Università degli Studi della Tuscia di Viterbo-Dipartimento per l'Innovazione nei Sistemi Biologici, Agroalimentari e Forestali
in agreement with
Consiglio Nazionale delle Ricerche-Istituto sull'Inquinamento Atmosferico

PhD Course in

Sciences, Technologies and Biotechnologies for Sustainability - XXXII Cycle

PhD Thesis Title

Multifunctional and eco-friendly nanofibrous based tools to control and reduce environmental impacts in agricultural systems

(SSD AGR/05)

PhD Student
Antonella Macagnano

Ph.D. Program Coordinator
Prof. Andrea Vannini

Supervisor
Prof. Giuseppe Scarascia Mugnozza

Co-supervisor
Prof. Nicola Pirrone

A.Y. 2018/19

Short Abstract

My PhD research activity proposes some innovative strategies to improve the technological infrastructure of agriculture practices by combining the development of novel agricultural products and sensors based on nanostructured smart materials, keeping competitiveness of yields and farms while improving the protection of natural resources. Consequently, by exploiting the potentials of electrospinning technology, a series of nanofibrous and eco-compatible fabrics were designed and investigated with the aim of: i) providing nutrients to plants, specifically iron, firstly by loading Fe chelating agents like phytosiderophores (mugineic acid) and phenolic compounds (catechol) on suitable supports, then releasing them in the surroundings, in order to mobilize this micronutrient and make it absorbable by plants, thus playing the role of biostimulants; ii) delivering nutrients to plants by supporting the successful colonization of soil (rhizosphere) by the adhesion and growth of beneficial microorganisms (plant growth promoting rhizobacteria, PGPR) on suitable supports, thus acting as biostimulants; iii) designing and testing of selective nano-composite conductive sensors based on biodegradable and recyclable polymers, capable of detecting some biogenic gases and volatile compounds in traces released in the soil upon treatments and metabolic activities. The exceptional specific surface area of the nanofibrous scaffolds created on purpose, together with the employment of biodegradable and biocompatible materials, resulted in efficient, eco-friendly and safe products for agriculture. Biomaterials and biodegradable polymers like polyhydroxybutyrate (PHB) and polycaprolactone (PCL) were selected and properly processed into freestanding nanofibrous membranes. The effectiveness of two non-woven fabrics differently designed and arranged to provide iron to plants from insoluble sources in the environment ($FeCl_3$) were tested in tomato (*Solanum lycopersicum* L. "Marmande") and duckweed (*Lemna minor* L.) plants grown in hydroponics and loading mugineic acid and catechol molecules, respectively. The resulting nanofibrous fabrics succeeded in providing iron to plants thus enabling them to recover the physiological and biometric features from previous Fe-deficiency conditions, thus acting as promising nanobiostimulants. A further approach concerned the investigation of PCL as a nanofibrous scaffold capable of hosting beneficial bacteria *(Burkholderia terricola*) to crop improving. The PCL nanofibrous scaffolds were inoculated with the bacteria cells and the dynamics of the consequent mechanisms involved in the specific adhesion of the cells to the nanofibers in both early and following stages of colonization were investigated in details. Since the nanofibrous framework was successful in enabling and stimulating the colonization by the plant growth promoting rhizobacteria (PGPR), then it could be suggested as a promising strategy for the creation of novel advanced nanobiostimulants for precision agriculture. To complete and maximize the expected benefits in an advanced and smart agricultural platform, miniaturized sensors based on similar nanofibrous and eco-friendly materials were also developed and investigated as selective and sensitive tools for monitoring biogenic gases and volatile organic compounds (VOCs) related to metabolic activities present in soils. In detail, conductive chemical sensors based on electrospun nanofibrous biodegradable (PHB) and recyclable (polystyrene, PS) polymers were arranged in both ternary and quaternary combinations with a conductive nanopowder of mesoporous graphene and a well-known sensing molecule (a free-base porphyrin, H2TPP). The resulting sensors were tested on biogenic gases and VOCs like amines, carboxylic acids, ketones, aromatic hydrocarbons, and nitrogen oxides. Their cost-effectiveness and ease of production, as well as reproducibility and environmental stability, confirmed that such sensors could be potentially used in monitoring soil in agro-ecosystems as well as in natural and perturbed conditions.

Keywords

Electrospinning, nanofibrous mats, eco-friendly materials, plant nutrition, agriculture, nanobiostimulants, low environmental impact, microorganisms, microbial inoculants, iron chelating agents, phytosiderophores, phenolics, nanostructured sensors, sustainability, environment preservation, VOCs, soil biogenic gases.

Extended abstract

1. Introduction

1.1. Nanofibrous Membranes for Eco-Friendly Iron Nutrition of Plants

Modern agriculture has been recently solicited to both improve crop yields and reduce the impact on environments and natural resources. The traditional approaches based on the large use of synthetic chemicals to control plant nutrient deficiencies and diseases have caused soil degradation, environmental pollution and risks to human health while level rates of yield growth for most crops have been decelerating at the global level **[1]**. The strategies here proposed employed nanostructured polymers capable of gradually releasing bioactive compounds supporting crop growth and productivity but reducing the impact on natural processes. The drug loading is a very easy process to implement via electrospinning technology and the high specific surface area and short diffusion passage length give higher overall release rate to the resulting nanofiber-based drug system than the traditional bulk material (e.g. film). Electrospinning, in fact, is a technology able to produce advanced multifunctional polymer nanocomposites (2D and 3D micro- or nanofibrous layers of inorganic and organic materials) and has been conceived as one of the most promising strategies to design and fabricate freestanding fabrics at low cost and with high production rates. The modulation of nanofiber morphology, porosity and composition can finely control the release of hosted compounds into the environment. Usually, in a controlled releasing system, the active substance is first loaded into a carrier or device, and then released at a predictable rate *in vivo* **[2-4]**. Since the limitation of iron availability is a crucial condition in plant physiology, the polymer fabrics here proposed, mimicking the peculiar natural strategy adopted by graminaceous species (Strategy II) **[5]**, were designed to make available to the plants the insoluble iron (Fe III) widely present in ecosystems by releasing selected phytosiderophores. My PhD thesis approach focused first on the production and functionality of a natural and biodegradable nanofibrous polymer (polyhydroxybutyrate-PHB) including aqueous drops of mugineic acid (MA) **[6,7]** extracted by barley root exudates onto tomato plants grown in hydroponics. Afterwards, due to the fragility of the nanofibrous fabrics, PHB was blended with polycaprolactone (PCL) and loaded with a phenolic compound, catechol, which is commonly involved in natural processes typical of nongraminaceous plants (Strategy I) with the aim of chelating iron (Fe(III)) from the surroundings and making it available to plants roots. This polymer blend, due to the physical properties of PCL, resulted softer and mechanically more resistant than the previous one (PHB) and it was poorly affected by sudden changes in temperature. Both polymers were selected since biodegradables, with low environmental impact, water insoluble and commonly investigated and used in drug delivery structures **[8-11]**. Electrospinning technology enabled different operative applications such as the direct coating of the root systems of tomato plants with soft gauze caps-like loading MA as well as the supply of the functional MA-releasing membranes as freestanding discs to the plants. Alternatively, freestanding mats of PHB/PCL were created and then fragmented into several parts and placed in proximity to the roots of duckweed (*Lemna minor*) **[12]**. In all the applications, hydroponic conditions were preferred to reduce, in these preliminary studies, the numerous variables present in tests with real soil.

1.2. Bacterial adhesion on polymer nanofibers

A further strategy pursued in this thesis was to design a peculiar polymeric fabric mimicking the soil structure and capable of enabling bacteria cells to adhere, colonize and develop biofilms and keeping bacterial populations viable for use in

agriculture. A bacterial strain (*Burkholderia terricola*) beneficial to plants because classified as plant growth promoting rhizobacteria (PGPR) was selected as a model microbial species for testing the interactions between microorganisms and polymer nanofibers and creating an eco-compatible fabric, easy to handle and store and to be used as a biostimulant tool in crop cultures **[13,14]**. Thus, a beeds-&-fiber model of electrospun 3D nanofibrous PCL scaffolds was designed on purpose to mimic the soil structure and then to be suitable for the development of bacteria biofilms. The bacterial communities grew on such a nanostructured fabric stored at room temperature, retaining their vitality up to 8 months upon storage in various moisture conditions. The adhesion mechanisms of bacteria cells to the nanofibers was investigated in details, specifically the phases of initial and reversible adhesion of bacteria to nanofiber surfaces, the orientation of bacteria cells relative to nanofibers, the following anchorage of bacteria to single and multiple nanofibers and the communication between cells. PCL is a biodegradable aliphatic polyester, which has been extensively employed in electrospinning processes to generate nanofibers and scaffolds for medical applications in tissue engineering **[9]**. Thus, based on the hydrophobic features of PCL nanofibers upon electrospinning, the bacteria strain was chosen also for its hydrophobic surface, thus aiding its adhesion **[15]**.

1.3. Nanofibers Doped with Porphyrin and Graphene for Chemiresistor Gas Sensors

Sensors aimed at measuring soil properties and treatments have been recently developed and used in precision agriculture. These sensors have been applied either to control variable rate application equipment in real-time or in combination with a Global Positioning System (GPS) to generate field maps of particular soil properties. Such sensor systems should allow crop farmers to recognize variations in the fields and to apply, at the right moment, variable type and rate of treatments with a much finer degree of precision than earlier possible. Together with information extrapolated from satellite or drone data (e.g. images analysis) and site-specific electrodes (e.g. ions-electrodes, moisture, etc.), soil status has been also successfully investigated by sensors capable of monitoring its volatile organic compounds (VOCs) and gases related to the "healthy" of the soil (e.g. microbial metabolism, pollution, etc.), providing valuable information on production and management plans. Sensors are desired to be able to work cooperatively with other sensors to measure simultaneously more parameters of the same soil, thus providing a more complete assessment. The electronic nose (E-nose) is a sensing technology that has been widely used to monitor environments in the last decade **[16]**. The capability of an E-nose, in combination with biochemical and microbiological techniques, proved to be able in measuring VOCs and/or gases evolution in soil headspace during microbial activity through a home-made E-nose based on a set of QCMs (quartz crystal microbalances) coated with different Me-porphyrins films. The resulting outcomes confirmed that the E-nose technology combined with both metabolic and biomass parameters could represent reliable indicators of the metabolic status of soil ecosystems. To further miniaturize the system and exploit the porphyrin sensing features, nanocomposite and conductive materials were designed, since considered more stable and being the most successful sensors on the market. Electrospinning technology has been confirmed to be a cost effective and attractive procedure to develop highly sensitive sensors **[17]** for detecting gases and VOCs. Therefore, a further strategy of my PhD thesis was dedicated to design, develop and test nano-composite conductive sensors based on biodegradable and recyclable polymers and capable of detecting selectively some gases and VOCs **[18,19]** as potential sensors for industrialized devices. In the present study, thin nanofibrous layers, comprising two insulating polymers (polystyrene (PS) and polyhydroxybutyrate (PHB)), a known percentage of nanofillers of mesoporous graphitized carbon (MGC) and a free-base tetraphenylporphyrin (H_2TPP), were deposited onto Interdigitated Electrodes (IDEs) by electrospinning technology to get miniaturized conductive sensors. The

effects of the porphyrin combination with the composite graphene–polymer system appeared evident when nanofibrous layers, with and without porphyrin, were compared for their morphology, electrical and sensing parameters. The potentials of the working temperature to drive both the sensitivity and the selectivity of the chemical sensors were studied and described.

2. Experimental procedure

Poly[(R)-3-hydroxybutyric acid] (PHB; natural origin), 2,2,2-trifluoroethanol (TFE), polycaprolactone (PCL) (M_n 45,000 g/mol), polystyrene (PS) (M_n 192,000 g/mol), mesoporous graphitized carbon nanopowder (MGC) (<500 nm; available surface area: 50–100 m^2/g; average pore diameter: 137 Å), hexadecyltrimethylammonium bromide (CTAB) (~99%), chloroform (≥99%), toluene (≥99.8%), acetic acid (≥99), catechol (1,2-Dihydroxybenzene, ≥99%) were purchased from Sigma-Aldrich (Merck KGaA, Darmstadt, Germany). Ethanol (≥99.8%) was obtained from Fluka (Buchs, Switzerland). All chemicals were used without further purification. A 5,10,15,20-tetraphenylporphyrin (H_2TPP) was prepared and provided by Prof. R. Paolesse, University of Tor Vergata, Rome, Italy. A mugineic acid (MA) aqueous suspension (0.112 μM) extracted by barley roots exudates (3%vol) and a set of *Solanum lycopersicum* L. "Marmande" plants in hydroponics were provided by prof. S. Astolfi (University of Tuscia – DAFNE, Viterbo, Italy); *Burkholderia terricola* strains (IF 25) cultures, previously isolated from a vineyard soil, were prepared by Dr. E. Di Mattia (University of Tuscia – DAFNE, Viterbo, Italy) and *Lemna minor* L. cultures, disposed in plastic vessels, were supplied by Dr. F. Pietrini (IRET-CNR, Monterotondo (RM, Italy)). Tomato plants were grown for 1 week in hydroponics in 40 μM Fe^{3+} and then for another week in Fe^{3+} deficiency (4.4 μM) before electrospinning (ES) treatment. Each nanofibrous layer was grown up by ES deposition using a single-needle. Duckweed cultures were prepared by cultivating fronds of *L. minor* in plastic vessels for 10 d in 1/10 strength Hoagland's nutrient solution in the presence (Fe-supplied) or absence (Fe-deprived) of 6 μM Fe(EDTA) (soluble chelated-Fe), then transferred into 24-well plates (well volume: 2.8 mL, well surface area: 2 cm^2), and each well was filled with 2.5 mL Hoagland's nutrient solution at pH 5.8. The 1 cm^2 polymer pieces, irrespective of their catechol content, were then placed on the bottom of the wells of 24-well plates for further incubation with duckweed plants. *Burkholderia terricola* cells were pre-cultured in a Luria-Bertani (LB) broth (30°C), agar plates (4°C) and then kept in a final suspension of 0.8 ± 0.02 x 106 CFU ml^{-1} where PCL samples were incubated. Electrospinning deposition parameters were properly modulated to optimize each type of fabric preparation. Optical micrographs were captured by Leitz-Wetzlar (Metallux 708082) microscope. Fibers morphological analyses were carried out by means of micrographs from Scanning Electron Microscopy (SEM, JEOL JSM 6010LA), Transmission Electron Microscopy (TEM, JEOL 1200 EX II, equipped with Olympus SIS VELETA CCD and iTEM software) and Atomic Force Microscopy (Nanosurf AG, Flex-AFM). UV-vis spectrophotometer (UV-2600 Shimadzu) was used to collect UV spectra. Water drops (8 μl) were deposited on the fibrous matrices and imaged using a USB-Digital Microscope (2.0 MPx, DIGIMICROSCOPE). Contact angles were measured after 5 s using DropSnake© (LBADSA method), a plugin in ImageJ. *L. minor* samples florescence was daily measured by MAXI-Imaging-PAM fluorimeter (Walz, Effeltrich, Germany). Chemosensors were housed in a measurement glass chamber (~100 mL volume) and connected to an electrometer (Keithley 6517) capable of measuring their electrical parameters and sending data to a PC (LabVIEW Software). The current was recorded by applying potential values at different temperatures (20, 40, 60, 80, 100°C). Different fluxes of gas withdrawn from a cylinder at fixed concentration were mixed to pure air; VOCs and water vapor concentrations were generated by a bubbler filled with liquid samples and mixed with the gas carrier (air).

3. Results and Discussion

Electrospinning deposition technique (Figure 1*a*) was used to create specific polymer mats with different features and potentials. Figure 1 (*b,c,d*) depicts a composite diagram of the different strategies based on ES technology and proposed for agriculture practices.

In a preliminary approach, a soft coating around the roots was performed by a direct deposition onto the samples. Tomato plants roots resulted thus encapsulated in porous and nanofibrous (100 nm fiber size) cocoons, and apparently, they were undamaged. When the ES-plants were grown in the presence of insoluble Fe^{3+}, chlorosis was clearly visible in NMs plants (i.e. plants nanofibrous membranes without MA) after 3 d treatment, due to lower chlorophyll content (measured by SPAD Chlorophyll Meter). Vice-versa, chlorophyll concentration increased in MA-NMs plants, thus confirming a proper functioning of the matrix. However, the membranes resulted to be too mechanically fragile to resist to the air bubbling typical of the hydroponic conditions and were then replaced by freestanding disc-shaped membranes.

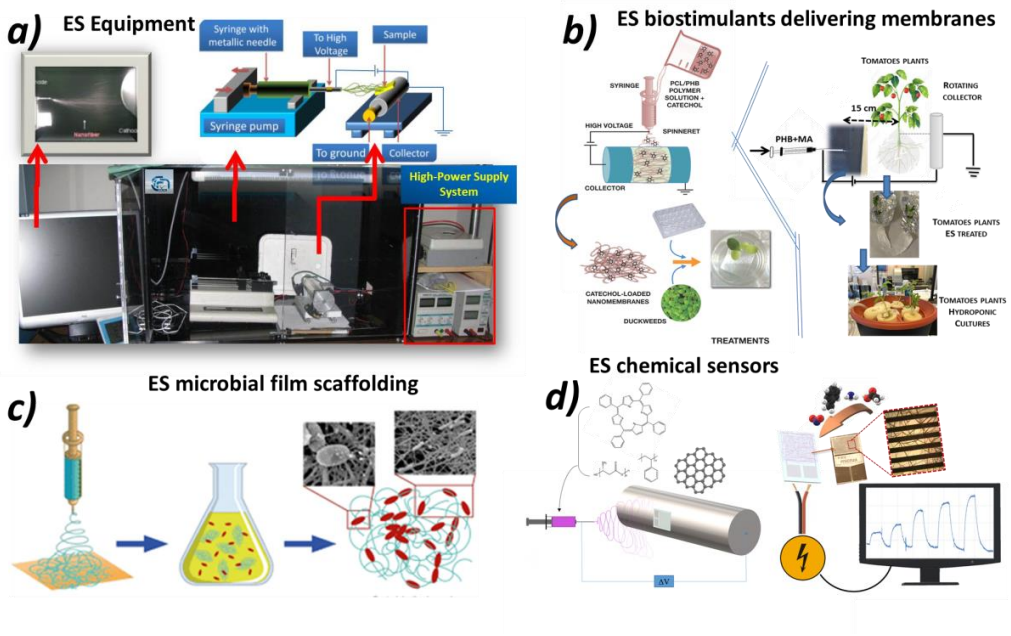

Figure 1. (a) electrospinning technique setup; ***(b)*** fabrication and application of polymer membranes loaded with biostimulants molecules for the plant growth and ***(c)*** with microorganisms after immersion in a culture broth; ***(d)*** Deposition of IDEs with composite and conductive nanofibers for chemical sensing

These nanoframeworks resulted to be more resistant and efficient than the wrapping cocoons previously tested so that the recovery of the chlorophyll content was prolonged to 5 d and was more substantial than before. Furthermore, discs with different surface-area-volume ratios involved different releasing times, suggesting the chance of modulating the efficiency of the membranes and their working time.

About the nanofibrous scaffolds morphology of the PHB/PCL blend, used to release catechol to duckweeds cultures, it appeared depending on the amount of catechol molecules solved in the polymer solution. More specifically, the fibers size distribution decreased when catechol amount increased (ranging by 0.526 ± 0.173 µm to 0.493 ± 0.148 µm) as well as wettability of the fibers seemed also depending on the quantity of molecules present in the polymer blend (WCA ranging by 118° to 82°), suggesting that catechol induced a rearrangement of the polymer fibers, thus affecting their physical properties which changed from hydrophobic to hydrophilic. The investigations on *L. minor* plants showed, in

fact, that upon addition of catechol loaded nanomembranes (CL-NM) to Fe-starved duckweeds, several improvements occurred in the plants (partially reported in Figure 2), such as enhanced chlorophyll synthesis (molecular level), greater photosynthetic activity (physiological and metabolic level), ultrastructural reorganization of the photosynthetic organelles (structural level), and reactivation and stimulation of plant growth (biometric level), so that all these parameters previously impaired by the Fe limitation were successfully recovered to a large extent or totally.

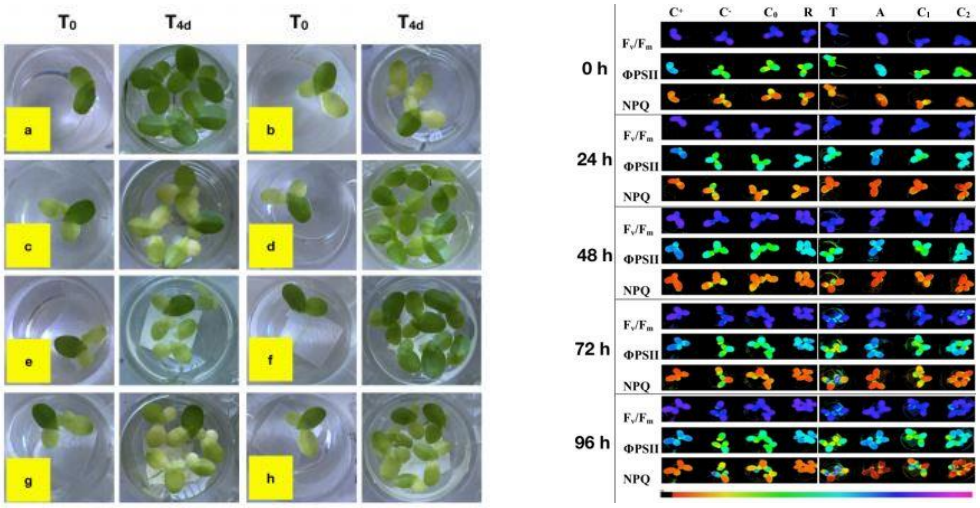

Figure 2. (left) Pictures of duckweeds fronds captured before (T_0) and after (T_{4d}) various treatments: a) C^+ = 6 μM Fe(EDTA) for both pre-treatment and treatment; b) C^- = no Fe for both pre-treatment and treatment; c) C_0 = no Fe (pre-treatment) + 6 μM $FeCl_3$; d) R = no Fe (pre-treatment) + 6 μM Fe(EDTA); e) T = no Fe for both pre-treatment and treatment + catechol free nanomembranes (CNMs); f) A = 6 μM Fe(EDTA) for both pre-treatment and treatment + CNMs; g) C_1L-MNs = no Fe (pre-treatment) + 6 μM $FeCl_3$ + C_1L-MNs (C_1 = 5 mM catechol); h) C_2L-MNs = no Fe (pre-treatment) 6 μM $FeCl_3$ + C_2L-MNs (C_2 = 100 mM catechol); ***(right)*** time courses of chlorophyll fluorescence parameters in *Lemna minor* L. fronds treated with different nutrient solutions and electrospun nanofibrous products for (4 days) after T_0. Images of the duckweed plants show: i) *Fv/Fm* = maximum quantum yield of PSII photochemistry in a dark-adapted leaf, ii) *ΦPSII* = quantum efficiency of PSII photochemistry and iii) *NPQ* = non-photochemical quenching measured at steady state. The arbitrary color code depicted at the bottom of each image ranges from 0.000 (black) to 1.000 (pink).

About the PCL nanofibrous mats designed to immobilize microorganisms, they appeared highly porous, with the external surface (exposed to the surrounding liquid growth medium) showing valleys and crests, while the internal portion presented cavities, channels and interconnected pores, similar to what observed in natural soils (Figure 3*a*). Relative to the overall 3D nanofibrous PCL structure, bacteria attachment and colonization started from the surfaces more easily intercepted by bacteria cells under stirring (incubation), typically the crests and the borders of the frameworks, but biofilms were firstly developed in the valleys and cavities of the structures, where maybe nutrients could be longer retained and concentrated. The biofilmed electrospun PCL nanoscaffolds, once removed from the growing medium, were stored for 2 months at 30°C in moist air conditions to assess the viability of the proposed microbial tools.

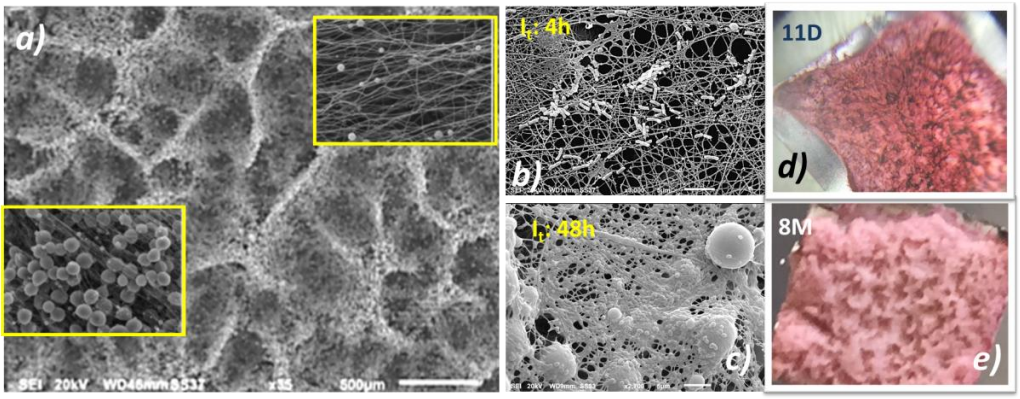

Figure 3. a) SEM micrograph of a PCL self-assembling beads-and-fibers 3D-framework mimicking the soil structure; ***b)*** microcolonies: bacteria cells attached to nanofibers after 4 h of incubation; ***c)*** biofilm formation: dense packing of cells attached to nanofibers to form a layer where cells are embedded into the matrix covering the whole electrospun framework (48h); ***d-e)*** respiration test of incubated and dry stored PCL membranes after 11 day *(d)* and 8 months *(e)*.

To test the viability/metabolic activity of the bacteria population during biofilm development and further storage, bacteria cells were specifically assayed periodically for INT (2-(p-iodophenyl)-3-(p-nitrophenyl)-5-phenyl tetrazolium chloride) reduction capacity (figure 3*d*). The bacterial communities resulted still viable after storage (Figure 3*e*). The nanostructured "artificial soil" here created resulted capable of providing a suitable surface to support the various phases of bacterial biofilm development, from initial unspecific attachment (facilitated by the "conditioning film"), specific adhesion (anchoring), extensive bacteria colonization (macro-colonies), EPS matrix release and bacteria embedment, development of a proper 3D biofilm. Interestingly, the PCL nanofibrous scaffolds appeared composed of nanofibers with an average diameter ≈64 nm, i.e. much smaller than the size of *B. terricola* cells. Different from most of the published studies, the fabricated nanofibrous fabrics appeared coated with a ≈15 nm thick conditioning film secreted by bacteria during the incubation aimed at facilitating their adhesion to the nanofibers. This coating consequently changed the surface morphology (from smooth to rough) and the physicochemical properties of the pristine material, thus resulting facilitating the bacteria colonization and storage **[15]**.

Finally, about the nanomembranes developed for designing chemical sensors, they were produced after a 2 min electrospinning deposition onto IDE (Interdigitated Electrode) microtransducers. Firstly, the 3-component nanofibers (i.e. without porphyrin loading), obtained from a mixture of PS and PHB (insulating thermoplastics) and a known concentration of MGC nanopowder, appeared highly rough on the surface and decorated with jagged islands but homogeneous in shape and diameter, with the nanofillers aggregated into clusters more or less densely packed through the fibers. The resulting sensor was conductive at room temperature and could work between 40 and 80°C without any apparent degradation. As the fibrous sensing layer was heated, the current increased and the sensitivity to some classes of VOCs such as an oxidizing gas drastically changed depending on the working temperature. More in detail, the sensor resulted highly sensitive and selective to acetic acid (an organic acid) at 40°C but the sensitivity fell down, decreasing by 96%, when the sensor operated at 80°C. On the other hand, although an increase in temperature caused a general decrease in sensitivity to the tested VOCs (with a maximum of 14, 81, and 78% for amine, acetone and toluene, respectively) and water vapors (with a maximum of 55%), higher temperature affected only slightly the amine permeation, thus modifying the partial selectivity of the sensor to these chemicals. Conversely, when the operating temperature

increased, the sensitivity to the detected gas, NO_2, increased too, reporting a ~2 ppb limit of detection (LOD), thus confirming that the temperature was able to drive the selectivity of nanocomposite polymeric sensors.

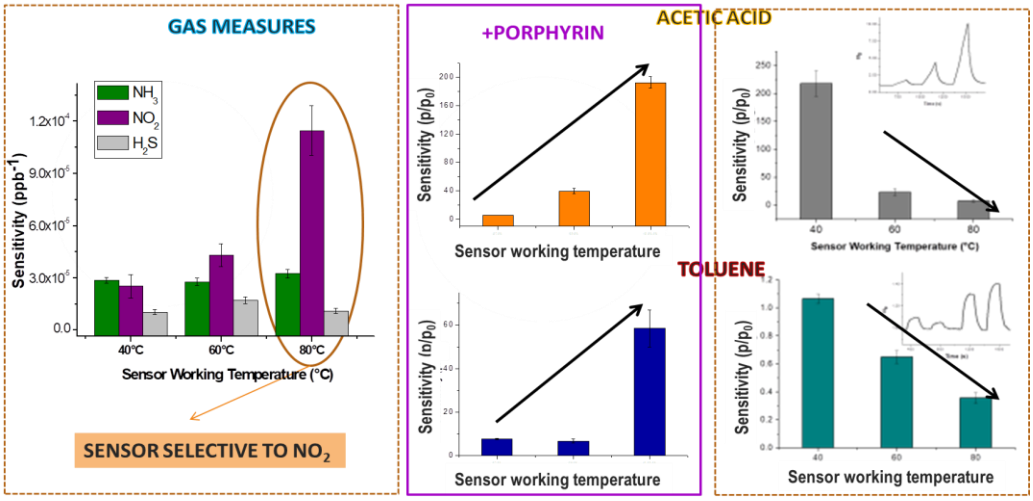

Figure 4. Sensors sensitivity values (calculated as the slope value of each sensor response curve) with- (pink rectangle) and without porphyrin (orange rectangles) have been reported at increasing working temperature and towards gas and VOCs.

Secondly, when the porphyrin free base was incorporated, it changed not only the fiber morphology, but also the electrical and sensing features making the novel material more sensitive to specific VOCs (as aromatics) at increasing working temperatures. Therefore, porphyrin not only increased the sensor sensitivity to toluene vapor (i.e., adsorption and diffusion were favored), which conversely was not revealed at all by the previous sensor (PS-PHB-MGC), but also increased with increasing temperature, differently from what occurred previously with the sensor porphyrin-free, whereas the sensitivity to VOCs decreased with heating (Figure 4).

4. Conclusions

Based on the features of the nanomaterials created in the present thesis (delivering natural Fe-chelating agents, keeping enormous surface area suitable for hosting large amounts of microorganisms) and the findings obtained (improvement of Fe nutrition in plants, good adhesion and long maintenance of the viability of beneficial microorganisms), the resulting products here proposed might reasonably represent promising efficient, eco-friendly and safe materials tools acting as nanobiostimulants in agricultural applications. These results could also assist in the future the development of further eco-friendly and safe materials for target low impact applications aimed at dealing with specific drug delivery systems and environmental problems. The use of the selected eco-friendly thermoplastics for designing sensors allowed the temperature to be a useful parameter for modulating their selectivity, similarly to what happens for the metal oxide sensors, so that arrays might be created based on the same sensor working at different temperatures.

5. References

1. Alexandratos, N.; Bruinsma, J. *World Agriculture towards 2030/2050: The 2012 Revision*; FAO: Rome, Italy, 2012; ISBN 9781844070077.

2. Pornsopone V., et al., Electrospun methacrylate-based copolymer/indomethacin fibers and their release characteristics of indomethacine, *J Polym Res* 14 (2007), 53-59
3. Kim T.G., et al., Controlled protein release from electrospun biodegradable fiber mesh composed of poly(epsilon-caprolactone) and poly(ethylene oxide), *Int J Pharm.* 338 (1-2) (2007), 276-283
4. Huang Z.M. et al., Encapsulating drugs in biodegradable ultrafine fibers through co-axial electrospinning, *J Biomed Mater Res A*. 77(1) (2006), 169-79.
5. Marschner H., Romheld V., Strategies of plants for acquisition of iron, *Plant and Soil* 165 (1994) 261-274
6. Takagi S., Kamei S., Yu M-H., Efficiency of iron extraction from soil by mugineic acid family phytosiderophores, *Journal of Plant Nutrition* 11(6) (2008), 643-651
7. Canarini, A.; Kaiser, C.; Merchant, A.; Richter, A.; Wanek, W. Root exudation of primary metabolites: Mechanisms and their roles in plant responses to environmental stimuli. *Front. Plant Sci.* 2019, 10, 157
8. Patra, J.K.; et al. Nano based drug delivery systems: Recent developments and future prospects. *J. Nanobiotechnol.* 2018, *16*, 71
9. Mondal, D.; Griffith, M.; Venkatraman, S.S. Polycaprolactone-based biomaterials for tissue engineering and drug delivery: Current scenario and challenges. *Int. J. Polym. Mater. Polym. Biomater.* 2016, *65*, 255–265.
10. Bugnicourt, E.; Cinelli, P.; Lazzeri, A.; Alvarez, V. Polyhydroxyalkanoate (PHA): Review of synthesis, characteristics, processing and potential applications in packaging. *Express Polym. Lett.* 2014, *8*, 791–808.
11. Lovera, D.; Márquez, L.; Balsamo, V.; Taddei, A.; Castelli, C.; Müller, A.J. Crystallization, morphology, and enzymatic degradation of polyhydroxybutyrate/ polycaprolactone (PHB/PCL) blends. *Macromol. Chem. Phys.* **2007**, *208*, 924–937.
12. De Cesare F., Pietrini F., Zacchini M., Scarascia Mugnozza G. and **Macagnano A.**, Catechol-Loading Nanofibrous Membranes for Eco-Friendly Iron Nutrition of Plants, *Nanomaterials* 2019, 9(9), 1315; https://doi.org/10.3390/nano9091315
13. T. Danhorn and C. Fuqua , Biofilm formation by plant-associated bacteria, *Annu. Rev. Microbiol.*, 2007, 61 , 401 —422
14. Egamberdieva D., Shrivastava S., Varma A., *Plant-Growth-Promoting Rhizobacteria (PGPR) and Medicinal Plants*, Springer International Publishing Switzerland 2015 DOI 10.1007/978-3-319-13401-7
15. De Cesare F., Di Mattia E., Zussman E. and **Macagnano A**., A study on the dependence of bacteria adhesion on the polymer nanofibre diameter, *Environ. Sci.: Nano***,** 2019,6, 778-797
16. De Cesare F., Di Mattia E., Pantalei S., Zampetti E., Vinciguerra V., Canganella F., Macagnano A., Use of electronic nose technology to measure soil microbial activity through biogenic volatile organic compounds and gases release, *Soil Biology & Biochemistry* 43 (2011) 2094-2107
17. Macagnano , A. Zampetti E. and Kny E., *Electrospinning for High Performance Sensors* , Springer International Publishing Switzerland, 2015
18. Avossa J., Zampetti E., De Cesare F., Bearzotti A., Scarascia-Mugnozza G., Vitiello G., Zussman E. and **Macagnano A.**, Thermally Driven Selective Nanocomposite PS-PHB/MGC Nanofibrous Conductive Sensor for Air Pollutant Detection, *Front Chem* 2018 https://doi.org/10.3389/fchem.2018.00432
19. Avossa J., Paolesse R., Di Natale C., Zampetti E., Bertoni G., De Cesare F., Scarascia Mugnozza G. and **Macagnano A**., Electrospinning of Polystyrene/Polyhydroxybutyrate Nanofibers Doped with Porphyrin and Graphene for Chemiresistor Gas Sensors, *Nanomaterials* 2019, 9(2), 280; https://doi.org/10.3390/nano9020280

“Solo vuela el que se atreve a hacerlo"

(L. Sepulveda)

To my beloved son and husband.

To my unforgettable mum and dad.

TABLE OF CONTENT

1. CHAPTER 1 - Introduction

The aim of the PhD thesis research project was to investigate the potential of innovative nanofibrous materials for the development of more sustainable agricultural ecosystems. Electrospinning technology was employed on purpose to create eco-compatible and eco-sustainable nanomaterials as suitable scaffolds addressed to: i) support plant growth employing advanced products based on natural agents and strategies to replace agrochemicals and ii) monitor soil ecosystems through novel sensing systems. Both the approaches were aimed at reducing the environmental impacts of agricultural systems by supporting more efficient practices, but preserving their competitiveness in crop productivity. Briefly, electrospinning was used to create nanofibrous materials to be used to improve plant growth through the fabrication of novel agrochemicals and products acting as nano-biostimulants and as nanofibrous sensors to monitor soil fertility through the detection of volatile compounds and gases related to soil health and quality. The two nanofiber-based approaches might also be coupled into smart fertilizing-&-monitoring integrated systems for applications in precision agriculture (in the field and nurseries) aimed at reducing the global amounts of synthetic agrochemicals in favor of natural compounds and more efficient and eco-friendly strategies. Consequently, the decrease in the exploitation of natural resources, the protection of soil and environment from contamination and eutrophication, and the enhancement in the use of biocompatible and recycled materials could be obtained. The main concept underpinning the present project is to exploit the outstanding features of the nanotechnological process named "electrospinning" (ES) to create a variety of tools for a multitude of possible applications in agriculture.

Therefore, the main objectives of this PhD project were the followings:

i) to preserve the soil ecosystem, considered as a natural capital that is part of the Earth's life support system;
ii) to develop resource-efficient, green and competitive approaches for agricultural systems based on the use of eco-sustainable materials (biological, biodegradable and recycled materials) aimed at creating nanofibrous matrices acting as both nano-biostimulants (i.e. (phyto)siderophores and microorganisms) and nanosensors for monitoring the ecosystem health, quality and safety;
iii) to protect the environment from eutrophication and contamination (e.g. through the slow release of natural compounds, the use of eco-friendly compounds, the employment of natural strategies);
iv) to propose a novel approach based on electrospinning technology and the generated nanofibrous materials for agricultural applications;
v) to suggest the ecosystems monitoring by novel sensors based on electrospun nanofiber technology;
vi) to design a future integrated platform composed of suitable nano-biostimulants and nanosensors capable of both providing nutrients (controlled release) and detecting and monitoring, directly or indirectly, the fertility status of the soil ecosystem (e.g. excessive nutrients), to reduce then superfluous fertilizations and prevent the possible contamination of natural bodies.

By exploiting electrospinning potentialities, a series of nanofibrous fabrics were designed and investigated. The exceptional specific surface area of the scaffolds combined with the employment of biodegradable and biocompatible materials were promising for creating efficient, eco-friendly and safe materials for agriculture. Biomaterials as polyhydroxibutyrate (PHB) and biodegradable

polymers like polycaprolactone (PCL), were selected and properly processed into freestanding nanofibrous membranes. The effectiveness of two fabrics differently arranged and designed to provide iron to plants from insoluble sources in the environment ($FeCl_3$) was tested in tomato (*Solanum lycopersicum* L. var Marmande) and duckweeds (*Lemna minor* L.) plants in hydroponics, loading mugineic acid and catechol molecules, respectively. A further approach concerned the investigation of PCL as a nanofibrous scaffold for hosting *Burkholderia terricola,* an agricultural beneficial bacterium (PGPR - plant growth promoting rhizobacteria). The PCL nanofibrous scaffolds were inoculated with the bacteria cells and the dynamics and mechanisms involved in the specific adhesion of the selected bacterial species in both early and following stages of colonisation were studied, as well as the maintaining of their viability on the fabric even after months of conservations. To complete and maximize the expected benefits in an advanced and smart agricultural managing model, also miniaturized sensors based on nanofibrous and eco-friendly materials were developed and investigated as selective and sensitive tools for monitoring gases and volatile organic compounds (VOCs) related to the soil metabolic activities and the soil fertility status. In detail, nanofibrous conductive chemical sensors based on a biodegradable (PHB) and a recyclable organic polymer (polystyrene, PS) were arranged in both ternary and quaternary combinations with mesoporous graphene in the form of conductive nanopowder and a free-base porphyrin molecule (H_2TPP) as model sensing molecules. The cost-effectiveness and ease of production, as well as the reproducibility and environmental stability of such sensors confirmed that they might be potentially used in monitoring soil ecosystems in natural and perturbed conditions.

CHAPTER 2 - State of the Art

Soil is an essential support for the life on the Earth, it regulates processes in terrestrial ecosystems, and interacts with the atmosphere and the hydrosphere (*Adewopo et al., 2014*). There is a close relationship between soil security (quality, resilience), water security (quality, renewability and availability), climate security (optimal temperature and moisture regimes, and low frequency of extreme events) and economic security (income and access to resources). Agriculture is the largest interface between humans and the environment, and is a major cause of climate change and ecosystem degradation (*Srilatha, 2011*). The damage and risk to the environment (croplands, forests and water sources) and human health consequent to agricultural practices (tillage, excessive fertilization and pesticide treatments, and deforestation) traditionally employed to improve crop productivity have enhanced the belief that such practices should be urgently replaced by more environmentally friendly processes and compounds (*Heege, 2013; Fares et al. 2015*). Nanomaterials and nanotechnologies can contribute to the transformation of actual agricultural systems towards more sustainable managements by adopting practices and bioactive substances aimed at maintaining an ecological equilibrium and encouraging natural regenerative processes such as nitrogen fixation, nutrient cycling, soil regeneration, and the protection of natural enemies of pest and diseases. An ideal agricultural system is defined as sustainable if it maintains and improves human health, benefits environment and produces enough food for increasing world population. The utilization of bio-fertilizers can reduce the use of urea, prevent the depletion of soil organic matter and decrease environmental pollution to a considerable extent. Notably, nanomaterials can enhance the productivity of crops by increasing the efficiency of agricultural inputs to facilitate site-targeted controlled delivery of nutrients, thereby ensuring the

minimal use of agri-inputs. They can find application for the development of smart nanotools for the immobilization of proper compounds and their slow or controlled release in soil. Nanomaterial engineering is the cutting-edge track of research that supports the development of high-tech agricultural fields by offering a wider specific surface area crucial for the sustainable development of agriculture systems. In conventional methods, agrochemicals are generally applied to crops by spraying and/or broadcasting. As a result, a little amount of agrochemicals reaches the target sites of crops, i.e. much below the minimum effective concentration required for successful plant growth. On the contrary, substantial losses are recorded because of chemical leaching, degradation by photolysis, hydrolysis and microorganisms. Therefore, nanotechnology can not only reduce the uncertainty, but also coordinate the management strategies of agricultural production as an alternative to conventional technologies (*Shang et. al., 2019*). In agriculture, novel and groundbreaking tools have recently been developed employing natural and engineered nanomaterials to deliver agrochemicals to plants (Figure 2.1) for both improving nutrition (nanofertilizers), stimulate plant growth (seeds treatments), improve the quality of the soil (nanozeolites, hydrogels) and protecting plants (nanopesticides), but reducing the impact of these compounds on the environment and human health by reducing the global amount provided and improving the efficiency of their actions (*Tuteja et al., 2013*; *Ingale et al, 2013*; *Ranjan et al., 2017*). In order to ensure eco-friendly agricultural practices, the recent advancement of nanotechnology-based synthesis of slow or controlled release fertilizers, pesticides and herbicides has received extra attention in agriculture farming. With the passage of time, nanotechnology has gradually moved from the lab-based experimental trials to practical applications. Controlled delivery techniques aim at releasing a measured amount of necessary and sufficient quantities of

agrochemicals over some time and obtaining the full biological competency with minimizing losses and harmful effects. Nanostructures, generally nanoparticles, offer the advantages of effective delivery of agrochemical due to their large surface area, easy attachment and fast mass transfer. For these reasons, micron or submicron particles have been incorporated into the agrochemicals through several mechanisms, such as encapsulation, absorption, weak bond attachments and entrapment into the nano-matrix of active ingredients. Nanomaterials improve stability of agrochemicals and protect them from degradation and subsequent release into the environment, which eventually increase the effectiveness and reduce the quantities of agrochemicals. Nanotechnology can find applications also in the development of analytical devices dedicated to the control of quality, bio/security, and safety not only in agriculture, but also along the food supply chain (*Fraceto et al., 2016*). In this context, nanosensors represent a powerful tool with advanced and improved features, compared to existing analytical sensors and biosensors. Nanosensors are defined as analytical devices having at least one sensing dimension no larger than 100 nm, fabricated for monitoring physicochemical properties in places otherwise difficult to reach. Nanotubes, nanowires, nanoparticles, or nanocrystals are often used to optimize the signal transduction deriving by sensing elements in response to the exposure to biological and chemical analytes having a similar size. They have unique surface chemistry, distinct thermal, electrical and optical properties, useful to enhance sensitivities, reduce response times, and improve detection limits, and can be used in multiplexed systems. Thus, nanosensors can be employed to maximize the benefits of these resources management by controlling soil nutrients, moisture, pH and temperature of soils as well as contaminants and microorganisms (*De Cesare et al., 2008; 2011*). Therefore, the potential of

nanomaterials encourages a new green revolution with reduced farming risks.

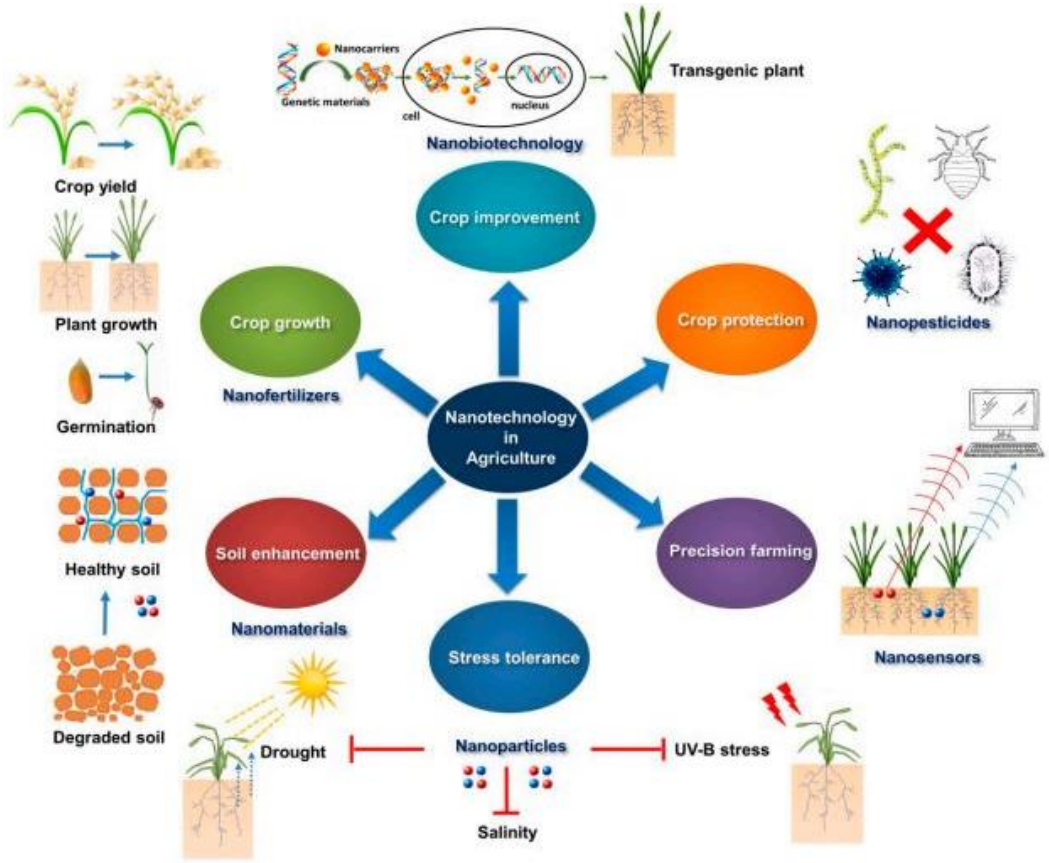

Figure 2.1. Layout of applications of nanotechnology in agriculture. Controlled released nanofertilizers improve crop growth, yield and productivity; nano-based target delivery approach (gene transfer) is used for crop improvement; nanopesticides can be used for efficient crop protection. Uses of nanosensors and computerized controls greatly contribute to precision farming. Nanomaterials can also be used to promote plant stress tolerance and soil enhancement (*Source Shang et al., 2019*).

However, there are still huge gaps in our knowledge of the uptake capacity, permissible limit and the ecotoxicity of different nanomaterials. Some regulatory aspects of nanotechnology in agriculture in EU and non-EU countries have been reported by *Amenta et al., 2015.* However, the major issue on potential toxicity of nanomaterials to ecosystems, in short and long time, is mainly supposed to be due to the possibility of nanostructures of penetrating inside the cells of living organisms. Electrospinning

(ES) is a highly versatile and inexpensive nanotechnology that allows to design and fabricate continuous non-woven fibers with diameters ranging from micrometer to nanometer when a strong electrical field acts on a droplet of a solution with sufficient viscoelasticity (*Wendorff et al., 2012*). Long fibrous structures are expected to be less harmful than NPs, since more difficult to incorporate. ES can be applied to natural polymers, synthetic polymers, ceramics, carbon, glass and metal. Such 2D-3D arrangements (Figures 2.2 and 2.3), while maintaining unchanged the potential related to nanosize, they are not expected to affect the toxicity related to their possible penetration into the cell at all. Additionally, fibers can assume complex shapes, such as micro-ribbon, porous, core-shell, or hollow, creating a multitude of structures (2D, 3D, ribbon-like, membranes, scaffolds, tissues) with a broad spectrum of different properties (porosity, permeability, high surface-to-volume ratio, non-woven fabrics, high fiber interconnectivity, nano-scale interstitial spaces, biomimetism and bioinspiration, etc.). ES technology is nowadays a widely known fiber-forming technique, but its principles and investigations have started many decades ago. For instance, John Francis Cooley filled the first patent of an electrospinning apparatus in 1900. Lately, efforts to understand the physics of fluids under an electromagnetic field received a great contribution from the mathematical work of John Zeleny in 1914. A seminal contribution to the field of fiber spinning was also given by Anton Formhals, who filled a series of patents from 1931 to 1944. In the 1960s, Sir Geoffrey Taylor, a prominent scientist in fluid dynamics, worked on the mathematical modelling of the cone formed by a droplet under the action of an electrical field, which was later named Taylor Cone. In the 1990s the technique started to be used in large scale by several researchers to produce a large variety of polymer nanofibers. During the last years, several patents and articles involving electrospinning technique have been published around

the world, evidencing this technique as highly suitable to obtain micro- and nanofibers of polymer and composite materials for varied applications. The main advantages of electrospinning compared to other conventional fiber-producing methods, such as spinneret extrusion, are the formation of fibers with low size scales, control of morphology and the versatility of materials that can be used to obtain the fibers. Fibers morphology is an aspect of extreme importance to direct the application of ESNFs in several technological fields. In order to improve and/or obtain different morphologies, several experimental parameters related to the polymer solution (e.g. polymer molecular weight, concentration, viscosity, conductivity) as well as those related to the process (e.g. applied voltage, spinneret-to collector distance, polymer solution feeding rate) need to be properly tailored. As previously mentioned ES technology provides several opportunities for the development of chemical (bio)sensors based on polymeric or composite nanofibers: i) to generate membranes designed with excellent (or tuned) interconnected porosity, predictable pore geometries and sizes, large global pore volumes; ii) to obtain nanofibers with desired diameters, then extending specific surface area; iii) to regulate, in a single electrospinning deposition step, the desired thickness of the applied membrane, from tens of nanometers to several micrometers; iv) to allow the use of a large variety of materials (polymers, polymer-blends, inorganic nanoparticles, carbon nanostructures) exhibiting distinct interacting properties. Moreover, the opportunity to customize and functionalize the nanofibers on large scale enables the electrospinning technique to match a wide range of requirements for specific sensing applications, giving it a benefit over other methods commonly used for the production of micro/ nanostructures (*Mercante et al., 2017*). The wide range of polymers and materials employable in ES and the possibility for electrospun nanofibers to be variously functionalized provide exceptional binding properties of the

resulting materials towards molecules of various chemical nature (food bioactive compounds, pollutants, gases, ions, VOCs, etc.), as well as macromolecules (enzyme, and proteins, DNA, etc.).

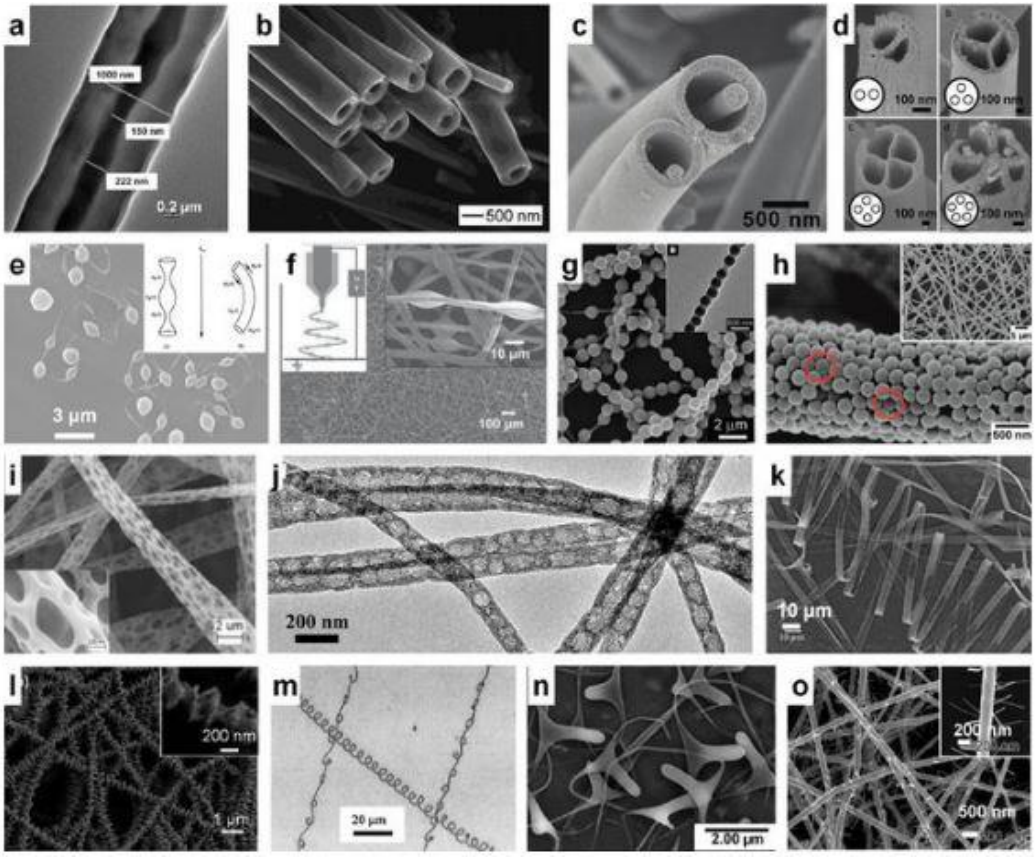

Figure 2.2. Structural diversity of the individual electrospun fiber. a) core-shell fibers produced by coaxial electrospinning; b) hollow fibers; c) nanowire-in-microtube structured fibers; d) multichannel microtube structured fibers; e) beaded-fibers; f) bead-on-string fibers produced by coaxial electrospinning; g) beaded (necklace-llike) fibers produced from electrospinning of blend of SiO2 particles and PVA solution; h) colloidal fibers produced from electrospinning of blend of PS nanoparticles and PVA solution; i) porous fibers; j) bamboo-like nanofibers with internal cavities; k) ribbon fibers; l) nanofibers with a nanohybrid shish-kebab structure; m) helical fibers; n) barbed fibers produced from electrospinning of 3 wt% PVA solution; o) barbed V2O5-TiO2 nanofibers and the barbs comes from the growth of V2O5 crystals during the calcining of V2O5-TiO2-Ta2O5 composite nanofibers. (Source *Yang et al., 2017*)

Similarly, ES fibers can be easily designed for immobilization of cells (endothelial and smooth muscle cells for blood vessels, fibroblasts for dermal substitution, osteoblasts for bone regeneration, hepatocytes for potential liver regeneration, neural stem cells, microorganisms, etc.), by using different binding

techniques: functional-binding, co-electrospinning, emulsion electrospinning, etc.). The outstanding versatility of ES has made it eligible for a multitude of applications in medicine, pharmaceuticals, catalysis, filtration, cosmetics, and flame-retardants. The findings obtained by scientists in nanomedicine using ES as concerns the release of substances in specific organs of human body (drug delivery), healing wounds through releasing drugs and antibacterial agents to prevent infections and providing support for cell regeneration and growth, prove the potentialities in the use of electrospinning for agricultural formulations and products for similar purposes. Similar tools can be designed to supply nutrient to plants, control pest and pathogen-induced disease in plants and fruits, provide wound healing and sensing. For instance, the employment of ES in drug-like delivery systems for agriculture (Figure 2.4) has been proven in releasing pheromones for pest control. Indeed a natural strategy of controlling insect pests is to use pheromones to lead them to traps. Electrospun nanofiber with its large surface area has been able to release effectively the pheromones for this purpose (*Krishnamoorthy et al., 2017; Bansal et al. 2010*). More effective resulted the blending of tert-butyl-2-methyl-4-chlorocyclohexane-1-carboxylate (Trimedlure, commercial name) in ethylcelluose, polyethylene glycol (PEG- PCL), polyvinyl acetate-vinyl pyrrolidone and polycaprolactone polymers using organic solvents and electrospun to form nanofibers. Up to 10% w/v of the active ingredient was added (*Bisotto-de-Oliveira et al., 2014*). Their studies in the field showed that the chemically-treated membrane were effective in attracting the flies. Given that different polymers may be electrospun to give fibers, selection of the polymers for encapsulation of pheromones need to be tested to find the best combination in attracting the targeted pests.

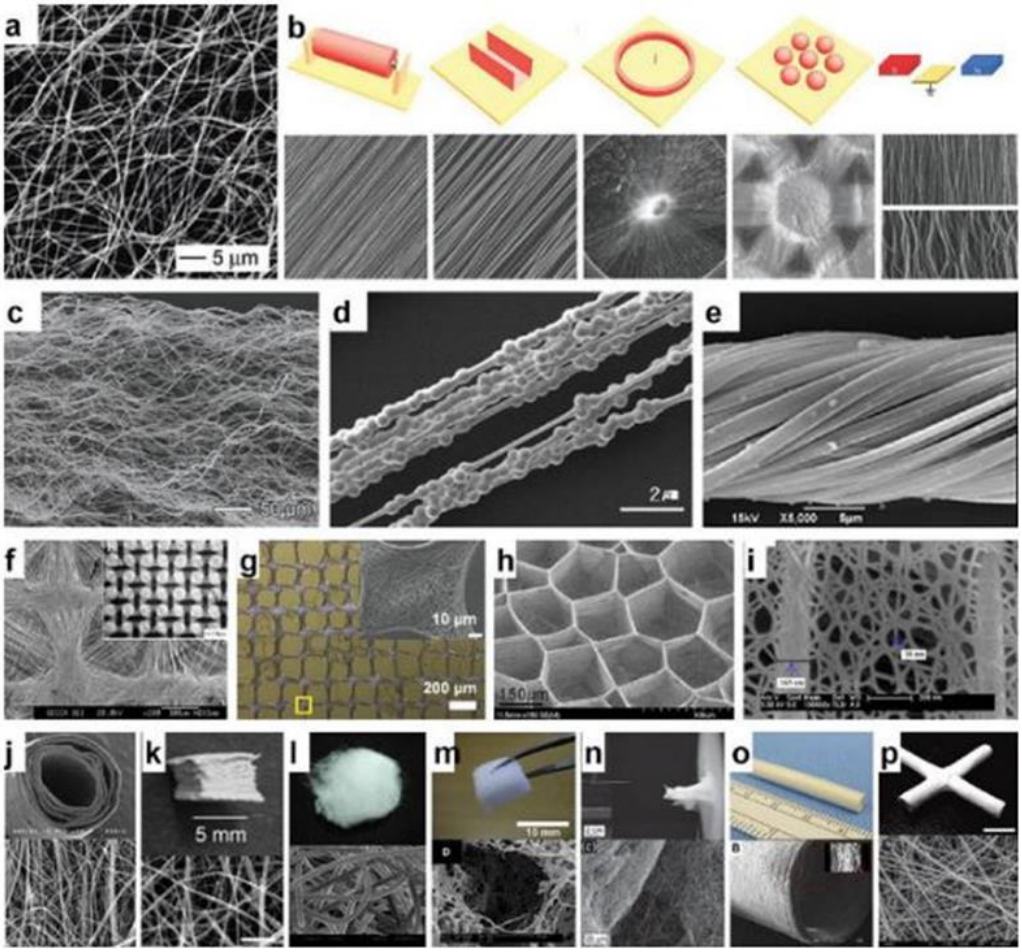

Figure 2.3. Structural diversity of the 3D-arrangements of electrospun fibers: **a)** random electrospun fibers; **b)** different aligned electrospun fiber collectors and SEM images of corresponding aligned fibers; **c)** aligned self-crimping fibers; **d)** aligned beaded fibers; **e)** electrospun fiber yarn**; f-i)** patterned fiber mats, **f)** patterned fibers fabricated by using a patterned fiber collector; **g)** stereomicroscopy images of fibrous patterns with localized nanofiber dissolution method; **h)** honeycombpatterned nanofibers from self-assembly of electrospun nanofibers driven by surface tension and electrostatic repulsion; **i)** nanofiber spider webs; **j-p)** the macroscopic photos and corresponding microscopic SEM images of different 3-D electrospun nanofibrous macrostructures, **j)** the fibrous tube fabricated from electrospun fiber mats by manual; **k)** 3D fibrous stacks; **l)** 3D fibrous structure from expansion of electrospun microfibers; m) macroporous and nanofibrous hyaluronic acid/collagen hybrid scaffold fabricated by concurrent electrospinning and deposition/leaching of salt particles; **n)** 3D fibrous structure fabricated by electrospinning the blend solution of alginate/PEO/F127; **o)** the fibrous tube produced by using a rolling stick collector; **p)** the crossed fibrous tube produced by using the perpendicular collecting stick. (Source *Yang et al., 2017*)

However the distribution of the molecules into the polymer are key parameters to get effective tools. For instance, the encapsulation of synthetic sex pheromone of *Grapholita molesta* (*Bisotto-de-Oliveira et al., 2015*) resulted different in the final amount inside

electrospun fibers depending on the kind of hosting polymer (polyvinyl acetate/polyvinyl pyrrolidone, PVAc/PVP), polycaprolactone (PCL) and the used organic solvents (tetrahydrofuran,THF and dichloromethane, DCM).

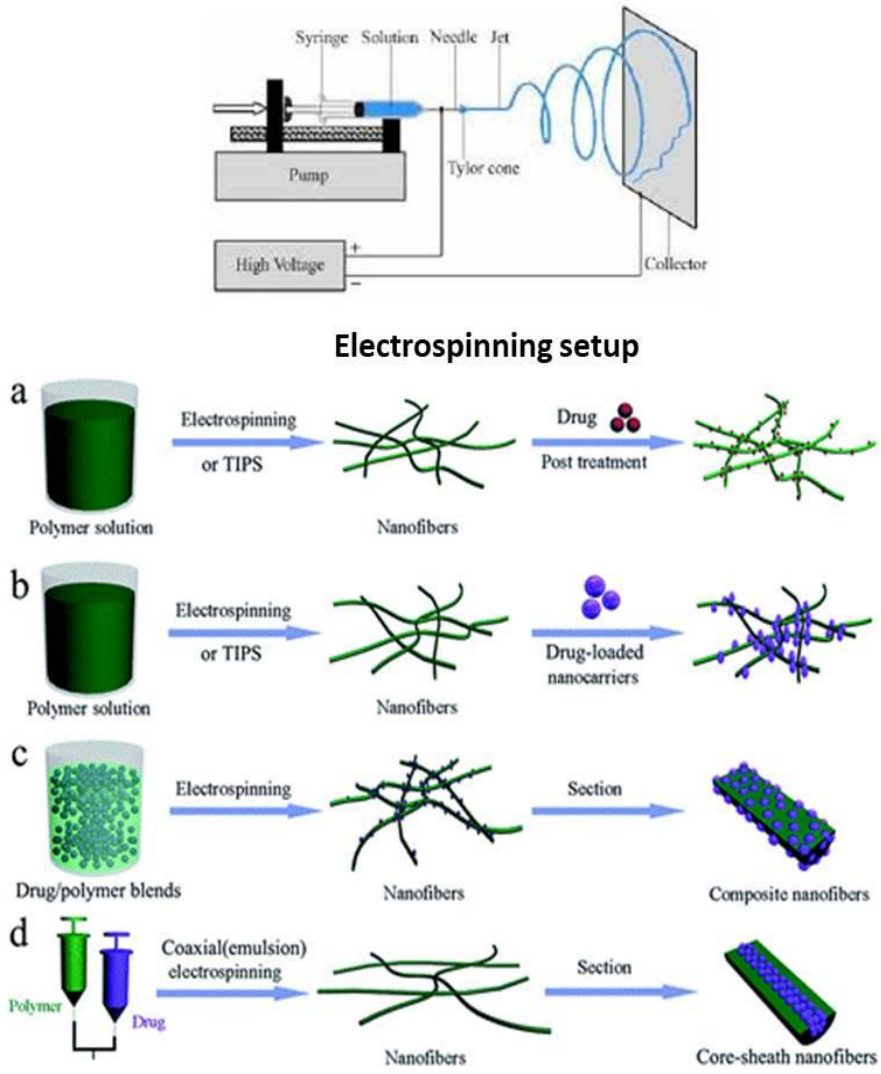

Figure 2.4. Sketch of electrospinning setup and several strategies to load compounds for drug delivery (Source *He et al., 2014*)

Such difference in load retention was supposed to be due to the loss of pheromone to the surrounding during electrospinning process. Electrospinning has been tested as a fungicide treatment for seeds. *Castaneda et al.* (2014) incorporated commercially available fungicide (Vitavax Thiram SC-200 and Carbex 500) into ethyl cellulose before electrospinning over rice seeds. The results

showed an improvement of rice germination to about 95% with the nanofiber coating, which is 8% more than the negative control (rice without coating). Referring to fertilizer application via ES, it sounds extremely promising since a network of fibers is much less likely to be washed away than particles. This will reduce the amount of fertilizer loss by the farmer and at the same time prevent pollution of the waterways due to fertilizer run-offs. Furthermore, in the dry season, a layer of fertilizer loaded fibers electrospun directly over the top soil may also be used to hold down the soil with the seed in place while waiting for rain to arrive in an exposed dry field. Seeds coated with fertilizers loaded electrospun fibers have been shown to facilitate germination (*Krishnamoorthy et al., 2017*). Depending on the polymer carrier and the structure of the fibers, the release rate of the fertilizers may be tailored (*Castro-Enriquez et al., 2012; Kampeerapappun et al., 2013*). Agriculture, with its use of fertilizers, pesticides, herbicides and fungicides to improve the yield of the crops is often a source of pollution that can sometimes be detrimental to the crops itself. Herbicides while meant to reduce growth of weeds, may act against seed germination or seedlings if the water source is contaminated with it. Pesticides and fungicides residues are always a concern for consumers while excess fertilizers washed into the streams and rivers may disrupt its ecosystem. In the removal of herbicides contaminants, *Palvannan et al. (2014)* tested functionality and performance of laccase immobilized on electrospun zein/polyurethane nanofiber. Retention of the functionality of laccase immobilized on the nanofiber surface was verified by the degradation of chloroxuron with up to 25 reuse cycles.

Bacteria and microbes are also important players in the soil ecosystem, and sometimes, in economically important crops, their presence is essential for the soil features. Beneficial soil microrganisms are able to fix atmospheric N, decompose organic wastes and residues, detoxify pesticides, suppress plant diseases

and soil-borne pathogens, enhance nutrient cycling and produce bioactive compounds such as vitamins, hormones and enzymes that stimulate plant growth. Cyanobacteria and PGPR are excellent model systems and can provide bioactive compounds with diverse uses in agriculture and environmental sustainability (*Singh et al., 2011*). However, microorganisms are effective only when they are provided with suitable and optimum conditions for metabolism including the available water, oxygen, pH and temperature of the ambient environment. Electrospun nanofibers may be suitable both for the encapsulation (*Damasceno et al., 2013*) and as a good substrate to immobilize PGPR (plant growth promoting rhizobacteria) (*De Gregorio et al., 2017*).

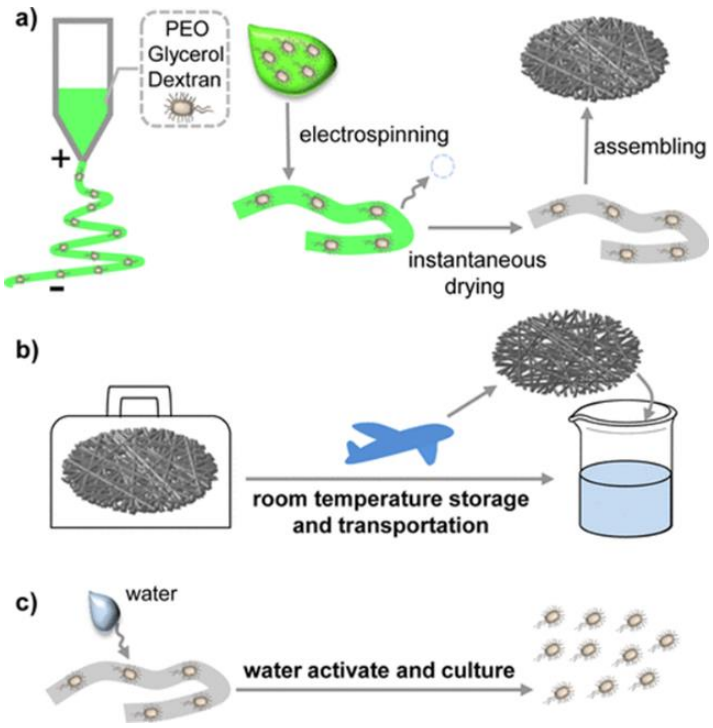

Figure 2.5. Schematic drawing of a microfiber-based strategy for room-temperature storage and transportation of microorganisms based on electrospinning technology; (a) fabrication of ES microfibers with encapsulated microorganisms through the instantaneous drying process; (b) microorganisms storage and transportation at room temperature; (c) activation of microorganisms by water adding (*Source Han et al., 2018*)

The polymer matrices were expected to protect the rhizobia from environmental stress such as temperature and dehydration (Figure

2.5). Indeed a comparison between the viability of rhizobia encapsulated in nanofiber and the negative control (unprotected rhizobia), reported a significant effectiveness of the role of the polymer. From recent literature, electrospinning has been confirmed to be also one of the best candidates among the various nanotechnologies for designing and developing smart and ultra-sensitive sensing systems, both for the uniqueness of the resulting nanostructures and for production rate and cost (*Macagnano et al, 2015*). Since the dimension of fibers is roughly comparable with that of interacting molecules, people may exploit the tiny size with some size effects, such as quantization, and the single molecule sensitivity. A powerful strategy to improve the sensing features of chemical (bio)sensors relies on increasing the specific surface area of the interacting material: the larger the surface area of a sensing material the higher its ability to interact with the medium, such as biological sensing structures do. The main advantages of electrospinning are the simplicity and low cost of the processing system, the short time required to prepare continuous 1D structures and its versatility, enabling the production of fibers and membranes with a wide range of morphologies and materials (Figures 2.2, 2.3 and 2.6). In addition, the versatility of the process provided by the polymer solutions, co-processing of polymer mixtures, chemical cross-linking of the formed nanofibers, can offer a variety of pathways for controlling the chemical composition of electrospun nanofibers with a wide range of final properties such as mechanical strength, density, elasticity, porosity, charged surface area, structure, etc. Finally, electrospinning can assemble inorganic, organic, and even biological components into 1D structures, which is an exciting direction for developing novel multifunctional nanomaterials for sensors. Therefore a series of ESNF high performing sensors have been employed for measuring ions in soil (nitrate, impedance sensors) (*Ali et al., 2017*) and gases from soil like H_2S, NH_3, NH_3,

NO_2, O_2, SO_2, NO_2, CO, C_6H_6 and C_2H_5OH (chemoresistor sensors based) (*Choi et al., 2012; Pang et al 2014; Khalil et al., 2016; Lee et al., 2015; Abideen et al., 2015*). Conductive polymer blends reported attracting sensing features and different affinity to several gases (NH_3, NO_2, NO), and arranged in a bioinspired configuration (electronic nose-like) (*Zampetti et al., 2011*). Similarly, when inorganic fibers (TiO_2) were joint to a conductive polymer, the resulting composite sensors were able to detect NO_2 up to 5 ppb of NO_2 in 90 s at room temperature (*Zampetti et al., 2013*). *Yoon et al.* (2007) by using polydiacetylene-encapsulated electrospun fiber mats developed a colorimetric sensor system for volatile organic compounds (VOCs), similarly *Schoolaert et al.* (2016) developed ES nanofibers for visual and continuous control of external stimuli by incorporating the halochromic dyes Methyl Red and Rose Bengal inside a chitosan/poly(ε-caprolactone) mat, proposing a biocompatible pH-sensor.

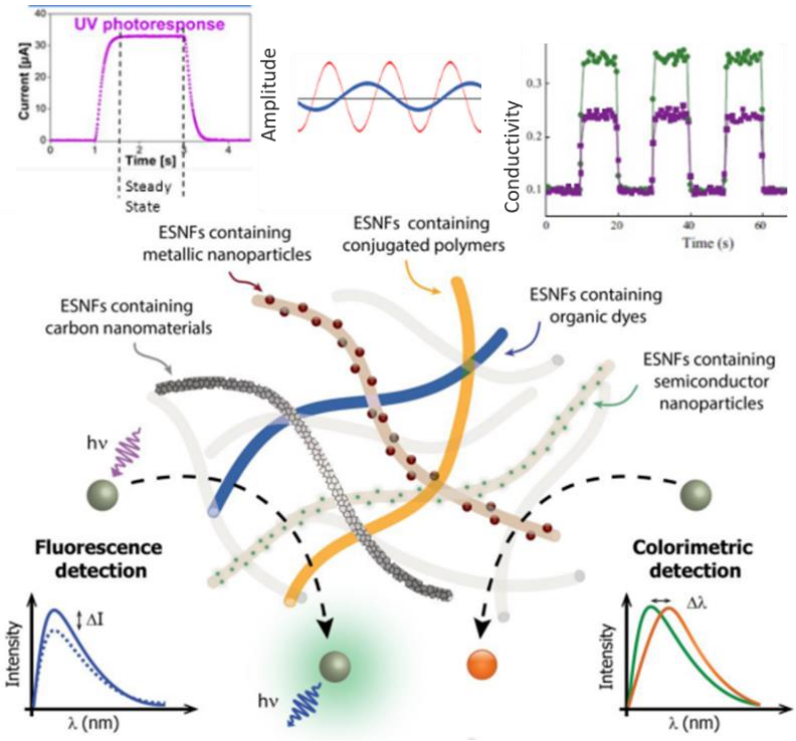

Figure 2.6. Drawing of ES nanofibers properly arranged to be used as sensing probes (Source: *Terra et al., 2017*)

CHAPTER 3 - Strategies for Eco-Friendly Iron Nutrition of Plants (APPROACH 1)

Iron is a microelement essential for plants to improve both crop productivity and produce quality, based on human requirements (*Briat et al., 2015*), because it is crucial in plant electron transport systems of mitochondria and chloroplasts, where Fe is also a pivotal component of the photosynthetic system (*Levi et al., 2009*). Iron is the most abundant metal on the Earth, but in diverse environments, it changes the state of oxidation so that both the various chemical species of iron and the relative amounts depend on the environmental conditions (*Darbani et al., 2013*). In oxic conditions (i.e. with oxygen), iron is mostly present in insoluble ferric hydroxide compounds especially at physiological pH (solubility $7.4 \cdot 10^{-18}$ M for ferric hydroxide). Hence, iron bioavailability is scarce, and the absorption of this essential element is consequently difficult for both plants and microorganisms living in aquatic environments and in soil so that plants often suffer for iron deficiency (*Prasad et al, 2016*), with a consequent decrease of food quality. Hence, iron is traditionally supplied to plants by farmers employing Fe fertilizers, where Fe is present in chelates (Fe-EDTA), which are applied mostly in foliar spraying but also in solutions to soil. The use of such formulations with Fe-chelates, however, is expensive and these compounds, as mentioned before, can be easily washed away from leaves by rainfalls, if not promptly absorbed by plants, and leached out from soils because of their high water solubility and mobility, thus causing groundwater and surface water pollution. Therefore, there is a current demand in agriculture for more efficient and effective formulations but also cheaper and more environmentally friendly products than the present fertilizers. To achieve these targets, natural strategies (as bioactive agents) and eco-friendly materials (as carriers) are alternative solutions in controlling plant nutrient deficiencies and diseases.

In natural ecosystems, both microorganisms and plants have evolved various strategies and mechanisms to get Fe from the surrounding environments to match their nutrient demand and prevent its deficiency. One of these strategies is based on the release of iron chelating organic compounds. A wide variety of molecules from diverse chemical classes has been employed or created on purpose by different organisms and even by a single organism, aimed at mining Fe^{3+} from insoluble sources. In the so called Strategy I (nongraminaceous) plants, additional to the acidification of the surrounding environment, the species also uses several classes of compounds, from organic acids (OAs) to phenolic compounds (PCs), that are released as part of exudates from roots outwards to chelate iron with different capacities (*Canarini et al., 2019*). Differently, in Strategy II (graminaceous) plants, highly efficient organic compounds called phytosiderophores (PSs) (siderophores, in the case of microbes (MSs)) are extruded from roots to act as scavengers for Fe^{3+} (*Hider et al., 2010*). Therefore, the employment of bioactive and biological agents capable of chelating iron could be useful in creating a novel type of iron-supplying products for plants to be applied in agriculture, plant nurseries, and gardening, aimed at being more efficient, effective, and environmentally friendly. Efficiency in such products can be linked to both the chemical features of the molecules employed and in the capacity of carriers possibly utilized to slowly release bioactive agents in the external medium to enable rapid absorption by the roots, thus preventing possible losses due to reduced bioavailability by adsorption, run-off, and leaching. Some slow/controlled release products based on chemical fertilizers are already commercially available, but they are expensive and often employ plastic coating materials that further contribute to ecosystem pollution (*Timilsena et al., 2015*). However, a similar strategy cannot be used to provide Fe directly to plants, because the released iron would easily precipitate at typical pH values of

both soil and water ecosystems. Moreover, the binding or loading of iron nanoparticles (NPs) to (nano)materials and their following release outwards has not yet been clearly demonstrated to provide Fe directly to plants (*Li et al., 2016*). It is worth noting that metal NPs are abundant in soils, hence the further addition of NPs might cause toxic effects (*Antisari et al., 2015*). Finally, the use of Fe-NPs would further increase the exploitation of natural resources to extract iron. Hence, more efficient and eco-friendly materials as carriers for the delivery of Fe-supplying bioactive agents, such as those afore mentioned, could be created by employing biodegradable nanomaterials. Electrospinning has been used to create bioactive nanostructured materials capable of supplying Fe to plants in different contexts through the slow release of Fe-chelating biological agents like those aforementioned. The use of biodegradable organic polymers could further offer the possibility to generate nanofibrous structures with low environmental impact. Polycaprolactone (PCL) is a biodegradable aliphatic polyester that has been employed, based on its hydrophobic properties, for several medical applications (*Mondal et al., 2016*), and it has also been used to encapsulate compounds in electrospun fibers for drug delivery (*Tampau et al., 2018*). Unfortunately, the low melting point value (≈60 °C) makes it useless when employed in some environmental applications. Polyhydroxybutyrate (PHB) belongs to polyhydroxyalkanoates, i.e., a class of polyesters produced by several bacteria species mostly as an intracellular storage source of carbon and energy to survive when nutrients become limiting. PHB is a material of interest to create biodegradable, bioderived, biobased, and non-toxic plastics for medicine and other types of applications. Differently from other similar bio-plastics that are water-soluble and sensitive to water, PHB is insoluble in water and shows some resistance to hydrolytic degradation (*Bugnicourt et al., 2014*). Unfortunately, the high crystallinity of PHB makes it rigid and stiff. The use of polymer blends instead of pure polymers is a

usual alternative to overcome the weakness of the single polymers and enhance their strengths. PCL exhibits good miscibility with PHB, is ductile, and has a significantly lower melting point than PHB. Thus, nanofibrous fabrics composed of a blend of PCL/PHB can be expected to be soft and mechanically resistant, able to sink, and be poorly affected by sudden changes in temperature, possibly occurring in nutrient treatments to plants, especially in field conditions.

3.1. A Polyhydroxibutyrate-Mugineic Acid nanofibrous system to supply insoluble Fe to plant roots (RESEARCH - 1)

A PHB membrane was loaded with mugineic acid (MA), a phytosiderophore extracted from root exudates of selected cultures of graminaceous plants (barley). The polymer, as mentioned before, was selected since non-toxic and water-insoluble, compostable and biodegradable and sinking in water. Mugineic acid (*Hider et al., 2015; Canarini et al., 2019*), an amino acid excreted from the roots by some graminaceous (grassy) plants (barley, oats, and wheat) under conditions of iron deficiency to solubilize Fe from the surrounding soil for uptake by the plant, was simply mixed to the polymer solution prior to the deposition. A set of tomato plants (*Solanum lycopersicum* L. "Marmande") was mounted on grounded collector and the roots of each plant were coated with loaded or unloaded fibers forming a sort of cocoon. In fact, the electrospinning technology allows the straight treatment of biological surfaces without any kind of damage (here except for the stress to the plants for staying out the hydroponic culture for a while).

3.1.1. Materials and Methods

Nanofibrous Membranes

EXPERIMENT-1

To obtain non-woven functional electrospun nanofibrous PHB membranes (NMs) to test in their capacity of supplying Fe to plants, 10 mL PHB solution in trifluoroethanol (THF) (5% w:w) was prepared at 65°C under stirring for 72 h, at least. Aqueous suspensions of mugineic acid collected from barley root exudates (provided by Prof. Astolfi, Dept. AFNE, University of Tuscia, Viterbo) at various concentration (0.037 mM, 0.075 mM and 0.112 mM) were mixed to the polymer solution (to obtain 1%, 2% and 3% v:v MA:PHB electrospinning solution, respectively) and vortexed for a few seconds just before the electrospun deposition. The distinct samples were sonicated in an ultrasonic water bath (Branson 1800) for 5 min to obtain homogeneous mixtures. Control electrospinning solutions without MA were prepared as before but replacing the MA solutions with the same ultrapure water volume to the PHB polymer solution. Nanofibers were then generated using a home-made electrospinning machine (CNR-IIA, Italy) composed of a high power AC-DC (alternative current-direct current) converter, a high voltage oscillator (100 V) to stabilize the electric field (ranging from 1 to 50 kV) and a syringe pump (Model KDS 200, KD Scientific). A single-needle electrospinning procedure was used to generate the PHB nanofibrous membranes in a single step. The electrospinning machine was placed in a homemade clean-box housing temperature and humidity sensors. The electrospinning procedure was set up as follows: the single-needle syringe holding the various polymer solutions was incorporated in the syringe pump working at 600-800 µL h^{-1} in feed rate (for 150 min at about 21°C, %RH:30%). A 6-8 kV electrostatic DC voltage was applied between the syringe stainless steel needle tip and the grounded collector. Since the different NMs loading various MA concentrations (MA-NMs) did not show any substantial morphological difference by SEM observations, only 3% MA-NMs were used for the following experiments with tomato plants, with the aim to supply as much phytosiderophore as possible to the

plants and obtain the greatest effects. In the first operative experiment, electrospun nanofibers were deposited directly on the root system of tomato plants previously fixed on a rotating aluminum collector placed at a distance of 15 cm from the syringe tip. Tomato plants were flipped after 70 min deposition to permit the entire coating of the root system. After the completed deposition of the electrospun NMs, plants were quickly placed in culture pots for hydroponic cultivation to test the functional effectiveness of the nanofabrics (MA-NMs) (Figure 3.1.1).

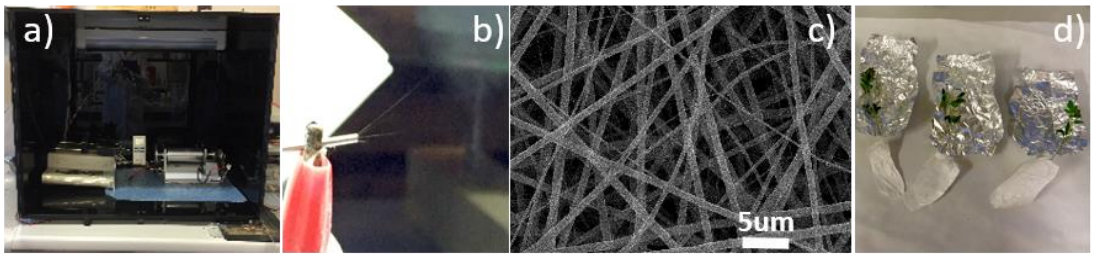

Figure 3.1.1. Experiment 1: Sequential steps of nanofibers fabrication for root coverage: **a)** electrospinning equipment, **b)** charged jet from droplet, **c)** polymer nanofibers (SEM), **d)** treated plants (roots coated with ES cocoons).

EXPERIMENT-2

In this experiment, non-woven functional electrospun nanofibrous MA-loading PHB membranes (MA-NMs) supplying Fe to plants were fabricated with the shape of discs with various diameters but loading the same amount of MA. In detail, 5 cm and 10 cm diameter nanofibrous PHB discs loading 3% MA were obtained upon deposition on paper discs firmly attached to aluminum foil coated round plates. The nanofibrous PHB discs were generated using the instrumentation and the procedure described in Experiment-1. The disc-shaped PHB NMs were collected on 5 cm and 10 cm diameters discs of filter papers soaked with a conductive polymer in water solution. Paper was used to facilitate the peeling of the deposited NMs and the conductive polymer was employed to make the paper more conductive and then more

suitable to collect fibers. The conductive polymer-soaked paper discs, attached onto the grounded rotating aluminum plate facing the needle tip at a distance of 5 cm, successfully collected the ejected fibers within the deposition cone. After deposition, PHB NMs with or without MA were peeled off the conductive paper discs used to collect them and placed in plastic pots containing tomato plants that were then incubated following the same experimental plan described in Experiment-1 (Figure 3.1.2).

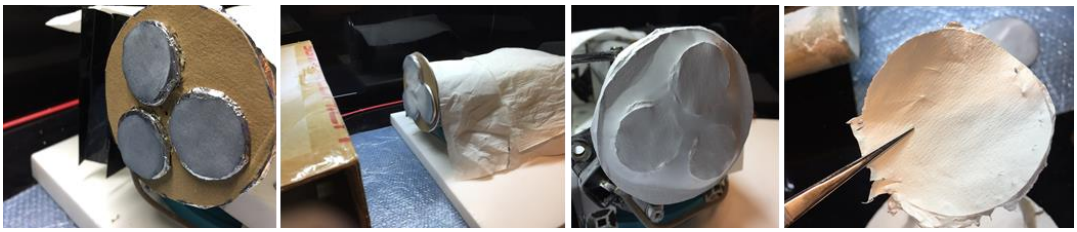

Figure 3.1.2. Experiment 2: Sequential steps of nanofibrous disks fabrication for dipping in hydroponics

Plant Materials

EXPERIMENT-1 and EXPERIMENT-2

Tomato plants (*Solanum lycopersicum* L. "Marmande") were provided by Prof. Astolfi (DAFNE, University of Tuscia, Viterbo). Seedlings were grown hydroponically for 14 *d* in plastic pots (six seedlings per pot) containing 2.2 L of nutrient solution (pH 6.2) of the following composition (mM): K_2SO_4 0.7; $MgSO_4$ 0.5; $Ca(NO_3)_2$ 2.0; KCl 0.1; KH_2PO_4 0.1; H_3BO_3 $1x10^{-3}$; $MnSO_4$ $1x10^{-3}$; $CuSO_4$ $2.5x10^{-4}$; $(NH_4)_6Mo_{27}O_{24}$ $1x10^{-5}$; $ZnSO_4$ $1x10^{-3}$; and further exposed to the following pre-treatments: 40 µM Fe^{III}(EDTA) (Control); 4.4 µM Fe^{III}(EDTA) for 1 week (-Fe-Step1), then 0 µM Fe^{III}(EDTA) for 1 week (-Fe-Step2). Afterwards, the plants were treated as reported in the next paragraph. The various nutrient solutions were continuously aerated and renewed every 2 *d*. Plants were grown in a growth chamber under 200 µmol photons $m^{-2}s^{-1}$ photosynthetic photon flux and a 14-h/10-*h* day/night regime

(27°C/20°C day/night temperature cycling and 80% relative humidity).

Experimental Design

EXPERIMENT-1 and EXPERIMENT-2

To assess the effectiveness of MA-NMs both deposited directly on the root systems (Experiment-1) and supplied as discs with various diameters (Experiment-2), after the completed deposition of the electrospun NMs, tomato plants were quickly transferred in new culture pots filled with the nutrient solution previously used and treated as follows: i) totally soluble Fe (40 μM Fe^{III}(EDTA)) (Cont, i.e. control), insoluble Fe (Fe_{ins}) ($FeCl_3$, 40 μM) and without iron (-Fe) (0 μM Fe^{III}(EDTA)). The global resulting treatments of tomato plants with or without MA-NMs were then the followings: a) totally soluble Fe, in both pre-treatment and treatment (Control, i.e. no MA-NMs); b) MA-NMs deposited directly on the root systems (MA-NMs) (Experiment-1) or as discs added in the incubation solution (large disc-MA-NML and small disc-MA-NMS, respectively) (Experiment-2) to plants pre-treated in Fe deficiency (-Fe) and then cultivated with Fe_{ins} (MA-NMs); c) NMs (i.e. without MA) applied to the root system or in discs to plants pre-treated and treated as in b) (NMs); d) plants grown in Fe deficiency pre-treatment and total Fe deprivation treatment and without any application of NMs (-Fe). Plants were then cultivated in hydroponic conditions in growth chamber as previously described (Figure 3.1.4). Plants were then harvested 17 d (Experiment-1) or 20 d (Experiment-2) after sowing. Chlorophyll content was monitored by a SPAD-502Plus meter (400-500 nm and 600-700 nm) to test the physiological status of tomato plants and then the effects of the various treatments.

Imaging

Samples for SEM analysis were pre-fixed in a solution of glutaraldehyde (2.5% v/v), ruthenium red (0.075% w/v) and

lysine acetate (0.075 M) dissolved in 0.1 M cacodylate buffer (pH 7.2), before SEM analyses. Fixation in glutaraldehyde (2.5% v/v) dissolved in 0.1 M cacodylate buffer (pH 7.2) was then performed for 2 *h* at 4 °C, after cold washings in the same buffer. Post-fixation in osmium tetroxide (2% *v/v*) in cacodylate buffer for 2 *h* at 4°C was then performed after washings. Then, a cold rinsing was applied to the processed specimens before dehydration in a graded ethanol series following the critical point method with CO_2 in a Balzers Union CPD 020. Samples were finally sputter-coated with gold in a Balzers MED 010 unit before observations using a JEOL JSM 6010LA electron microscope.

Imaging from a digital microscope integrated with a HD camera was also used for measuring the water contact angle (WCA) of the NMs from water drops (8 µl) deposited on the electrospun NMs with or without phytosiderophore molecules. The WCA of the thin membranes was quantified after 5 *s* from water dripping by using DropSnake© (LBADSA method), a plugin implemented for ImageJ software (open source image processing program).

The AFM (atomic force microscopy, Nanosurf AG, FlexAFM)) micrographs were taken in tapping mode using a 190Al-G tip, 190 kHz, and 48 N m^{-1} on the electrospun NMs. The roughness of the fibrous layers after AFM scanning was measured using SPIP 6.7.6 software (Image Metrology, Denmark) over image areas of 900 μm^2 (30x30 µm).

3.1.2 Results and Discussion

Experiment-1

The NMs wrapping plant roots within white and soft gaze-like cocoon showed the presence of smooth fibers with size ranging between 90±30 nm (Figure 3.1.3.c). The WCA of the overall nanoframework changed by 117°±2°a 79°±3° when PHB nanofibers were added with mugineic acid (Figure 3.1.3a).

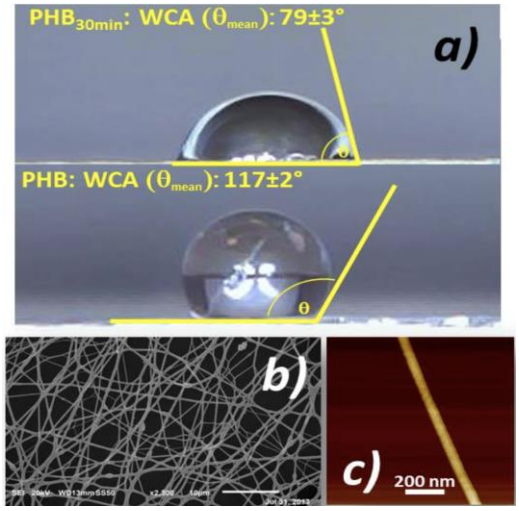

Figure 3.1.3. Physical parameters of the PHB NMs utilized to delivery mugineic acid to tomato plants; a) WCA pictures of MA-NMs (top) and NMs (down); b) SEM micrograph of a nanofibrous fabric of PHB deposited onto silica wafer; c) AFM micrograph of a single PHB nanofiber.

Plants after NM deposition directly on the root system showed some stress symptoms (wilting) due to the absence of aqueous supply during the deposition itself, but they recovered their turgor after a few hours regardless of the specific treatment (Figure 3.1.4). After the incubation, tomato plants treated with NMs showed very different physiological (photosynthetic) conditions when supplied with or without MA (NMs vs MA-NMs). Relative to T_0 (Figure 3.1.4.A,B), plants were visibly grown also when in deficiency of Fe (Fe_{ins}) and without phytosiderophore addition (NMs), but the plants supplied with MA resulted higher and greener than NMs, which showed chlorosis symptoms in the leaves (Figure 3.1.4.C). These results were confirmed by the chlorophyll content measurement (Figure 3.1.4.D). It is worth noting that NMs plants showed lower content of chlorophyll even relative to -Fe plants maybe because of the stress undergone during the NM deposition, as visible from the lower content at T_0, although a slight recover was observed during the incubation until reaching similar values. Plants coated with MA-NMs (PHB-NMs loaded with the phytosiderophores) after fourteen days of Fe-limitation showed a recovery in the photosynthetic activity consequent to higher

chlorophyll content (+21%) than NMs, thus supporting the greener color of the leaves (Figure 3.1.4.B,C). However, in spite of the higher photosynthetic activity of plants due to the presence of phytosyderophore in the incubation medium of MA-NMs relative to both the conditions of total deprivation of iron (-Fe) (+15%) and Fe-deficiency, when only NMs without MA and Fe_{ins} were applied, and despite the amazing recovery relative to T_0 (+60%), tomato plants treated with MA-NMs and Fe_{ins} still showed a lower chlorophyll content (-14%) relative to control plants at the end of incubation (Figure 3.1.4.D). The lower performance than expected was probably due to the evident physical and chemical degradation of the nanofibrous membranes observed at the end of the incubation (data not shown). This result was consequent to the continuous air bubbling of hydroponic conditions and the non-sterile conditions adopted in the experiment, so that the organic materials of the NMs tended to degrade and break away from the roots because they were rapidly used as substrates by microorganisms present in the incubation medium and also the phytosiderophore molecules were broken down (data not shown).

Experiment-2

Plants after the incubation with or without the various disc-shaped NMs and phytosiderophores showed different responses when investigated in their growth, chlorosis symptoms and chlorophyll content (Figure 3.1.5). In detail, tomato plants undergoing Fe deprivation were remarkably affected in all the parameters, showing strong decrease in the growth and evident chlorosis symptoms due to substantial chlorophyll decrease (Figure 3.1.5.Bb,Bc,Bd). Plants treated with disc-shaped MA-NMs showed differences in the photosynthetic response when phytosiderophores were supplied with thin and large (Figure 3.1.5.Ab) or thick and small (Figure 3.1.5.Aa) disc-shaped membranes (MA-NML vs MA-NMS).

MA-NMS plants showed slightly smaller growth than MA-NML plants and more evident chlorosis symptoms in the leaves (Figure 3.1.5.B-cd). Such results were also confirmed by the lower recovery in the chlorophyll content of MA-NMS plants relative to MA-NML ones (Figure 3.1.5.Cab). Interestingly, when compared to the T_0 values, plants in Fe-deficiency but treated with MA-NMs, irrespective of their size, showed higher recovery of the chlorophyll content even relative to the increase of full-Fe supplied control at the end of incubation (+40% vs +30%) (Figure 3.1.5.Ca). Additionally, when compared to the values of -Fe plants, MA-NMs plants displayed increased chlorophyll content until +30%, although it was constantly smaller (17%) than that of Cont (+47%) (Figure 3.1.5.Cb). It is worth noting that the mentioned effects seemed to be dependent on the different mode of supply of phytosiderophores to tomato plants (MA-NML vs MA-NMS). The MA-NML discs displayed a more rapid effect on the chlorophyll content of plants than the MA-NMS until +32% after 1 d incubation that instead decreased in the following days until +10% (percent relative to T_0) or no difference (percent relative to -Fe treated plants) (Figure 3.1.5.C).

Furthermore, such a prompt increase in the effect induced by MA-NML, however, did not further improved during the following incubation, while MA-NMS, despite the lower initial effect, improved during the incubation, irrespective of the specific percent evaluation reckoned (Figure 3.1.5.C).

These differences were probably due to the diverse flow rate crossing the NMs. In the case of MA-NML, in fact, the thinner and larger configuration of the MA-NML discs provided a higher flow rate in and out the MA-NML consequent to a reduced resistance of the fabrics along the perpendicular direction to the flat surface of the MA-NML discs and then a faster release of MA molecules.

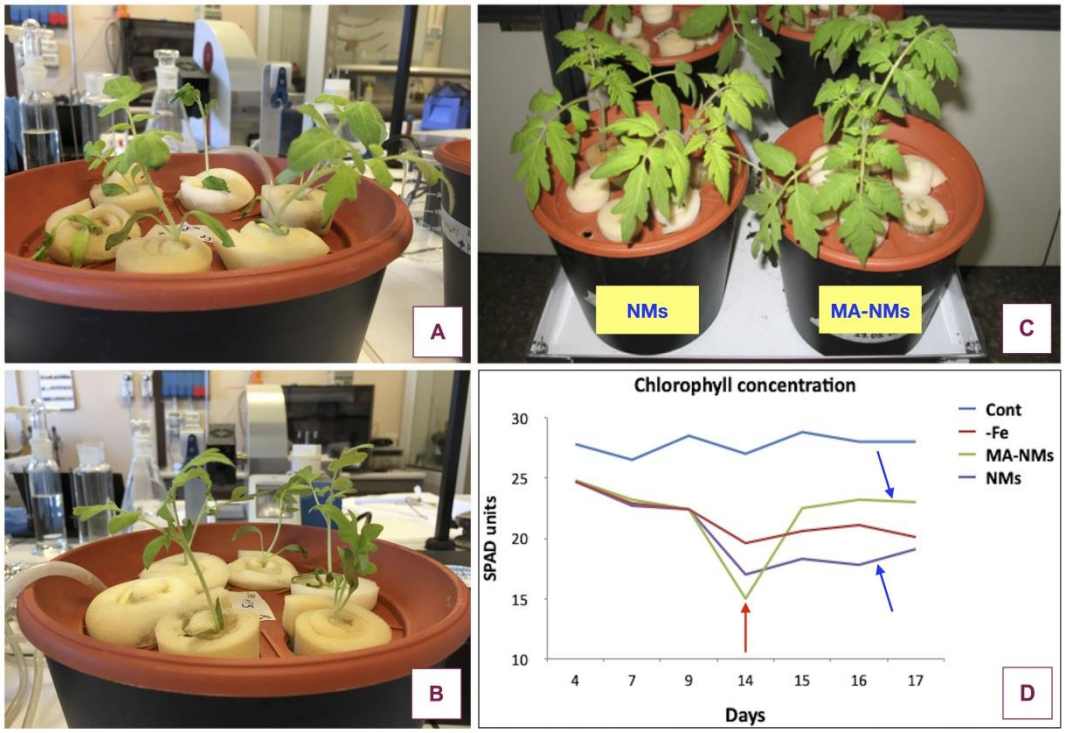

Figure 3.1.4. Tomato plants after pre-treatment, root system wrapping upon NM deposition (T_0) and the various treatments. A) Plants at T0 pre-treated in Fe deficiency and then treated with NMs + Feins (NMs). B) Plants as in A) but added with MA-NMs + Feins (MA-NMs). C) Tomato plants soon after treatments: NMs (left), MA-NMs (right). D) Chlorophyll content of tomato plants measured by a SPAD meter during the pre-treatments and treatments as follows: Cont, -Fe, MA-NMs, and NMs. The red arrow indicates the beginning of treatments (T0). Blue arrows highlight the treatments with NMs in the presence or absence of MA, as in the legend.

On the contrary, the thicker discs of MA-NMS, but with the same mass than MA-NML ones, offered a greater resistance to the solution flow crossing the fabrics and then reduced the release rate of MA molecules. Hence, in the case of MA-NML, the phytosiderophores molecules were quickly almost totally released within 1 d (Figure 3.1.5.Ca,b), while in the case of MA-NMS, MA molecules were released more gradually.

Therefore, for agricultural applications of possible products composed of nanofibrous membranes similar to those here proposed, the use of thicker fabrics is more promising. Finally, at the very end of the incubation, the MA-NMs, regardless of the size, displayed a decrease in the performance in terms of chlorophyll content relative to -Fe plants.

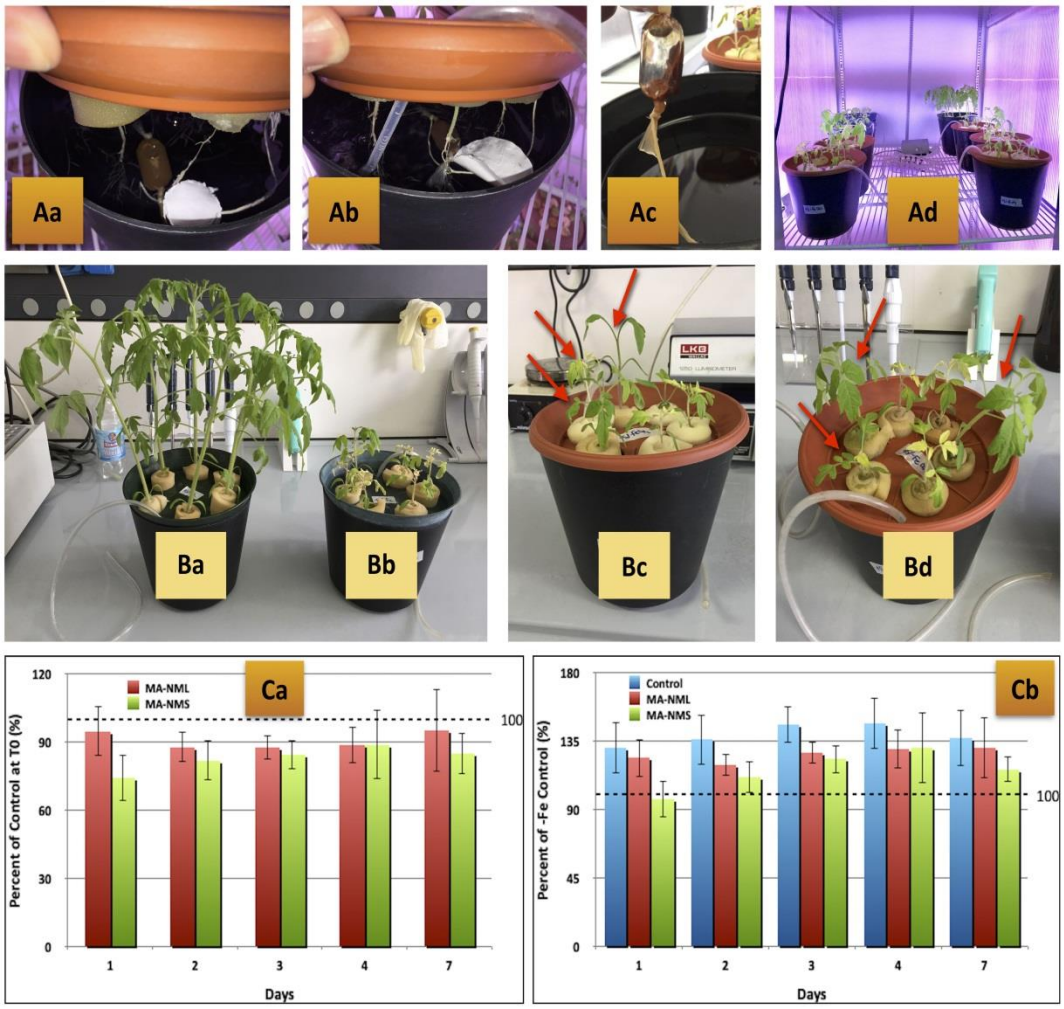

Figure 3.1.5. A) Tomato plants at T_0, i.e. after pre-treatment and before the treatments: (Aa and Ab) plants added with 5 cm and 10 cm diameter disc-shaped NMs, respectively (here regardless of the presence of MA); (Ac) dialysis membrane sack containing the Fe_{ins} ($FeCl_3$) solution; (Ad) tomato plants incubated in a growth chamber. B) Tomato plants after the incubation with various treatments: (Ba) totally soluble Fe (Control); (Bb) -Fe; Bc) MA-NMS; Bd) MA-NML. Red arrows indicate the plants of interest (the others were mutant plants belonging to another experiment not included in the PhD thesis). C) Percent of variation in the chlorophyll content of tomato plants undergoing the indicated treatments: Control, MA-NML;, and MA-NMS; Ca) Percent relative to Control at T_0; Cb) Percent relative to -Fe samples at the same date. Error bars depict the uncertainty in the measurements (error propagation).

This result was due probably to the non-sterile conditions of the experiment and then from the microbial degradation of the NMs that reduced the global amount of both the fabrics releasing MA

and the phytosiderophore molecules themselves, which were used as C substrates by microbes. Such explanation was confirmed by SEM micrographs of the disc-shaped MA-NMs captured at the end of the experiment (Figure 3.1.6).

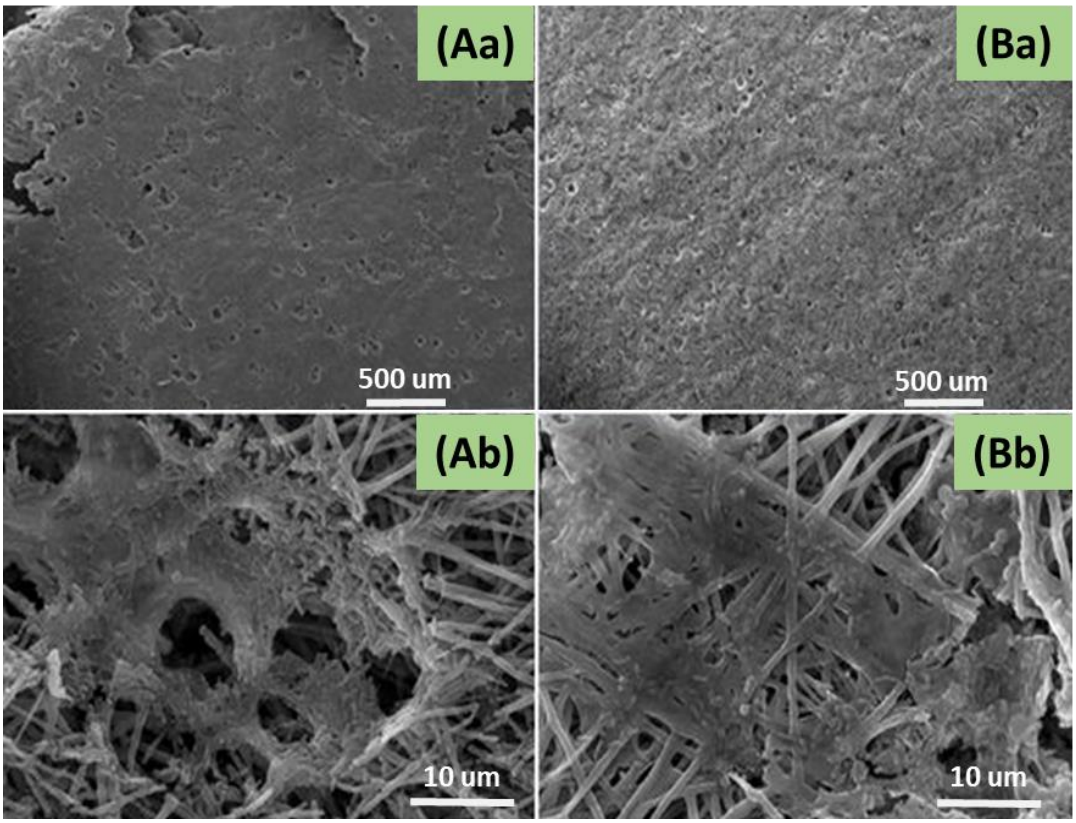

Figure 3.1.6. SEM micrographs of the disc-shaped MA-NMs at the end of incubation with tomato plants: **A)** MA-NML discs at different magnification (37x) (a) (2500x) (b); **B)** MA-NMS discs at different magnification (37x) (a) (2500x) (b).

The wider degradation was observed in MA-NML, where areas with the destroyed nanoframework appeared more frequent and proper holes could be identified (Figure 3.1.6.Aa). At higher magnification, the broad presence of bacteria attached onto the nanofibers and in biofilms was observed and the nanofibres appeared broken and heavily degraded (Figure 3.1.6.Ba).

In MA-NMS, although more frequent degraded areas were observed, they appeared less deeply destroyed than in MA-NML

(Figure 3.1.6.Ab). At higher magnification, in fact, the less degradation of the nanofibres was confirmed (Figure 3.1.6.Bb).

3.1.3 Preliminary Conclusions

In conclusion, the disc-shaped NMs loading MA seemed to be more promising than MA-NMs deposited directly on the root systems of tomato plants, because the plants undergoing direct deposition were stressed during this process. Furthermore, the effects due to NMs lasted for longer time (5 d *vs* 3 d), when provided in separate discs since they appeared to be more resistant to physical and microbial degradation and they released phytosiderophore molecules more gradually than those of NMs attached to roots. Additionally, the effects on the photosynthetic activity were more evident (+30% *vs.* +15%) relative to -Fe.

3.2 A Polyhydroxibutyrate-polycaprolactone nanofibrous system loaded with catechol as a model to provide insoluble Fe to non-graminaceous plants (RESEARCH-2)

In another set of experiments, PHB composing the functional membranes aimed at supplying iron to plants utilized in Research-1 was replaced by a blend of PHB and PCL (polycaprolactone) because of some mechanical fragility of the electrospun nanofibrous PHB membranes tested in the previous research. MA was also replaced by catechol as an iron-chelating agent to improve the global amount of the bioactive agent loaded in the nanofibrous fabrics and remove the time wasted for the collection of MA from the barley root exudates, since catechol is a substance that is also commercially available. Indeed, among the various natural substances capable of chelating iron and utilized by organisms to collect this element from external environments and

fulfill their demand for this micronutrient, catechols are a group of aromatic compounds containing a 1,2-benzenediol moiety that provides them with the capacity of forming stable complexes with a number of di- and trivalent metal ions (*Schweigert et al., 2001; Dalla Torre et al., 2018ù; Schmid et al., 2014*). The hydroxyl groups of the catechol ring can strongly coordinate ferric ions because the oxygens in the molecule behave like Lewis bases and hard donor atoms and Fe acts like a hard Lewis acid, thus determining the affinity with iron. Catechol, in fact, is part of the phenolic compounds that are the major components of root exudates released in response to iron (Fe) deficiency in Strategy I plants, and the catechol motif is present in several other soluble phenolic compounds of root exudates, such as coumarins (esculetin, fraxetin, and sideretin) and flavonoids (quercetin, catechin) (*Clemens et al., 2016; Kasprzak et al., 2015*), where this structural moiety is specifically devoted to iron binding.

Hence, the aim of this study was to create freestanding thin membranes made of electrospun biodegradable PCL/PHB nanofibrous fabrics and loading catechol molecules (namely, catechol-loading nanofibrous membranes—CL-NMs) to provide Fe to plants, thus mimicking Strategy I principles. Catechol was preferred as a model and simple iron chelator to phyto- and microbial siderophores because the plant species that was intended to be used, i.e. duckweed (*Lemna minor* L.), is a nongraminaceous plant and then it is not expected to have the proper transporters for (phyto)siderophores. Catechol also has high solubility in water, making it suitable for both hydroponic growth and dissolution in biphasic mixtures of hydrophilic and hydrophobic solvents used to prepare the polymer blend solutions for the fabrication of the bioactive thin membranes by electrospinning. The nanofibrous framework of the scaffold was also preferred to mimic both structurally and functionally the release process of Fe chelators

(catechol molecules, in this case) by plant roots. Then, CL-NMs were tested for their effectiveness in providing iron to duckweed plants from insoluble sources ($FeCl_3$). *L. minor* is the smallest representative of vascular plants, and it is also a model plant frequently used in studies on plant physiology, biochemistry, and ecotoxicology. It is also considered to be, in fact, a biological indicator of chemical contamination in aquatic environments, because of its sensitivity to pollutants and other toxic substances (*Mikandawire et al., 2014*). Due to their remarkable ability to absorb and accumulate macro- and micro-nutrients, duckweeds play a crucial ecological role in cycling nutrients in water environments and in reclaiming wastewater.

To test such a capacity of CL-NMs, two catechol concentrations (dose-dependence effect) and distinct iron treatments (from starvation to optimal concentration) were fixed in hydroponic culturing conditions. Hydroponic conditions were preferred in this preliminary study to reduce the numerous variables present in tests with real soils. Photosynthetic and biometric parameters were measured in *L. minor* plants undergoing the various treatments. SEM and TEM imaging and analyses were also carried out to investigate the nanostructured materials and the possible effects of the various treatments on plant photosynthetic ultrastructures. The possible successfulness of CL-NMs in supplying Fe to duckweeds would point out the capacity of these plant species of absorbing iron from Fe–catechol complexes, although such findings has never been reported to date in these plants to the best of our knowledge, and would classify the CL-NMs here created as nanostructured biostimulants or nanobiostimulants (NBs) (*Du Jarden et al., 2015*).

3.2.1 Materials and Methods

Nanofibrous Membranes

The polymer mixture composed of a blend of PCL and PHB (1:0.26, *w*/*w*) was added with catechol, as a model iron-chelator

(CL-NMs) dissolved at two concentrations (C_1 = 5 mM and C_2 = 100 mM). Control NMs were created deprived of catechol (CNMs). To create non-woven electrospun nanofibrous thin membranes, 10 mL PHB solution in TFE/$CHCl_3$ (trifluoroethanol/chloroform, 9.9:0.1, v:v) was prepared by solving 0.515 g of powder at 65°C under stirring for 72 *h*, at least. Similarly, 1.22 g PCL was dissolved in 10 mL TFE/$CHCl_3$ (2:8, *v:v*) at 60°C for 24 *h*. Finally, the PHB and PCL solutions were mixed in order to obtain a polymer blend with a mass ratio of 1:0.26 (*w:w*), respectively. Two catechol solutions were prepared separately by dissolving catechol in ultrapure water at two concentrations (5 mM and 100 mM). Electrospinning solutions containing catechol at the two concentrations and the PCL/PHB polymer blend were prepared by incorporating 0.10 mL catechol solutions (5 mM or 100 mM) in 5 mL PCL/PHB polymer solution (2% *v/v*). The distinct samples were then sonicated in an ultrasonic water bath (Branson 1800) for 5 min to obtain homogeneous mixtures. Control electrospinning solutions without catechol were prepared as in the previous treatments but mixing the same ultrapure water volume to the PCL/PHB polymer solution. Nanofibers were then generated using the instrumentation described in Research-1. The electrospinning procedure was set up as follows: the single-needle syringe holding the polymer solution was incorporated in the syringe pump working at 1000 µL h^{-1} in feed rate (for 3 *h* at about 28°C and 30% RH) to generate PCL/PHB nanofibrous membranes in a single step. The operating electrostatic DC voltage between the syringe stainless steel needle tip and the grounded collector was set up at 4.0-4.5 kV. The PHB/PCL nanofibers were collected on an aluminum disc placed on a rotating collector fixed at a distance of 5 cm. The disc diameter was suitable to provide enough 1 x 1 cm squared membranes for all the duckweed samples treated with CL-NMs at the relative catechol concentrations.

After deposition, PHB/PCL nanofibrous membranes were removed from the conductive paper discs used to collect them and then cut into 1 × 1 cm (1 cm^2) pieces. Each squared fragment of the CL-NMs contained approximately 0.50 μmol (C_1L-NM samples) and 10 μmol (C_2L-NM samples) catechol. The 1 cm^2 pieces, irrespective of their catechol content, were then placed on the bottom of the wells of 24-well plates for further incubation with duckweed plants. Some physical properties of both the NMs, such as the hydrophobicity (contact angle) and morphology (by AFM and SEM imaging analyses), were investigated. More specifically, the contact angle of the NMs was measured from water drops (8 μl) deposited on the electrospun nanofibrous PCL/PHB fabrics with or without catechol molecules. The water contact angle was quantified in the thin membranes after 5 *s* of water drip by using DropSnake© (LBADSA method), a plugin implemented for ImageJ software (open source image processing program).

The AFM (atomic force microscopy, Nanosurf AG, FlexAFM)) micrographs were taken in tapping mode using a 190Al-G tip, 190 kHz, and 48 N m^{-1} on the nanofibrous layers. The roughness of the fibrous layers after AFM scanning was measured using SPIP 6.7.6 software (Image Metrology, Denmark) over image areas of 900 μm^2 (30x30 μm). A plane correction process was performed on all of the AFM topographical images. The roughness parameters here analyzed within the defined area were the roughness average (i.e. the difference in the height of each point compared to the arithmetical mean of the surface) (Sa), the root mean square value of ordinate values (Sq), the sum of the largest peak height value and the largest pit depth value (Sz), the absolute value of the height of the largest pit (Sv) and the height of the highest peak (Sp). NMs were properly treated and sputter-coated with gold in a Balzers MED 010 unit before observations by electron microscope (JEOL JSM 6010LA).

Plant Materials

Duckweed (*Lemna minor* L.) plants (*provided by CNR-IRET, Dr. Pietrini*) were purchased from a specialized company (Anubias, Villanova (BO), Italy) and sterilized. Stock cultures were maintained for one month in a modified Hoagland's nutrient solution (Pietrini et al., 2015), adjusted to about pH 6, in a growth chamber at 25 ± 2 °C, photoperiod 16 h light/8 *h* dark, and an irradiance of 60 µmol m^{-2} s^{-1}, provided by cool white fluorescent lamps (T8 L 58 W/840; Osram AG, München, Germany). Plant cultures were grown under static conditions and sub-cultured weekly until the beginning of the experiment.

Some photosynthetic and biometric parameters were used to test the effectiveness of the CL-NMs created here in supplying iron to duckweed plants undergoing various Fe treatments. A non-invasive approach based on chlorophyll fluorescence imaging analysis was used to monitor the same samples over a period of time. Specifically, chlorophyll fluorescence parameters such as F_v/F_m (maximum quantum yield of PSII photochemistry), *ΦPSII* (quantum efficiency of PSII), *NPQ* (non-photochemical quenching), and *ETR* (electron transport rate) were measured using saturating light pulses to estimate photosynthetic activity under different environmental conditions, while total plant chlorophyll content (*Chl*) was monitored by measuring the absorptivity of the frond surface (*Abs*), and calculating *ΦPSII*, *ETR*, *NPQ*, and *Chl*. Chlorophyll fluorescence analysis has been used for many years as a rapid non-destructive tool to evaluate the state of the photosynthetic apparatus in many plant species. In the last years, with the introduction of imaging instrumentation that maps chlorophyll fluorescence parameters, it has been possible to identify spatial heterogeneity of leaf photosynthetic performance (*Baker et al., 2008; Pietrini et al., 2016*). Recently, the use of chlorophyll fluorescence imaging has been utilized to investigate the impact of iron deficiency and resupply on the photosynthetic performance of strawberry plants

(*Osorio et al., 2014*). The chlorophyll fluorescence imaging was then used to monitor the temporal changes in both the photosynthetic efficiency and the chlorophyll content during the overall 14 day-period of treatments of plants, i.e. the 10 day-pre-treatment and the following 4 day-treatments (i.e. at T_0 and after 24, 48, 72 and 96 *h* of 98 exposure), consequent to the various treatments of plants in the presence or absence of Fe. The Fv/Fm ratio is a parameter frequently used to detect disturbances in the photosynthetic system favored by several stress, because its decrease indicates a reduction in the photochemical efficiency of PSII and damages to the photosynthetic apparatus. ΦPSII is the most useful parameter to measure the efficiency of PSII photochemistry. It measures the proportion of the light absorbed by chlorophyll associated with PSII that is used in photochemistry and, under laboratory conditions, there is a strong linear relationship between this parameter and the efficiency of carbon fixation. Moreover, ΦPSII can be used to calculate linear 105 electron transport rate (ETR) contributing to represent the plant photosynthetic capacity in vivo. Differently, NPQ is often used as an indicator of the excess-radiant energy dissipation to heat in the PSII 107 antenna complexes. This photoprotective process removes excess excitation energy within 108 chlorophyll-containing complexes and prevents the likelihood of formation of damaging free radicals. As concerns the biometric parameters, image analysis was applied to measure the frond number (*FN*), the doubling time (T_d), and the average specific growth rate ($\mu_{t(0-4)}$) with the aim of testing the effects on *L. minor* plants induced by iron deprivation and its resupply with or without CL-NMs. The biometric parameters were measured at T_0 and after 24, 48, 72 and 96 *h* of treatment exposure using imaging analysis software (ImageJ, IJ 1.46r, http://imagej.nih.gov/ij/). Specifically, Td and (μt(0–4)) were calculated based on the total frond number. The latter was determined in duckweed plants present in each replicate of the

various treatments in the presence or absence of Fe. The fronds in each plate well were counted, and their area was recorded preventing possible overlapping. The average specific growth rate ($\mu t_{(0-4)}$, expressed in day^{-1}, based on the total FN) was calculated over the 4 d-period (96 *h*) of treatment ($\mu t_{(0-4)}$) from the following equation (1):

$$\mu_{t_{(0-4)}} = \left({(ln(FN_{t4})) - ln(FN_{t0}))} \Big/ {(t4 - t0)} \right) \quad (1)$$

while the doubling time (Td), expressed in days, of the FN was determined according to the Test No. 221 of the 152 *OECD Guidelines* for the Testing of Chemicals, Section 2 from the following equation (2):

$$T_d = {ln2} \Big/ {\mu_{(0-4)}} \quad (2)$$

Finally, the effects of the various Fe nutritional treatments on duckweeds were also evaluated by optical and electronic microscopy (TEM) observations of the treated plants. Investigations were focused mostly on the structures and ultrastructures of the plant organelles involved in the photosynthetic process, i.e., the chloroplasts, in both the leaves and roots, where the presence of chloroplasts has also been confirmed by the literature (*Leng, 1999*).

Experimental Design

To assess the capacity of CL-NMs in supplying Fe to duckweeds, plants were pre-treated under Fe-starving conditions and then added with CL-NMs in the presence of insoluble Fe sources. Fully Fe-supplied plants were also tested as controls. To also investigate the singular and combined effects of the various Fe sources and NMs, additional control treatments were also analyzed. Duckweeds undergoing the various Fe treatments were incubated for 4 days and samplings were carried out periodically, i.e., at

T_0 and after 24, 48, 72, and 96 *h*. Each treatment was carried out in six replicates (Figure 3.2.1).

More in detail: two stocks of duckweed cultures were then prepared, after another sterilisation step, by cultivating fronds of L. minor L. in plastic vessels for 10 *d* in 1/10 strength Hoagland's nutrient solution in the presence (Fe supplied, Stock1) or absence (Fe-deprived, Stock2) of 6 µM Fe(EDTA) (soluble chelated-Fe). After this period (T_0), duckweed colonies from Fe-supplied and Fe-deprived cultures were transferred into 24-well plates (well volume: 2.8 mL, well surface area: 2 cm^2; BD, USA), and each well was filled with 2.5 mL Hoagland's nutrient solution at pH 5.8 ± 0.1, regardless of the specific iron treatment, and 1-2 colonies (1-2 visible fronds each) of L. minor were placed therein. In order to investigate the recovery from Fe deficiency, distinct experimental treatments were planned for specific purposes as follows: i) C^+ = duckweeds from Stock1 grown in optimal Fe supply, i.e. where iron was supplied as 6 µM Fe(EDTA) during the entire experiment; this treatment represented the reference control for duckweeds growing in optimal conditions for all of the nutrients throughout the experiment, i.e. without any limitation for iron. ii) C^- = Fe-starved duckweeds from Stock2 further grown in Fe deprivation; this treatment corresponded to the reference control of duckweeds grown in the total absence of Fe throughout the experiment. iii) C_0 = plants from Stock2 then resupplied with 6 µM $FeCl_3$ (insoluble-Fe), that means they were grown under Fe limitation since only very few ions were present in the soluble form because of the very low solubility of Fe^{3+} at pH 5.8; this treatment was the primary reference control for duckweeds added with the CL-NMs; iv) R = Fe-starved duckweeds from Stock2 resupplied with 6 µM Fe(EDTA) (soluble-Fe); this treatment was another reference control for duckweeds added with CL-NMs, because it aimed at discriminating the effectiveness of CL-NMs in resupplying Fe to plants (mediated bioavailability), as compared with more direct iron resupply

composed of soluble Fe (promptly bioavailable). v) T = Fe-starved duckweed plants from Stock2 further grown in Fe deprivation, like C^-, and added with catechol-free (control) electrospun NMs (CNMs); this treatment was aimed at testing the possible toxicity induced in L. minor plants by CNMs and also represented another reference control for duckweeds added with CL-NMs. vi) A = full Fe-supplied duckweeds from Stock1 then grown in optimal Fe supply, like C^+, and further added with CNMs; this treatment was focused at testing possible Fe adsorption caused by CNMs. Such event, in fact, might induce inhibition in the plants caused by the reduction in the amount of soluble-Fe. vii) C_1L-NMs = Fe-starved duckweed plants from Stock2 then grown under Fe limitation since resupplied with insoluble $FeCl_3$, like C_0, and further added with C_1L-NMs (C_1 = 5 mM catechol concentration). This treatment was aimed at testing the capacity of C_1L-NMs to provide duckweeds with Fe(III) that could only be made bioavailable upon the release of chelating agents, the Fe(III)-chelation from insoluble sources (FeCl3) and the Fe-chelate absorption by plants). viii) C_2L-NMs = duckweeds grown and treated as in C_1L-NMs but using C_2L-NMs (C_2 = 100 mM catechol concentration) instead of C_1L-NMs. The scope of this treatment was the same as in C_1L-NMs, but employing NMs with a higher content of catechol to test possible dose effects. A diagram of the various treatments of duckweeds included in the experimental plan is reported in Figure 3.2.1. Plates with duckweed cultures trialing various treatments were then covered with transparent lids, to minimize evaporation and accidental contamination, and further incubated under the same photoperiod and temperature used for the preparation of stock cultures, and without renewal (static) of the test solutions. The cultures of duckweed plants were incubated until 96 *h* and analyses were carried out periodically, i.e. at T_0 and after 24, 48, 72 and 96 *h*.

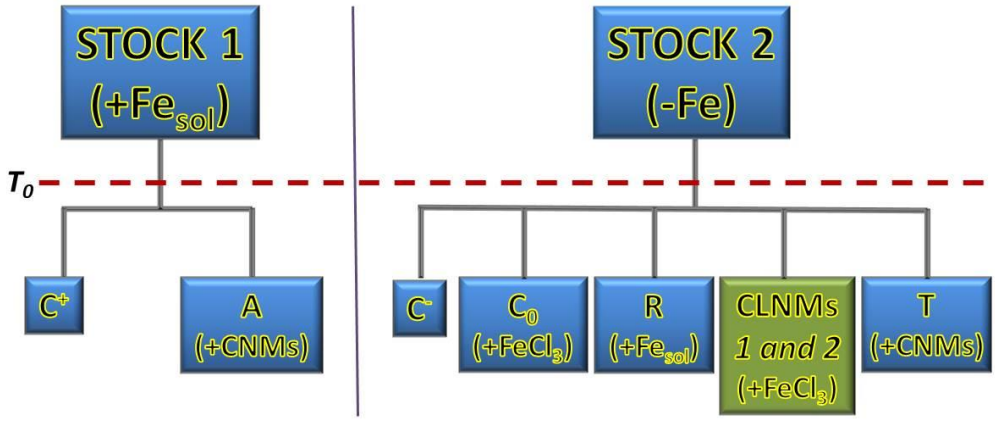

Figure 4.1. Sketch of the experimental plan in *Lemna* describing the various Fe-treatments of duckweed plants to test the performances of the distinct catechol-loaded nanomembranes (CL-NMs)

Statistics

Normally distributed data were processed by one-way ANOVA, when applicable, using the SPSS 16.0 (Chicago, IL, USA) software tool and a suitable number of replicates per treatment (as indicated in the figures and tables). The statistical significance of the mean data was assessed by the Fisher's Least Significant Difference (LSD) Test ($p \leq 0.05$). The Normal probability distribution (Gaussian curve) of the fiber diameters was obtained from the SEM images of the fibers analyzed by Gwyddion© 2.3 software (GNU General Public License) to calculate the fiber size that were then processed by Microsoft Excel© 2011. The distribution analysis of the nanofiber diameters was performed on 150 nanofibers (n = 150).

3.2.2 Results and Discussion

Because of the problems of scarce effectiveness and efficiency of the PHB nanomembranes utilized in the previous research due to the continuous air bubbling and microbial degradation, we searched for an alternative strategy so that both the polymer scaffold and the plant species and the hydroponic growth conditions were modified. Similarly, the release rate was tentative

delayed and slowed to prevent the loss of the bioactive molecules previously observed.

In detail, PCL/PBH depositions were carried out onto filter papers soaked with a conductive polymer dissolved in water solution. Paper was used to facilitate the peeling of the deposited NMs and conductive polymer was employed to make the paper more conductive and then more suitable to collect fibers. The conductive polymer-soaked paper discs, attached onto the grounded rotating aluminum plate facing the needle tip, successfully collected the ejected fibers within the deposition cone. Despite the presence of a little water fraction (2% *v*/*v*) in the electrospinning PCL/PHB polymer mixture due to the incorporation of the aqueous solution containing catechol molecules, the electrospun liquid jet streams were formed without discontinuity, micro-drops, or nozzle blocks so that fibers could be collected for some hours without interruptions. The various electrospun PCL/PHB NMs, regardless of the catechol loading, were peeled off and analyzed in the morphological and physical features as follows. The distribution of fibers in the thin membranes observed by SEM differed in CNMs, C_1L-NMs, and C_2L-NMs nanofabrics. For example, CNMs showed an overall smooth surface at low magnification (×65) (Figure 3.2.2, inset), despite a sort of bundle arrangement of fibers present at the surface and visible at higher magnification only ×185) (Figure 3.2.2.A). The nanofibrous structure appeared as intricate but quite porous (Figure 3.2.2,A). Differently, the global aspect of C_1L-NMs (C_1 = 5 mM catechol initial concentration) at low magnification (×65) looked from the top view like a desert surface with sand ripples shaped by the wind (Figure 3.2.2.B, inset). At higher magnification (×185), this motif appeared to be derived from a configuration similar to that of CNMs but with larger groups of nanofibers arranged in bundles and generating higher ridges and alternated with wider valleys.

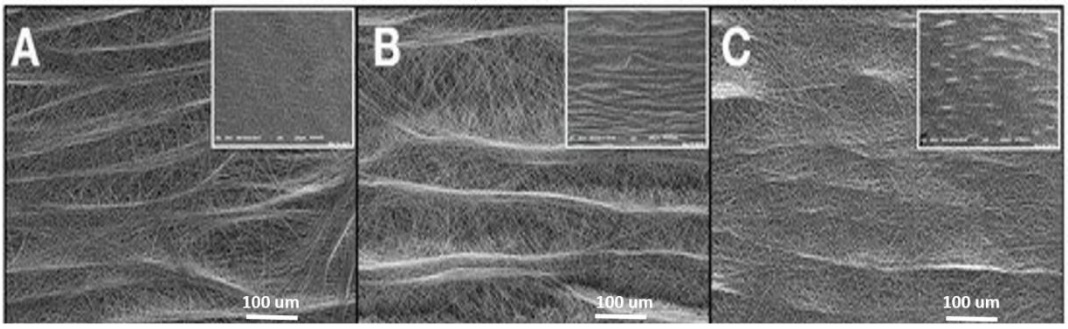

Figure 3.2.2. SEM micrographs of the polycaprolactone/polyhydroxybutyrate (PCL/PHB) thin nanomembranes (NMs) after electrospinning deposition and before the incubation with duckweed plants: (**A**) control PCL/PHB nanofibrous scaffolds (CNMs); (**B**) electrospun PCL/PHB NMs loading lower (C_1) and (**C**) higher (C_2) catechol concentrations (C_1L-NMs and C_2L-NMs, respectively) (magnification ×185); insets = top views of the same nanostructures (magnification ×65). Scale bars in the micrographs correspond to 100 μm and to 200 μm (relative insets).

In any case, the C_1L-NMs framework apparently seemed more porous than that of CNMs (Figure 3.2.2 A,B). In C_2L-NMs (C_2 = 100 mM catechol initial concentration), the whole aspect of the scaffold appeared quite different from the previous ones whatever the magnification used (Figure 3.2.2.C). The ridges appeared as replaced by isolated crests resulting from fiber coalescence more than from proper bundle aggregation. The resulting nanofibrous membrane looked much denser and more compact than in the other samples and with visible smaller pores (Figure 3.2.2.C). The various NMs were further analyzed at higher magnification by both AFM and SEM. The micrographs obtained by AFM from the scanning in the air of 900 μm^2 NM areas (30 μm × 30 μm) showed no clear difference in the nanofiber morphology of CNMs and C_2L-NMs samples. A smooth surface, in fact, characterized both the nanofiber types, which appeared deprived of pores notwithstanding the presence of 2% (*v*/*v*) water fraction in the electrospinning polymer mixture (Figure 3.2.3 A,B). A similar smooth aspect of the nanofiber surfaces was also confirmed in SEM micrographs of the two frameworks. AFM images were also used to measure the roughness of the overall nanofabrics. Figure 3.2.3 C,D reports 3D-AFM images of both the CNMs and C_2L-NMs samples, respectively,

and the relative topography profile. The selected colors, changing from orange to yellow and to blue, represented the nanofibrous membranes from top to bottom, and highlighted the roughness of the ridges, the entangled structure of the nanofibers, and the void volumes (pores) of the frameworks, respectively. The CNMs sample appeared slightly rougher than the C_2L-NMs, when measured as *Sa* and *Sq*, since these parameters showed 3% to 5% decrease in C_2L-NMs (Table 1). Interestingly, the void volume ($Void_{vol}$) of C_2L-NMs showed a substantial decrease relative to CNMs (−16%), thus suggesting that a more compact and less porous fabric resulted from the addition of the high catechol concentration to the polymer blend.

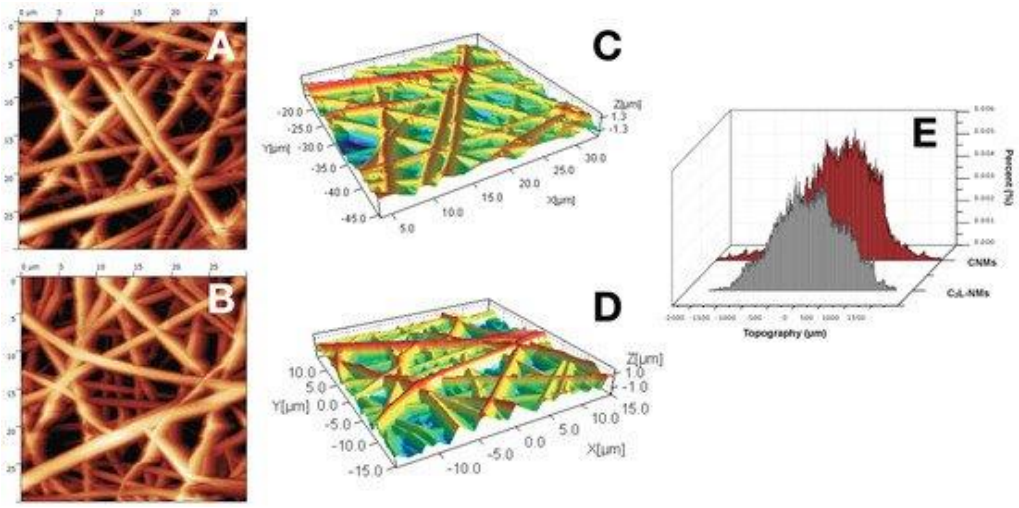

Figure 3.2.3. AFM micrographs of 30 × 30 µm scanned areas of PCL/PHB NMs before the incubation with duckweed plants: (**A**) control NMs (CNMs); (**B**) NMs loading higher C_2 catechol concentration (C_2L-NMs); (**C**,**D**) 3D-plot of images of (**A**,**B**); (**E**) roughness analysis reporting the percent distribution of peaks and depths in the topography (µm) of the scanned areas of the NMs shown in (**C**,**D**) (positive and negative values of the distribution, respectively

However, since the whole material volume (Mat_{vol}) was also substantially reduced (−18%), the global volume of C_2L-NMs was shrunk. This effect was confirmed by the decrease in *Sz* (the sum of the largest peak height value and the largest pit depth value), *Sv* (the maximum pit height—depth), and *Sp* (the highest

peak height) (17%, 18%, and 16% decrease, respectively). However, since the whole material volume (Mat_{vol}) was also substantially reduced (−18%), the global volume of C_2L-NMs was shrunk. This effect was confirmed by the decrease in *Sz* (the sum of the largest peak height value and the largest pit depth value), *Sv* (the maximum pit height—depth), and *Sp* (the highest peak height) (17%, 18%, and 16% decrease, respectively).

The bi-plot, reported in Figure 3.2.3 E, confirms the changes of the fabric topography due to the addition of catechol, with a decrease in both the peak and depth distribution in C_2L-NMs. In addition, the thickness of the electrospun nanofibrous membranes appeared reduced from about 60 μm in CNMs to about 40 μm in C_2L-NMs (Figure 3.2.4 A,B insets). Hence, the void ratio ($e = V_{v/vs}$, in this case: $Void_{vol}$ to Mat_{vol} ratio) of the nanoscaffolds with or without catechol was mostly unchanged in C_2L-NMs when compared with CNMs material (0.86 *vs*. 0.84, respectively) so that the calculated porosity ($P = e/(1 + e)$) was as large as 46% *vs*. 45%, respectively. These results thus confirmed the observations of C_2L-NMs s in favor of a more compact overall structure (Figure 3.2.2) but without a substantial decrease in the apparent global porosity. The analysis of the nanofiber distribution based on SEM micrographs of the nanoframeworks showed that both types of the CL-NMs displayed a smaller diameter than the CNMs samples (Figure 3.2.4 C). Moreover, a dose dependence in the fiber morphology was observed, with the diameter of the fibers decreasing when the catechol concentration loaded increased so that C_2L-NMs < C_1L-NMs < CNMs.

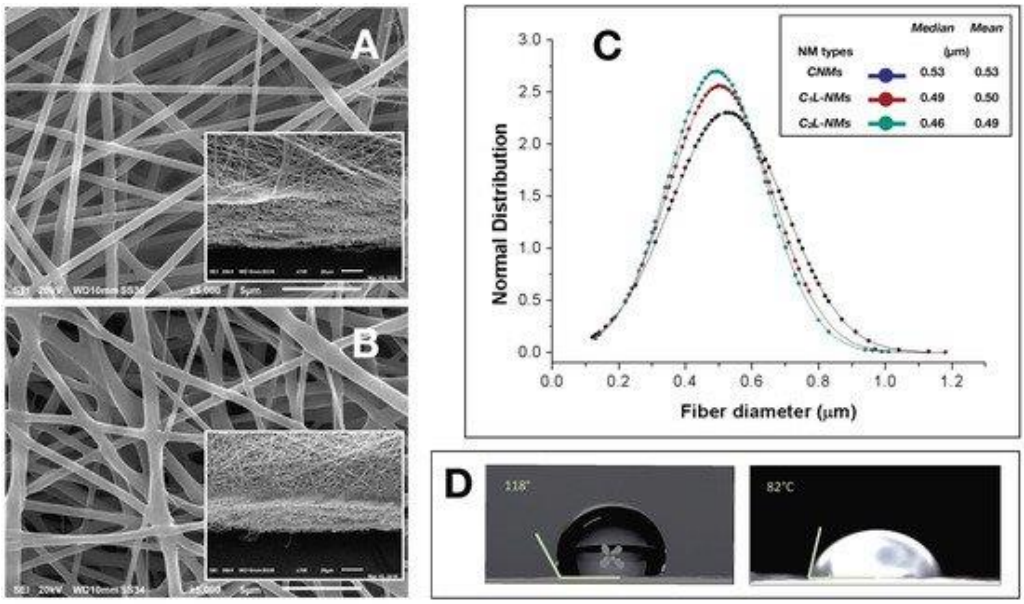

Figure 3.2.4. SEM micrographs of CNMs (control) (**A**) and C_2L-NMs (high concentration catechol loading NMs) (**B**) before the incubation with duckweed plants (magnification ×5000)—insets: tilted cross sections of the same NMs (magnification ×700); (**C**) distribution analysis of the nanofiber diameters present in CNMs, C_1L-NMs, and C_2L-NMs (n = 150); (**D**) Contact angles of CNMs (left) and C_2L-NMs (right). Scale bars in the micrographs correspond to 5 μm (**A**,**B**) and 20 μm (relative insets).

In detail, the distribution of the C_2L-NMs nanofibers ranged from 0.130 to 1.010 μm, with a mean diameter of 0.493 ± 0.148 μm; while the C_2L-NMs nanofibers ranged from 0.140 to 1.180 μm, with a mean diameter of 0.502 ± 0.156 μm; and the CNM nanofibers ranged from 0.120 to 1.130 μm, with a mean diameter of 0.526 ± 0.173 μm. Therefore, since the global amount of the material deposited was the same in both CNMs and C_2L-NMs, the reduced dimensions of the nanofiber diameters in C_2L-NMs caused an increase in the specific surface area that could favor the diffusion of catechol molecules in the external medium. Since the aqueous volumes added to the three polymer solutions were the same, it seemed that the effects on the morphological features of the electrospun nanofibers were independent of the water added but depended on the concentration of catechol in the polymer blend, thus suggesting that catechol induced a rearrangement of the polymer fibers.

Table 1. Roughness parameters of the electrospun nanofabrics CNMs and C_2L-NMs. Area = area scanned by AFM; Mat_{vol} = volume of the material; $Void_{vol}$ = volume of the voids within the scanned area; S_a = roughness average (i.e., the difference in height of each point compared to the arithmetical mean of the surface), S_q = the root mean square value of ordinate values, S_z = the sum of the largest peak height value and the largest pit depth value, S_v = the absolute value of the height of the largest pit, and S_p = the height of the highest peak.

Parameters	CNMs	C_2L-NMs	Variation
Area (µm²)	900	900	—
Mat_{Vol} (µm³)	2160.7	1776.1	−18%
$Void_{Vol}$ (µm³)	1819.2	1533	−16%
S_a (µm)	0.542	0.525	−3%
S_q (µm)	0.678	0.642	−5%
S_z (µm)	4.388	3.648	−17%
S_v (µm)	2.378	1.958	−18%
S_p (µm)	2.011	1.690	−16%

In any case, the presence of the catechol-containing aqueous solution in the PCL/PHB polymer blend seemed to profoundly affect the physical properties of the resulting nanofibrous membranes that changed from hydrophobic to hydrophilic (Figure 3.2.4 D). Such a deep modification might be related to changes in the morphology of both the single fibers, which appeared smaller in diameter, and the overall surface of the nanostructured fabrics, which became smoother than the control. In addition, modifications of the surface chemical properties of nanofibers cannot be excluded. The wettability of the fibers did not display, in this case, a clear linear dependence on the quantity of the catechol molecules in the polymer blends, as it was observed instead in the nanofiber size aforementioned, because the contact angle of the C_1L-NMs could not be measured for the inhomogeneity of the sample. The nanofiber arrangement in bundles at the fabric surface of C_1L-NMs forming high ridges alternating with large valleys was maybe the cause that inhibited the possibility of having a mat surface regular enough to measure the contact angle.

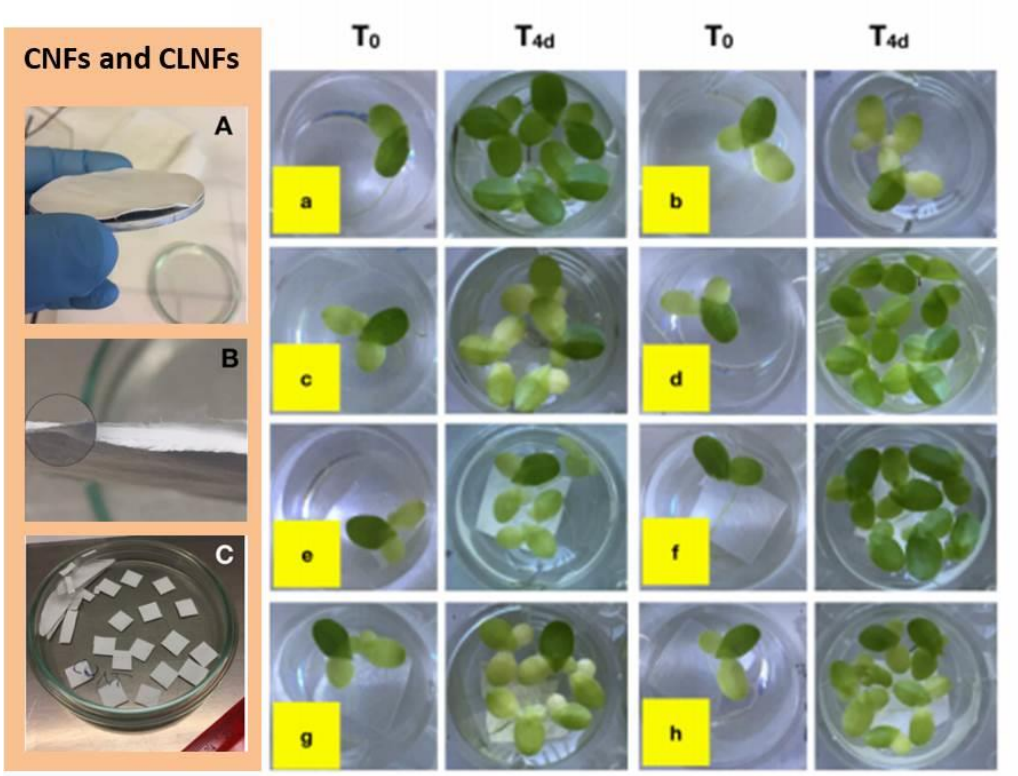

Figure 3.2.5. Electrospun nanomembranes (NMs) (irrespective of the catechol loading) after deposition onto the PEDOT-soaked paper attached to an aluminum disk (**A**); (**B**) NMs pealed off the mentioned supports; (**C**) NMs after cutting into 1 cm^2 pieces; Pictures of duckweeds fronds captured before (T_0) and after (T_{4d}) various treatments: **a**) C^+ = 6 μM Fe(EDTA) for both pre-treatment and treatment; **b**) C^- = no Fe for both pre-treatment and treatment; **c**) C_0 = no Fe (pre-treatment) + 6 μM $FeCl_3$; **d**) R = no Fe (pre-treatment) + 6 μM Fe(EDTA); **e**) T = no Fe for both pre-treatment and treatment + catechol-free nanomembranes (CNMs); **f**) A = 6 μM Fe(EDTA) for both pre-treatment and treatment + CNMs; **g**) C_1L-MNs = no Fe (pre-treatment) + 6 μM $FeCl_3$ + C1L-MNs (C_1 = 5 mM catechol); **h**) C_2L-MNs = no Fe (pre-treatment) 6 μM $FeCl_3$ + C_2L-MNs (C_2 = 100 mM catechol).

The various electrospun NMs, regardless of the catechol loading, were used for duckweed incubations after peeling off from the conductive paper and cutting into 1 × 1 cm pieces (Figure 3.2.5 C). Regarding the physiological and biometric parameters of the treated plants, it is worth noting, as a general result, that in almost all experimental treatments, F_v/F_m values were mostly within the 0.75–0.85 range, which indicated non-stressed conditions in the plants under study (*Bolhar-Nordenkampf et al., 1989*). It is noticeable that plants used in this experiment did not show irreversible symptoms of Fe deficiency at the photosynthetic

level due to the Fe-free pre-treatment and that our results were in agreement with data from the literature. It has been shown, in fact, that Fe deficiency leads to decreases in light-harvesting pigments, mainly chlorophylls (*Morales et al., 2000*), while several reports suggested that a reduction in the F_v/F_m (value <0.75) occurred only with severe Fe deficiency. In the present study, even when the F_v/F_m values were <0.75, no decrease in the chlorophyll content was observed, suggesting that the effect of Fe deficiency was not dramatic.

About PHB/PCL nanofibers tools, possible drawbacks, such as iron adsorption and toxicity on the *L. minor* plants were assessed in separate samples from the other treatments to distinguish the effects caused by the bioactive agents from those due to the carrier material utilized, which might combine in the resulting values. The possible capacity of NMs to adsorb soluble iron (Fe-EDTA) (A treatment) was assessed indirectly by evaluating possible Fe-deficiency effects on the physiological and biometric parameters induced by Fe binding on NMs from the growth solution during the incubation that might reduce the amount of Fe bioavailable for plant absorption. The duckweed plants treated with pieces of the pristine nanofibrous fabrics (i.e., without catechol) as large as those used for the other treatments did not show any apparent Fe deficiency induced by NMs. The biometric parameters of the A-treated samples were comparable with the control C^+ as concerns the frond number (FN) and even better than C^+ as concerns both T_d and $\mu_{t(0-4)}$. It is worth noting that T_d measures the time required for the frond number to double in value, and since the replication of cell structures and organs requires energy to be spent, only healthy plants can afford to double, thus indicating the degree of stress undergone by plants. As a result, the smaller the doubling time value, the faster the growth is and thus the plant is healthy (low stress). Hence, these results demonstrated that the growth of A-treated plants was even stimulated by the presence of

NMs (Table 2). The reasons for such stimulation are still unknown, but the possible concentration of some nutrients by NMs favoring plant nourishment could not be excluded. Besides, these findings were further confirmed by the analyses of possible chlorosis effects in L. minor plants and of the chlorophyll fluorescence imaging. At the end of the four-day incubation period, in fact, duckweeds did not show any chlorosis symptoms induced by the reduction of available Fe. As concerns the possible temporal changes of the photosynthetic parameters of duckweed plants measured by fluorescence imaging analyses, the only presence of NMs in the growth medium showed no apparent adverse effects on the photosynthetic activity (ΦPSII) and chlorophyll content (Chl) of L. minor plants with respect to the control (C^+), with no significant symptoms of nutrient deficiency, consequent to possible Fe adsorption. On the contrary, even an improvement (as hypothesized for the biometric parameters) as concerns NPQ values, which were lower than those of C^+ (−45%), was observed. Therefore, the apparent lack of any inhibition by NMs of both the biometric and photosynthetic parameters of duckweeds pointed out that the electrospun thin membranes did not induce iron limitation by removing Fe^{3+} ions from the nutrient solution by adsorption. The biometric parameters of the T-treated plants highlighted a recovery relative to the poorest conditions of C^- plants, as concerns FN, T_d, and $\mu_{t(0-4)}$ (Table 2), suggesting that some stimulating effect was carried out by the electrospun PCL/PHB NMs on the *L. minor* plants. Such "non-toxic" and even improving behavior of the electrospun NMs on duckweed plant growth, instead of the initially hypothesized inhibitory influence, seemed to confirm the nutrient concentration hypothesis suggested for the A treatment. These biometric results were confirmed by the observations of the visual aspect of duckweeds after 96 h of incubation, which showed reduced chlorosis symptoms in the plants, relative to C^-. Additionally, the analyses of the

photosynthetic activity and chlorophyll content of duckweed plants grown in the presence of NMs in the growth medium when iron was absent presented values significantly higher than those of C^- plants, thus reducing the Fe-deficiency symptoms and showing no toxic effects of NMs on the photosynthetic apparatus, i.e., additional to the absence of Fe as in C^-. For what concerning iron deficiency and starvation effects, duckweed plants undergoing iron starvation throughout the experiment (C^-), i.e., both before and after T_0, highlighted severe alterations showing the lowest values in all of the biometric parameters tested, especially relative to C^+: *FN* (−19%), $\mu_{t(0-4)}$ (−41%), and T_d (+26%, i.e., retardation of duplication) (Table 2). Iron deficiency in C^- also negatively affected the photosynthetic performances of *L. minor* plants relative to the C^+ control. The photosynthetic activity of *L. minor* plants was notably altered in all of the parameters tested (*ΦPSII*, *NPQ*, *ETR*, and *Chl* content), so that the values measured in total Fe deprivation (C^-) after the four-day incubation displayed the most significant difference from C^+ (−37%, +158%, −57%, and −76%, respectively) (Figure 3.2.6B–E). Furthermore, the decrease in the photosynthetic activity caused by the Fe deficiency was confirmed by the evident chlorosis symptoms in plants after the 96 *h* incubation period from T_0 although these dramatic conditions did not cause a reduction of the F_v/F_m values under 0.75.

The addition of iron in the insoluble form ($FeCl_3$) to duckweed plants previously starved for iron (Fe-free pre-treatment) *(C_0)* showed a slight attenuation of the negative effects on the growth of *L. minor* plants observed in C^--treated plants, with only a partial (not significant) recovery of the biometric parameters (Table 2). Such improvements indicated that *L. minor* plants after 10 days of Fe-free growth were still preserving their resilience because they were capable of recovering the main functions even when a minimal amount of Fe was available in the medium.

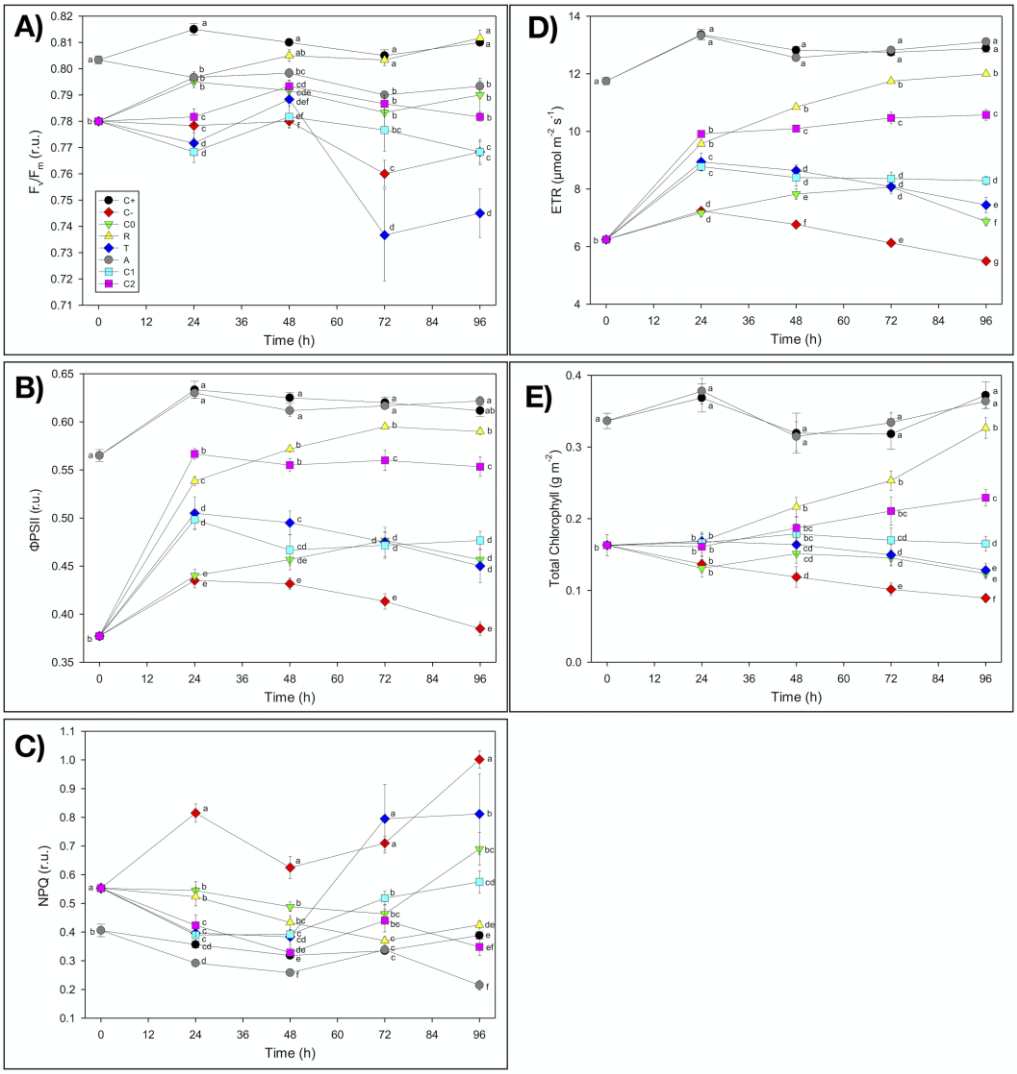

Figure 3.2.6. Quantitative analyses of the chlorophyll fluorescence parameters measured in *Lemna minor* fronds treated with different nutrient solutions and electrospun NMs over a 96 h incubation period: (**A**) F_v/F_m = maximum quantum yield of PSII photochemistry; (**B**) *ΦPSII* = quantum efficiency of PSII photochemistry; (**C**) *NPQ* = non-photochemical quenching; (**D**) electron transport rate (*ETR*); (**E**) total chlorophyll content. Black circle: C^+; Red diamond: C^-; Green triangle: C_0; Yellow triangle: R; Blue diamond: T; Grey circle: A; Cyan square: C_1L-NMs (C_1 = 5 mM catechol); Pink square: C_2L-NMs (C_2 = 100 mM catechol). Data points and vertical bars represent means (n = 6) ± S.E., respectively. One-way ANOVA was applied to each photosynthetic parameter; different letters indicate significant differences between treatments at each incubation period, according to the LSD test ($p \leq 0.05$).

Similarly, a slight recovery was also observed in the temporal values of the photosynthetic parameters of C_0 relative to C^-: *ΦPSII*, +19%; *NPQ*, −31%; *ETR*, +25%, and *Chl*, +38%.

Table 2. Growth parameters of *Lemna minor* L. measured after treatments for 96 h (4 days) with different nutrient solutions and nanofibrous products (NMs): *FN* = frond number; T_d = doubling time of the *FN*; $\mu_{t(0-4)}$ = average specific growth rate; C^+ = fully Fe-supplied duckweed plants; C^- = totally Fe-deprived duckweed plants; C_0 = duckweeds grown in Fe-limiting conditions; *R* = *L. minor* plants resupplied with soluble Fe after an Fe-free pre-treatment; T = plants grown as C^- and also incubated with NMs (catechol-free); A = duckweeds grown as C^+ and also incubated with NMs (catechol-free); C_1L-NMs = plants as in C_0 and also incubated with NMs loading catechol at a low concentration (C_1 = 5 mM catechol); C_2L-NMs = plants as in C_0 and also incubated with NMs loading catechol at a high concentration (C_2 = 100 mM catechol) (check the text for more details). Data are the mean values of six replicates ± standard error (SE). One-way ANOVA was applied, and data followed by different letters in the same row are significantly different (LSD test, $p < 0.05$).

Parameters	C^+	C^-	C_0	R	T	A	C_1L-NMs	C_2L-NMs
FN (n_{14})	6.8 ± 0.1 ^{ab}	5.5 ± 0.6 ^{b}	7.5 ± 1.0 ^{ab}	8.1 ± 0.9 ^{a}	6.5 ± 1.9 ^{ab}	7.3 ± 0.5 ^{ab}	6.5 ± 1.9 ^{ab}	7.3 ± 0.5 ^{ab}
T_d (days)	2.20 ± 0.04 ^{de}	2.78 ± 0.12 ^{a}	2.51 ± 0.07 ^{ab}	2.21 ± 0.07 ^{cde}	2.41 ± 0.03 ^{bcd}	2.01 ± 0.06 ^{e}	2.41 ± 0.03 ^{bcd}	2.01 ± 0.06 ^{e}
$\mu_{t(0-4)}$ (days^{-1})	0.22 ± 0.01 ^{b}	0.13 ± 0.02 ^{d}	0.16 ± 0.01 ^{cd}	0.22 ± 0.02^{b}	0.18 ± 0.01 ^{bc}	0.27 ± 0.02 ^{a}	0.18 ± 0.01 ^{bc}	0.27 ± 0.02 ^{a}

The resupply of iron in the soluble form (Fe(EDTA)) allowed duckweed plants previously grown in the absence of Fe (R treatment) to remarkably recover plant growth, relative to C^-. This treatment induced a strong significant ($p < 0.05$) improvement of all biometric parameters: *FN* (the highest values), $\mu_{t(0-4)}$, and T_d (Table 2). The *R* treatment promoted the almost complete recovery of the photosynthetic parameters in duckweed plants after 96 h of incubation, thus approaching C^+ values with no significant difference, in some cases. The results of the R treatment highlighted that duckweed plants were not altered at the physiological level by the 10 days of Fe-free pre-treatment since these characteristics were considerably recovered by the Fe(EDTA) addition to these plants.

Based on the aforementioned absence of any negative interference by NMs due to nutrient adsorption or toxicity on the physiology and growth of duckweed plants, the effects by CL-NMs on *L. minor* could be reasonably ascribed to the catechol molecules loaded in the nanofibrous fabrics.

The addition of catechol-loading nanofibrous PCL/PHB membranes (CL-NMs) containing catechol and $FeCl_3$ to previously Fe-starved duckweed plants showed different trends and results depending on the concentrations of the active compound in the nanofibers. These results indicated that, even at the lowest catechol concentration, the CL-NMs was effective, since these bioactive nanofibrous membranes succeeded in providing an adequate amount of iron to *L. minor* plants to support chlorophyll biosynthesis and consequently, the entire photosynthetic process, thus permitting duckweeds rapid recovery from Fe starvation until approaching the nutrient conditions typical of the fully Fe-supplied control.

The improvements observed in duckweeds following the application of CL-NMs and $FeCl_3$ to *L. minor* plants were confirmed by the modifications induced in the structures and ultrastructures of duckweeds grown in total Fe-deficient conditions (similar to those in C^-). Investigations by optical microscope and TEM of C_2L-NM-treated plant leaves and roots showed a chloroplast abundance and distribution similar to those of C^+-treated plants. TEM micrographs of the internal membrane organization of the chloroplasts of leaves from C_2L-NM-treated *L. minor* plants displayed the presence of a diffused membrane system in plant leaf chloroplasts from C_2L-NMs similar to that of the optimal Fe supply conditions (C^+) (≤21% of grana stacks and 20% of stromal lamellae relative to the total thylakoid membranes) (*Albertsson et al., 2004*) and different from that of Fe-starved plants (C^-), as reported in the literature (Figure 3.2.7A–C, red arrows) (*Varsano et al., 2003*). In C^--treated plants, in fact, a residual presence of immature grana composed of two to four thylakoids embedded in the stroma (Figure 3.2.7B, red arrows) was observed, further reduced to hardly visible faint lamellae immersed in the granular and electron-dense stroma. Other pieces of evidence on the ultrastructural effects induced by the addition of CL-NMs to Fe-

deficient (insoluble Fe) duckweeds were the presence, additional to starch granules, of some circular electron-dense structures visible by TEM in leaf chloroplasts and named plastoglobules (PGs) (Figure 3.2.7C). PGs are lipoprotein bodies also containing tocopherols (vitamin E) and other isoprenoid lipids and related metabolites that are localized in chloroplasts and other plastids and are related to lipid storage and metabolism and to various types of stress responses. Depending on the stressing cause, the presence and number of PGs vary, as well as their association with and connection to thylakoid membranes. PGs have been related to stresses, like high light, Fe-deficiency, salt concentration, and heavy metals *(Saito et al., 2014; Paramonova et al., 2004)*.

In the present study, PGs were present in both leaf and root cells of plants from all treatments and displayed different types of structures assorted distinctly between the treatments and might be related to diverse functions or degree of maturation (Figure 3.2.7A–C green arrows and yellow arrowheads) (*Lichtenthaler et al., 2013*). It is evident that the heavily stressing growth condition induced by Fe deprivation in C^- plants clearly affected the ultrastructural organization of the photosynthetic organelles, which were profoundly altered in the thylakoid membrane distribution and organization. It appears that the modifications (dismantling) in the membrane organization from C^+ to CL-NMs to C^- were closely related to the number (and maybe the function) of PGs in the chloroplasts. Such modifications might be related to the role of PGs in the reconstitution and repair of the thylakoid membranes upon stressing events. Regardless of the performances of the CL-NMs in supplying Fe to duckweeds, it is worthy to note that this study provided pieces of evidence, for the first time to our knowledge, that *L. minor* plants are capable of using catechol to absorb Fe for their nutrition and metabolic activities. Duckweeds are known generally to absorb iron from the outer environment by a constitutive system for transmembrane transfer of electrons (using

cytosolic NAD(P)H) aimed at reducing extracellular acceptors like Fe^{3+} (reduced to Fe^{2+}). However, this Fe-transport system is also able to get iron from Fe^{3+} chelates (Fe-EDTA) so that the chelate reduction rate in Fe deficiency is even higher than that of the free ions. Catechol is known to be used by nongraminaceous plants to chelate iron present in the external environment to facilitate its uptake by plants. However, duckweeds have not been reported to date to have the capacity to use this molecule with this aim.

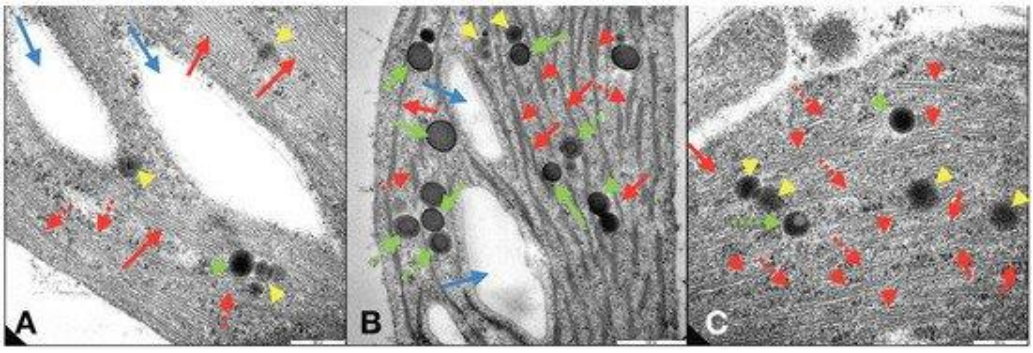

Figure 3,2.7. TEM micrographs of *Lemna minor* L. chloroplast ultrastructures in leaf cell cross-sections from plants grown in the presence of total Fe supply (C^+ control) (**A**), in total Fe deprivation (C^-) (**B**), and in the presence of C_2L-NMs and insoluble iron ($FeCl_3$). Graphical arrows and arrowheads in the micrographs represent the following: (**A**) light blue arrows = starch granules; solid red arrows = stacked thylakoids in grana; dotted red arrows = single thylakoid stromal lamellae; yellow arrowheads = Type2 plastoglobules (PGs); green arrowheads = Type1 PGs. (**B**) light blue arrows = starch granules; solid red arrows = double thylakoid stromal lamellae; dotted red arrows = grana composed of three stacked thylakoids; red arrowheads = grana composed of ≥four stacked thylakoids; yellow arrowheads = Type2 PGs; green arrowheads = Type1 PGs; solid green arrows = Type3 PGs; dotted green arrows = Type4 PGs. (**C**) solid red arrows = single thylakoid stromal lamellae; dotted red arrows = double thylakoid stromal lamellae; red arrowheads = grana composed of ≥three stacked thylakoids; yellow arrowheads = Type2 PGs; green arrowhead = Type1 PG; dotted green arrow = Type3 PG. Scale bars in the micrographs correspond to 200 nm (**A**,**C**) and 500 nm (**B**).

Lemna spp. have also been reported to absorb even ferrichrome, a hydroxamate siderophore synthesized and released by bacteria, through the plasmalemma, similar to other Strategy I plants, may be by mechanisms other than those typical of these plants (e.g., endocytosis) (*Lemanceau et al, 2009*).

3.2.3 Preliminary Conclusions

In conclusion, the findings reported here demonstrated that the combination of natural strategies and biodegradable materials could result in a successful approach to create novel and valuable low-impact and sustainable nanobiostimulants capable of overcoming the limitations caused by the scarce bioavailability of Fe for plants in hydroponic cultivations and, potentially, in croplands. The application of such bioactive products in agriculture (but also in nurseries and gardening) could be powerful in improving crop production and consequently contributing in fulfilling the demand by human populations for healthy and safe foods and environment preservation.

Further studies are necessary to assess whether the effectiveness of the nanofibrous PCL and PCL/PHB membranes in releasing biostimulants depends only on the concentration gradient of this model molecule between the interior of the fibers and the outer solution, or also on the physical properties of the fibers induced by the presence of the specific Fe chelator used.

3.2.4 Outlooks

The novelty of this study is that a natural strategy of iron nutrition typical of plants based on the release of organic Fe chelators was integrated with a nanofibrous fabric as the carrier of such bioactive natural molecules to mimic the release from the plant roots (mostly root hairs) of such Fe-mobilizing compounds aimed at providing Fe to plants. Two different strategies were applied proved an improvement of Fe uptake. It is worth noting that additionally to the findings aforementioned concerning the effectiveness of the created NBs in supporting the Fe nutrition of plants and their inherent low impact, further valuable advantages consequent to the use of these NBs in plant culturing (in agriculture, nurseries, and gardening) could be the following: (i)

The use of eco-friendly biodegradable polymer materials as carriers could replace the plastic materials commonly used in the commercial slow-release fertilizers. (ii) The use of CL-NMs employing a natural Fe-chelating agent, such as catechol, could replace the use of synthetic chemicals (Fe chelates like Fe(EDTA)), typically utilized in traditional fertilizers, thus reducing the global impact on the environment and health. (iii) The encapsulation of catechol molecules into the nanofibers since causing the slow release of these bioactive agents in the external medium, the mobilization of Fe from insoluble natural Fe sources and its rapid absorption by organisms would prevent the leaching of Fe chelates and the possible pollution of water sources as happens with synthetic chemical Fe chelates (Fe(EDTA)), and would also reduce the global amounts of fertilizers. (iv) The employment of Fe-chelating compounds, like catechol, in the CL-NMs to supply iron to plants was aimed at mobilizing Fe from the natural insoluble sources present in the environment surrounding the plants (e.g., natural stocks in soil and sediments). Oppositely, the use of synthetically preformed Fe chelates would require the previous mining of Fe from some natural resources to then be bound to the synthetic Fe chelator (or in the use of Fe-NPs). (v) Finally, the utilization of reusable organic chelating agents, like catechol (until degradation), that after Fe transfer to plant cells can be reused for the same activity and purpose would prolong the Fe-supplying effect of the NBs created (CL-NMs) here for a longer time relative to that of other Fe supplying products (e.g., Fe-NPs, sulphur, FeS), thus making these NBs more efficient.

This research activity has been published as:

De Cesare F., Pietrini F., Zacchini M., Scarascia Mugnozza G. and Macagnano A., Catechol-Loading Nanofibrous Membranes for Eco-Friendly Iron Nutrition of Plants, **Nanomaterials 2019**, 9(9), 1315; https://doi.org/10.3390/nano9091315

Funding

The research was funded by ERA-NET COFUND—ERA-PLANET (H2020-SC5-2015): The European Network for Observing our Changing Planet—IGOSP Project: "Essential Variables workflows for resource efficiency and environmental management". Grant Agreement: 689443.

Acknowledgments

Acknowledgments to A.R. Taddei for sample preparations for Scanning Electron Microscopy (SEM) and Transmission Electron Microscopy (TEM) and investigations at the Electron Microscopy Section of the High Equipment Centre, at Tuscia University (Viterbo, Italy) and Prof. S. Astolfi (University of Tuscia) for providing tomatoes plants and chlorophyll measurements.

CHAPTER 4 - A strategy model for improving crop yield using beneficial microorganism strains (like *Burkholderia terricola*) and biodegradable nanofibrous scaffoldings (like PCL) (APPROACH 2)

As mentioned previously, an objective of my research activity was dedicated to design, develop and investigate an innovative tool as a model for supporting PGPR growth to make crop benefits according to a sustainable approach.

It is known that, in the portion of soil surrounding plant roots, named rhizosphere, microorganisms mostly live in biofilms attached to both soil particles and root surfaces. More specifically, rhizosphere identifies the soil ecosystem surrounding the roots where plant, microbes and soil particles mutually interact with resulting advantages or disadvantages (i.e. beneficial or negative effects) for the distinct participants to such an "interacting trinity", in nutrition, growth promotion and defense. In the rhizosphere, microbes actively and mutually interact with plants through their roots, mainly supporting their growth (beneficial effects), but also competing with them for nutrients and even causing diseases (pathogens) (negative effects). Examples of benefits include nutrient supply and reduced damages from toxic substances, pollutants, pathogens and environmental fluctuations (water stress and pH) (*Figueiredo et al., 2010*).

There are a wide variety of PGPR and its allies, their role and usages for sustainable agriculture remains controversial and restricted. There is also variability in the performance of PGPR that may be due to various environmental factors that might affect their growth and proliferation in the plants. These gaps and limitations can be addressed through use of modern approaches and techniques such as nano-encapsulation and micro-encapsulation along with exploring multidisciplinary research that combines applications in biotechnology, nanotechnology, agro

biotechnology, chemical engineering and material science and bringing together different ecological and functional biological approaches to provide new formulations and opportunities with immense potential (*Gouda et al., 2018*). Some successful applications of PGPR, reported that Pseudomonas (a few strains), treated with gold, aluminum and silver coated nanoparticles were responsible of significant increasing plant growth, but also of inhibiting the growth of harmful fungal parasite within rhizosphere, thus acting as potential nano-biofertilizers.

Currently, nanobased products and technology for agricultural growth are practices in some of the developed countries like USA, China, Germany, France, Japan, Switzerland, and South Korea. However one concern is obviously in stabilizing (industrial purposes) and making these living organisms stable in time and easy to handle to the consumer. In the past decades, a multitude of observations in some distinct contexts demonstrated that microbes mostly live attached to surfaces (sessile attitude) rather than suspended in aqueous solutions (planktonic attitude), as previously believed, to intercept nutrients in flowing media, or adsorbed onto the surfaces (*Dunne, 2002; Palmer et al., 2007*) and their persistence is determined by the formation of biofilms. Biofilms can be developed on different types of surfaces including natural (*e.g.*, soil particles, wood, or plant/root tissues) and artificial materials (*e.g.*, metals, plastic, clothes, glass, food, rubber, silicon and other materials for medical implants). The evolutionary benefit of biofilm organisation is that microorganisms can survive successfully under adverse conditions. Therefore a suitable substrate promoting bacteria adhesion and colonization could be extremely advantageous to generate tools for specific applications, where the resistance of biofilms to adverse conditions is a prerequisite for the success of the application (*Flemming et al. 2016*).

An electrospun nanofibrous scaffold as the support for microbial cell growth has been developed in such research

approach, to try to recreate artificially a portion of soil where bacteria could develop more naturally to better compete with resident soil microbial population in future agricultural applications. Specifically, a bacterial species with the ability to colonize the rhizosphere of several crop plants (e.g. maize, wheat, rice, oat, coffee) has been grown on electrospun 3D polycaprolactone nanofibers (*De Cesare, et al., 2017*). Since electrospinning conditions (polymer solution, potential, rate of deposition, collecting tool, rotation speed and distance from the spinneret) strongly affect the morphology of the materials deposited, several trials were performed aimed at generating an artificial 3D scaffold mimicking the micromorphology of the soil structure, i.e. resembling the features of surface distribution in soils. Microbial inoculum composition and environmental conditions for microbial growth were set according to those suitable for biofilm formation and development in conventional microbial media. The electrospun nanoscaffold was capable of providing a suitable surface for bacterial attachment, colonization of the framework and development of a proper biofilm, and finally, of preserving its viability and vitality for months.

Furthermore, the specific interactions of bacteria cells with fibres, the orientations of bacteria cells relative to fibres, the dependence of interactions on the fibre diameters and their combined effects have been matter of investigation since they are still open questions.

In the present study, PCL was selected because it is a cheap, biocompatible and biodegradable polymer with a slow degradation rate (*Grossen et al., 2017*), but mostly because it has already been proven to have the capacity of binding bacteria from incubation media (*De Cesare et al., 2017*).

The first target we fixed was to create a nanostructure scaffold that mimicked the morphological structure of soil rhizosphere at nano-micro scale deriving from the distribution of soil mineral particles and organic fibrous materials present therein and with

abundant voids and channels to make it porous enough to permit the possible movement of microbial cells. The bacterium employed on purpose as a model species was *Burkholderia terricola*. *Burkholderia* is a genus of proteobacteria including both human and plant pathogens, and environmentally remarkable species, and it is characterized by its hydrophilicity (contact angle in the range 50–75°) and the electrical properties (negative zeta potential) of its cell surface (*Chakraborty et al., 2010*). Specifically, *B. terricola* is a species typical of terrestrial ecosystems, where it is prevalently located in the soil volume attached to and surrounding the plant roots (rhizosphere). Here, these bacteria interact with plants to support their growth and prevent diseases, *i.e.* the typical properties of the plant growth-promoting rhizobacteria (PGPR). The PCL nanofibrous scaffolds were inoculated with *B. terricola* cells and the dynamics and mechanisms involved in the specific adhesion of the selected bacterial species in both early and following stages of colonisation were studied.

4.1. Materials & methods

PCL-based scaffolds were created by depositing electrospun nanofibres on a rotating collector (400 rpm) to develop 3D self-standing nanofibrous structures. The pristine solutions were 9.5, 10.7 and 11.7% (w/w) PCL (45 kDa) in $CHCl_3$: C_2H_5OH; 4 : 1 (v/v) (anhydrous chloroform >90%, anhydrous ethanol >90%) and all chemicals were purchased from Sigma-Aldrich. The fibrous layers were named PCL1, PCL2 and PCL3. The home-made electrospinning setup (CNR-IIA, Italy) consisted of a high voltage oscillator (100 V) driving a high voltage (ranging from 1 to 50 kV), a high power AC–DC (alternating current–direct current) converter, and a syringe pump (KDS 200, KD Scientific).

The PCL fibrous matrices were obtained by applying 4.9 kV of electrostatic DC voltage between the tip of a 5 cm long stainless steel

equipped syringe and a grounded collector set at a distance of 7 cm below the syringe tip and a constant flow rate of the solution of 950 μL h^{-1}. A home-made clean-box equipped with temperature and humidity sensors housed the electrospinning deposition set up. Six centimeter diameter disks wrapped with aluminum foil were used as conductive collectors. The depositions were carried out for 3 h at about 24 °C and 30% RH. To analyze the possible interactions between microbial cells and the PCL nanofibres, the electrospun matrices were incubated with cells of the *B. terricola* strain IF25 (presumably assigned to this species) chosen for its PGPR properties and previously isolated from a vineyard soil.

The suspension of bacterial cells to be used for producing the active *B. terricola* IF25 cellular population was maintained in liquid culture of Luria Bertani Broth (LB) (*Moore et al., 2008*). Before incubation with the electrospun PCL fabrics, *B. terricola* cultures from agar plates were pre-cultured (30 mL) overnight in LB media and then promptly inoculated in glucose mineral broth (GMB) to obtain a standardised pre-culture to be used in the incubation trials with fibrous matrices. To perform the experimental trial, a GMB solution containing (gL^{-1}) 2.2 Na_2HPO_4, 1.4 KH_2PO_4, 0.6 $MgSO_4 \cdot 7H_2O$, 3.0 NH_4SO_4, 2.0 glucose and trace elements was prepared. The incubation of PCL nanofibrous scaffolds and *B. terricola* IF25 cells was performed by inoculating aliquots of bacteria pre-cultured cells in Erlenmeyer flasks containing 25 mL of GMB to obtain a suspension of 0.8 ± 0.02 × 106 CFU mL^{-1} (2% v/v final concentration of the inoculum). The interaction of *B. terricola* cells with PCL nanofibres was then assessed by placing 1 cm^2 pieces of electrospun PCL nanofibrous mats into the inoculated flasks and incubating them aerobically and under orbital shaking (80 rpm) in the dark at 30 °C for about 30 *h*. PCL samples housing bacteria cells were collected after 2 *h*, 4 *h* and 21 *h* of incubation.

WCA measures were carried out as described in the previous chapter (Materials and Methods).

B. terricola inoculated and non-inoculated samples of electrospun scaffolds collected from suspensions incubated for increasing periods were analyzed by SEM and TEM.

Samples for SEM were pre-fixed in a solution of glutaraldehyde (2.5% *v/v*), ruthenium red (0.075% w/v) and lysine acetate (0.075 M) dissolved in 0.1 M cacodylate buffer (pH 7.2), before SEM analyses. Fixation in glutaraldehyde (2.5% v/v) dissolved in 0.1 M cacodylate buffer (pH 7.2) was then performed for 2 *h* at 4 °C, after cold washings in the same buffer. Post-fixation in osmium tetroxide (2% *v/v*) in cacodylate buffer for 2 *h* at 4 °C was then performed after washings. Then, a cold rinsing was applied to the processed specimens before dehydration in a graded ethanol series following the critical point method with CO_2 in a Balzers Union CPD 020. Samples were finally sputter-coated with gold in a Balzers MED 010 unit before observations using a JEOL JSM 6010LA electron microscope. Samples for TEM analyses were fixed and dehydrated as with SEM samples, infiltrated with various percentages of LRWhite resin/ethanol mixtures and then embedded in LRWhite resin for 2 *d* at 50 °C. Blocks were cut into ultra-thin sections (60–80 nm) using a Reichert Ultracut ultramicrotome and stained with uranyl acetate and lead citrate. Micrographs were captured using a JEOL 1200 EX II electron microscope equipped with Olympus SIS VELETA CCD and iTEM software.

The bacteria vitality was assessed by the cell-mediated reduction of a tetrazolium salt following the method of *Ladd and Costerton (1990)*. Specifically, 2-(4-iodophenyl)-3-(4-nitrophenyl)-5-phenyl-2*H*-tetrazolium chloride (INT) was used in this study to assess the dehydrogenase activity, which is an expression of the bacterial redox activity (respiration) that bacteria use to obtain the energy for metabolic and physiological activities. Briefly, to test the bacteria vitality during the incubation of the nanofibrous scaffolds with bacteria, four electrospun PCL samples were collected from batch cultures of microbial populations after 2*h*, 4 *h* and 21 *h* incubation

periods. They were then washed in sterile deionized water, placed in flasks containing the INT solution (0.01% *w/v* redox indicator in 0.1 M phosphate buffer, pH 6.8, and LB 1 : 20 *v/v* final dilution) and finally incubated in the dark for 4 *h* at 30 °C, for color development. After washing and drying, the PCL pieces with immobilized bacteria were treated with absolute alcohol for formazan extraction.

4.2. Results and discussion

Various polymers and relative fabrics resulting from homopolymer and blend solutions were tested in preliminary studies, but were unable to create frameworks satisfactorily similar to soil structure. We found that PCL was the most suitable to obtain final frameworks similar to the morphological structure of soil, which is basically composed of particles and fibrous materials. A number of recipes for the PCL electrospinning solutions were also tested to optimize this achievement. Although several solvents capable of dissolving PCL were tested to reduce the employment of toxic organic solvents in the electrospinning process for possible future applications of the final products in distinct environments, only $CHCl_3$ mixed with C_2H_2OH successfully provided soil-like frameworks.

PCL1 and PCL2 nanofibrous fabrics showed 3D frameworks similar to microcarpets, where protruding microstructures were visible by camera (1-2 mm), stereomicroscope and SEM, respectively (Figure 4.1). The distribution in the nanofabrics of the self-assembled fibrous networks presented in both the matrices a sort of repetition of holes and pinnacles and flakes in the overall structure in top views. These structures were self-created during electrospinning by self-assembling of microbeads and nanofibres arranged in honeycomb-like shaped structures. As expected, when PCL concentration augmented, the beads number decreased favoring fibres creation (Figure 4.2). Polymer concentration is one of the most important parameters in the electrospinning process, because it is strongly related to the polymer

viscosity and the degree of entanglement. SEM images of Figures 4.1 and 4.2 depict fibres from the PCL solutions with different concentration (*w/v*). Electrospinning of PCL2 solution (Figure 4.1.b) led to the formation of a honeycomb pattern, but this polymer concentration also produced numerous beads inside the fibrous mesh. The honeycomb cells showed diameters in the range 200-500 μm (300 μm on average). In PCL1, with a lower concentration of the polymer, the jet would be broken down into more beads (drops) due to the lowering of the surface tension. When the concentration of the PCL solution increased to 11.7 wt%, a self-assembled and flatter honeycomb pattern emerged with less bead formation (Figure 4.2). In literature has been reported that honeycomb self-assembly generally disappeared at higher solution concentration (*Yan, et al., 2011*) as increased the fibres size. Such a nanofibers formation is driven by the competitive actions of surface tension and electrostatic repulsion. A biomimetic honeycomb pattern shows large surface area, high structural stability and good permeability, which have been proven to be crucial, in nanomedicine, for proliferation and differentiation of eukaryotic cells, promoting uniform cell distribution as well as providing a stimulant environment for tissue regeneration (*Yao et al, 2019*). However PCL1 framework degraded under stirring due to mechanical friction by the liquid media, presumably due to nano-microdimensional framework, thus it was not suitable to grow bacteria for periods long enough to develop biofilms on the nanofabrics with repeatable results. Conversely, PCL2 resulted more stable and more similar to the soil-like nanostructure (particulates and fibres) as desired, i.e. to create an artificial nanostructured scaffold mimicking the rhizosphere framework and principles to be used as a model for specific studies a structure enriched of internal voids, a dense network of fibers (0.096±0.042 mm) and particles (6.87±3.9 mm). The first evidence of adhesion of *Burkholderia* cells at nanofibres was observed as soon as upon 4 h incubation (Figure 4.3 A) whereas microcolonies could be noticed with rod shaped bacteria cells attached to nanofibres.

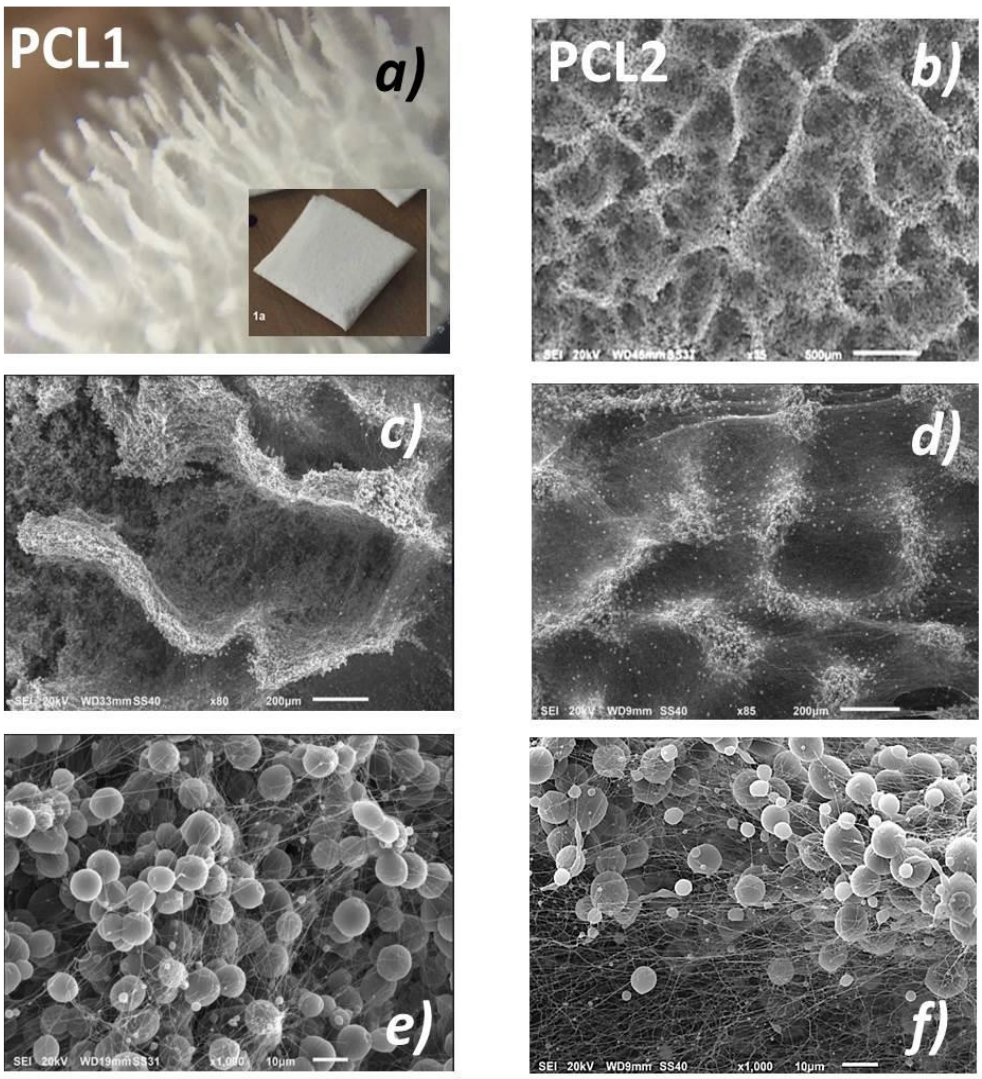

Figure 4.1. **a**) camera pictures of the PCL1 carpet-like fabrics (inset) highlighting the polymer macro- and micro-(**c**) extrusions and a composition mainly made of microspheres (≈6.5 μm) held by numerous but very fine fibers (≈60 nm) (SEM pictures); **b**,**c**) SEM micrographs of PCL2 honey-comb arrangement with a scaffold consisting of (**f**) microspheres (≈7 μm) and a very dense network of nanofibers (≈66 nm)

By increasing the incubation period, bacteria adhesion extended to beads, provided they were at least partially coated with nanofibres (Fig.4.3 B,C), with a diffused dense and extended colonization of fibres. It is peculiar, in effect, that after 48 *h* and even after 7 *d* incubation and an extensive colonisation of the nanofabrics, some beads (i.e. without nanofibres at surface) still appeared in SEM micrographs as completely naked, i.e. deprived of bacteria.

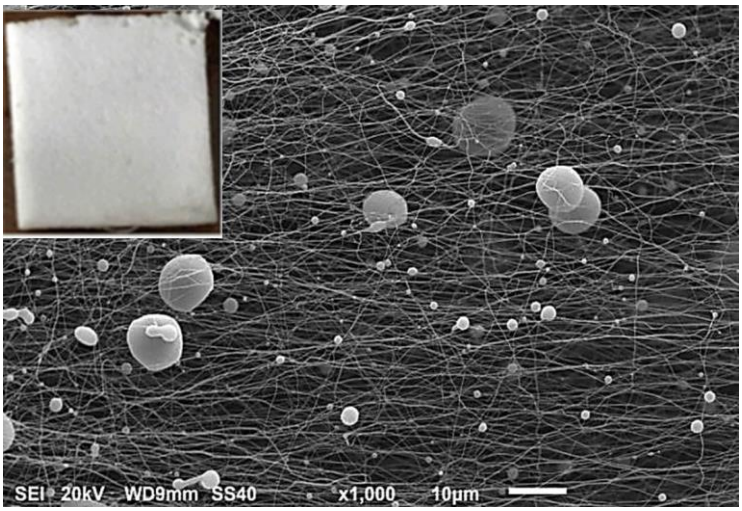

Figure 4.2. SEM picture of PCL3 and camera photo of a piece of the fabrics

In conclusion, adhesion always (or prevalently) seemed to occur to nanofibres. Figure 4.3.D shows dense packing of cells attached to nanofibres to form a layer progressively transformed into a biofilm with cells embedded into the matrix covering the whole electrospun framework as a pellicle (7*d*). After 11 *d* incubation a mature biofilm with microbial population embedded in the matrix and coated with a thick protective layer was generated. The viability of microbial population in the PCL nanofibrous fabrics was assessed during biofilm development and storage by respiration, i.e. the reduction of INT to the relative formazan (INT-F). The assay showed (Figure 4.3.F-D) interestingly that the colonization of the PCL nanofibrous fabrics started from the outer parts of the electrospun framework (4 h, Figure 4.3.F). Specifically, the outer borders and the top of the pinnacles and flakes of the nanoscaffolds were the first to be colonized then followed by a rapid diffusion and colonization of the fibers inside (Figure 4.3.D).

A deeper investigation focusing on bacteria adhesion onto PCL3 fibres has been recently reported in *De Cesare et al., (2019-a*).

A shorter description follows below. About the bacteria anchorage and adhesion, both PCL2 and PCL3 were extensively covered with organic materials that was absent in the nanostructured fabrics

incubated with the same medium but without bacterial cells (controls).

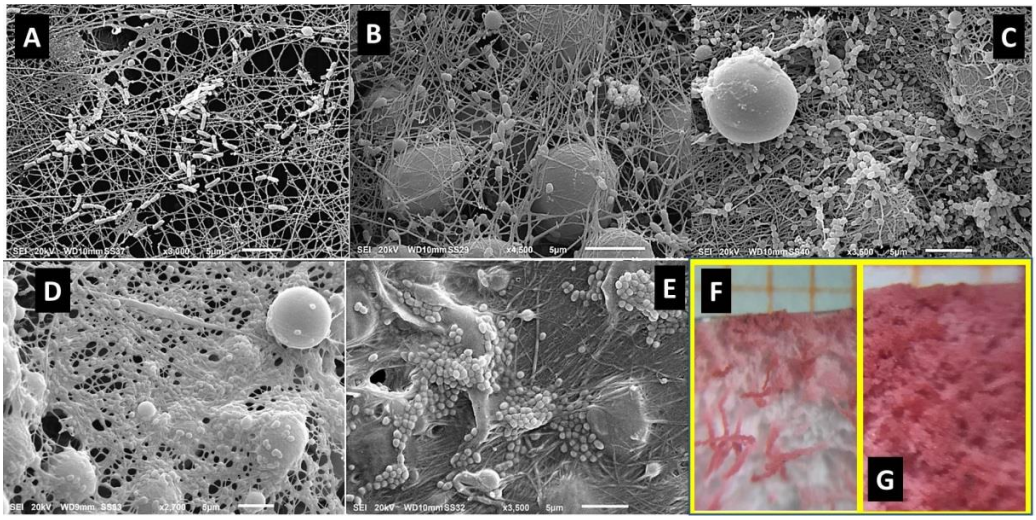

Figure 4.3. SEM pictures reporting the different stages of anchoring, adhesion and colonization up to the formation of a biofilm by *B. terricola* on PCL nanofibers; **A**) 4*h*; **B**) 28*h*); **C**) 48*h*; **D**) 7*d*; **E**) 11*d*. **F**) bacteria respiration assay after 4h and (**G**) 28 h

Therefore, such deposited materials should be specifically released by microorganisms and not consequent to the mere adsorption of organic materials of the growth medium. This matter is commonly named "conditioning film", and it is known to be produced by bacteria to facilitate adhesion of cells to surfaces. The SEM images of the pristine 3D self-standing fibrous matrices show a relatively smooth surface (Figure 4.4.A). The distribution of the pristine nanofiber dimensions indicated a mean diameter of 64.18 ± 27 nm, a median of 58 nm, and a diameter range of 10–129 nm, while more than 90% of nanofibres have a diameter <100 nm (Figure 4.4.C). The fibrous matrices were characterized by a remarkable decrease in contact angle with values of 109° ± 3.8° for pristine PCL nanofibres (Figure 4.4.D), relative to the typical values (115–136°) of other electrospun unaligned nanofibrous PCL (pristine). This effect might be due to a higher degree of porosity of the studied system that is usually related to higher hydrophilicity. When incubated with

bacteria, however, the fibrous matrices did not maintain the pristine morphology because of the coating with additional organic materials produced by bacteria, so that the original features of the pristine artificial material were remarkably modified (Figure 4.4.B). The coated fibers appeared larger in size, in fact, than the pristine nanofibers so that the analysis of the nanofiber population indicated a distribution of their dimensions in the range 22–300 nm, with an average diameter of 96.34 ± 41.21 nm, a median of 88 nm and more than 65% of nanofibers with diameter <100 nm. By considering the difference in the average values of the two populations of fibres, pristine and coated, a ≈30 nm thickness on average can be estimated for the fiber coating, then resulting in more than 50% increase in fibre size because of the coating deposition. The coated nanofibers displayed a rough surface with some spheres attached to the nanofiber surface. The various phases that drive bacteria cells from the planktonic to a stable sessile condition include the approximation and initial contact with an animate or inanimate surface (reversible adhesion), firm attachment, interactions between cells and formation of micro- (at first) and macro-colonies (later) (stable adhesion). The complex process of adhesion is driven by the activation and expression over time (of incubation, in the present case) of several specific genes that induce modifications in the cells (*e.g.*, flagella removal, pili formation, exopolymeric matrix release and cell envelope modification). The SEM micrographs of the nanofibrous scaffolds after 2 *h* of incubation show an additional organic material deposited onto nanofibers (Figure 4.4.B). Since no coating material was present on the nanofibers of control samples incubated with the same growth medium in the absence of bacteria, and a smooth surface and a smaller average diameter were observed (Fig. 4.4.A), it is reasonable to assign the presence of such a conditioning material to *B. terricola* cells. The composition of the CFs is often compared to that of extracellular polymeric substances (EPS) comprising the matrix. In species of the genus *Burkholderia*, polysaccharides are the major components of the

CF (named *Cepacian* in *Burkholderia cepacia*), although in most bacteria species proteins tend to prevail.

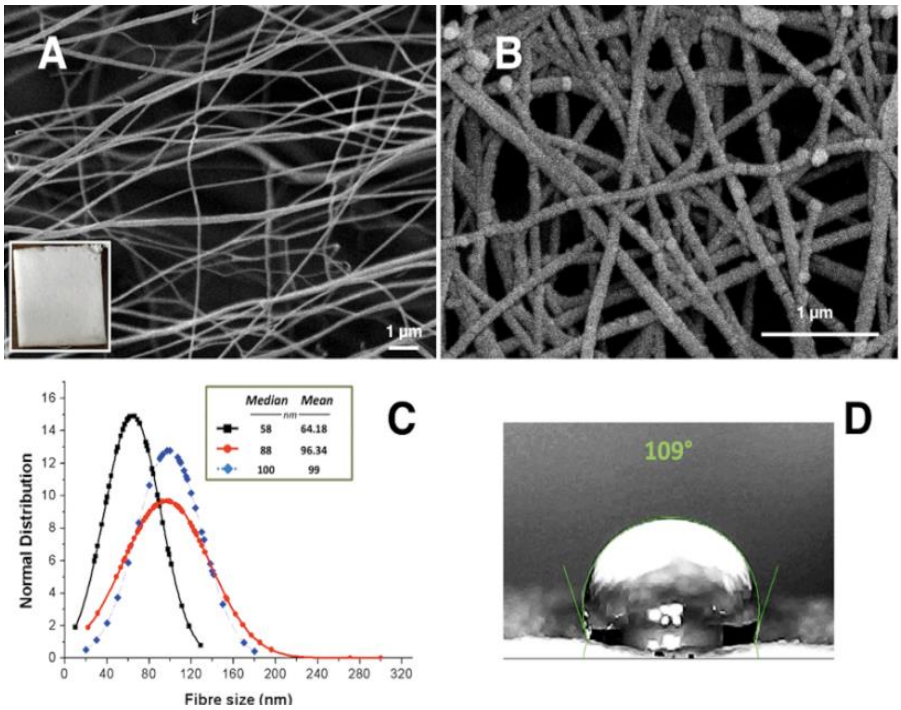

Figure 4.4. SEM micrographs of the nanofibrous PCL scaffold: **A**) soon after electrospun deposition; inset = image of the 3D nanofibrous fabric (1 × 1 cm) captured using a camera; **B**) after 2 h of incubation in the *B. terricola* cell suspension and showing the deposition of the conditioning film onto the nanofibrous framework. **C**) Distribution of the nanofibers, based on their diameter, measured soon after the electrospun deposition (*black line*), after CF deposition (*red line*) and binding *B. terricola* cells (*blue line*). **D**) Contact angle of the electrospun nanofabric (drop volume = 8 µl; drop surface = 1.79 mm^2; surface of contact = 6.04 × 10^{-1} mm^2). Scale bars in A and B = 1 µm.

Additionally, the presence of the conditioning material not only dramatically modifies the original chemical and physicochemical characteristics of surfaces such as hydrophobicity/hydrophilicity (wettability), surface charge and free energy, but also the topography of the underlying surface that might be consequently irrelevant (*Flemming et al., 2015*). It is worth noting that the CF deposited on the nanofibres and displayed in Figure 4.4.B resulted from the incubation of the electrospun PCL nanofibrous fabrics with bacteria

carried out under stirring and from washings for sample preparation for SEM analyses. This fact highlighted that the CF material produced by *B. terricola* cells, though bound unspecifically to the pristine PCL, was found to be tenaciously fixed to the PCL nanofibers underneath. Based on the interactions of bacteria with nanofibers observed in the present study, it seems that the CF deposited onto surfaces (and its properties) is confirmed to be the primary driver affecting bacterial adhesion to materials, in agreement with Garrett *et al.* (2008). Unfortunately, it was not possible in the series of experiments here carried out to test the adhesion of bacteria in the absence of the CF. This organic material, in fact, was released by bacteria themselves when exposed to the nanofibrous PCL fabric and was rapidly adsorbed onto the mat surface as soon as the incubation started, and its chemical or physical extraction would have required previous bacteria removal and preservation of the PCL scaffold, *i.e.*, conditions that would be difficult to perform without mutual alterations. However, some preliminary results obtained in another set of experiments exploiting distinct experimental strategies using the same bacteria strain and electrospun PCL nanofibrous mats seemed to support this hypothesis, because the same but uncoated material appeared to be unable to support bacteria adhesion (data not shown). Consequently, it might be concluded that the presence of the CF is a prerequisite for *B. terricola* adhesion.

In the present study, diverse types of interactions between *B. terricola* cells and nanofibers were observed in both SEM and TEM micrographs captured from electrospun nanofibrous scaffolds after incubation in the bacteria inoculated medium (Fig. 3.2.5). It is known that the adhesion of bacterial cells to surfaces generally takes place following the CF deposition, and it occurs through distinct steps involving unspecific and specific mechanisms, both originating essentially from weak bonding like physicochemical (electrostatic, van der Waals, and acid–base interactions) and hydrophobic interactions (*Costerton et al., 1999*). These ties occur,

in both natural and most of the artificial environments, between bacteria and the surfaces coated with various compounds of the CFs (*e.g.*, proteins and polysaccharides) (*Beech, et al., 2000; Yang et al., 2016*).

Since these types of bonding are weak, they are unstable and short-range effective and then reversible, especially under agitation or in flowing media, as is the case for the experiment carried out in this study. These interactions, then, do not permit a stable relationship between bacteria cells and surfaces and their colonization and host infection, in the case of biotic surfaces, until they do not become more stable.

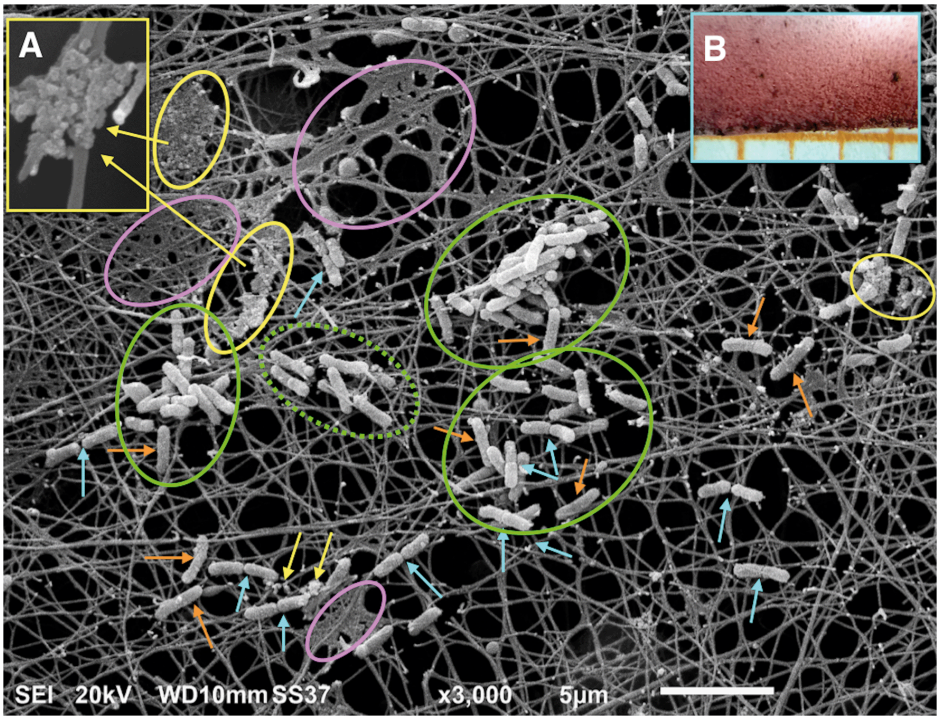

Figure 4.5. SEM micrographs of the nanofibrous PCL scaffold after 4 h of incubation in the *B. terricola* cell suspension: yellow arrows, circles and inset (**A**) indicate OMVs deposited onto the nanofibrous network; pink circles = conditioning film forming membranes when deposited onto crossing interlaced nanofibres; light blue arrows = replicating bacteria; orange arrows = elongating bacteria; green circles = cell aggregates and microcolonies (the dotted circle identifies a group of cells aligned with single nanofibres except for a cell that moves towards another cell which is oriented transversely to the fibre) (scale bar = 5 µm). (**B**) Electrospun PCL nanofibrous scaffold after 4 h of incubation with *B. terricola* cells and testing for bacteria vitality (respiration) (orange grid intervals = 1 cm).

Adhesins mediate both types of mechanisms, and the main difference between the two types of mechanisms is mostly the distance they operate.

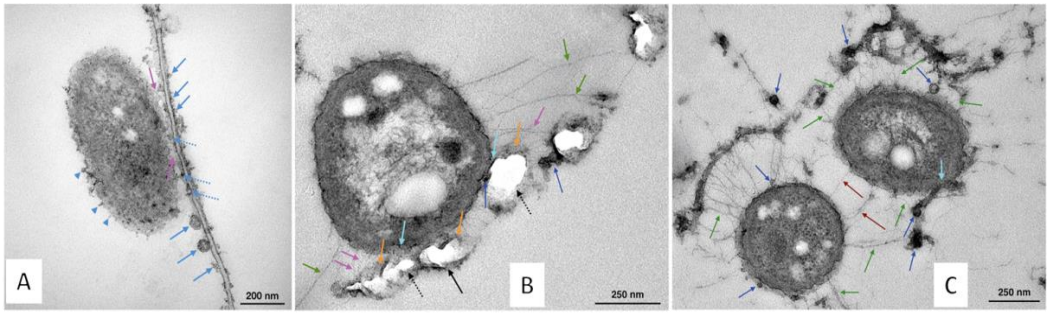

Figure 4.6. TEM pictures of B. terricola joining PCL NFs with different strategies: (**A**) surface-to-surface interaction; (**B**) generation of OMVs (outer membrane vesicles) and (**C**) appendages like fimbrie/pili protruding from all round the body of the bacteria

SEM and TEM micrographs were after different periods of incubation, but mostly Figure 4.6.A (pink arrows) clearly show a close contact between bacteria cells and nanofibres, typically a surface-to-surface interaction, which was here identified as type1-interaction. In these micrographs, this type of interaction seemed to be mediated by a sort of gel-like amorphous material surrounding *B. terricola* cells (maybe classifiable as a capsule-like material). This TEM micrograph not only provided the visual evidence that very thin nanofibers were generated during the electrospinning deposition and that they were coated by a ≈30 nm thick conditioning film but more interestingly allowed the analysis of the interactions between *B. terricola* cells and suitable thin nanofibers. Specifically, the capsule-like material of *B. terricola* cells seemed to merge with the CF and deposited onto the nanofibers. Furthermore, in some cases, the bacteria cells looked like not only lying on the conditioned nanofibers but almost surrounding them with their capsule materials all along the area of contact. Therefore, the adhesion of *B. terricola* cells to nanofibers here observed seemed to result from the interactions between macromolecules present in the capsule-like material and the

macromolecules comprising the bacterial CF. In Figure 4.6.B, TEM micrograph reports a further strategy of interaction between bacteria and fibre through the generation of OMVs (outer membrane vesicles) that appeared as electron dense disks 20-300 nm sized in diameter. These structures have been proven to be standard constituents of biofilms. After 21 *h* of incubation a more stable attachment of bacterial cells was observed with the generation of appendages like fimbrie/pili protruding from all round the body of the bacteria (3-10 nm diameter and variable length) (Figure 4.6.C). They should be related not only to adhesion but also to motility and colonization.

The present research activity has been awarded with a runner up cover competition in Materials Today 2016 (De Cesare et al. 2017) and with a back cover page in Environmental Science Nano Issue 6 Anno 2019 (v. pag. 98).

4.3. Preliminary Conclusions

This study aimed at testing the possibility of bacteria to interact with and adhere to fibres with nanoscale dimensions, different from that published to date in the scientific literature, to the best of our knowledge. The novelty of this study is that fibers with nanosized diameters so as to be classified appropriately as nanomaterials (*i.e.* ≤100 nm in at least one of the three spatial dimensions) were used to test the possible effects on the adhesion of bacteria with a much larger diameter. Specifically, PCL fibrous scaffolds composed of nanofibers with an average diameter ≈64 nm were created by electrospinning and incubated with *B. terricola* cells. Different from the published studies, the fabricated nanofibrous fabrics were coated with a ≈15 nm thick conditioning film secreted by bacteria during the incubation to facilitate their adhesion to nanofibers. This coating consequently changed the surface morphology (from smooth to rough) and the physicochemical properties of the pristine material so that the resulting nanofibers were characterized by an average

diameter of ≈96 nm and a size range of 22–300 nm. Because of the new features of the nanofibrous materials, maybe, bacteria cells preferentially adhered to 20–180 nm wide nanofibers and mostly to those with 99 nm diameter so that the bacteria-to-nanofiber (BFR) ratio was as large as BFR = 5.2, with a maximum of BFR = 25. Differently, the BFR values calculated in published studies ranged from 0.03 to 1.7, with a single case where it was ≈7. Additionally, we also observed for the first time to our knowledge that specific interactions occurred at this early stage of association between bacteria and nanofibers. Therefore, the usual events of surface colonization by bacteria preceding the formation of biofilms were confirmed to occur when *B. terricola* cells colonized the electrospun PCL fibrous matrix consisting of nanofibers with average pristine diameter <65 nm, without any evident inhibiting effect on the adhesion, proliferation and vitality of the bacterial cells.

4.4. Outlooks

All of these findings can have remarkable potential on the creation of advanced nanofibrous materials for various applications. The presence of ≤100 nm nanofibers will result in scaffolds with an enormous surface area suitable for hosting large amounts of microorganisms for applications of interest. The creation of 3D self-standing scaffolds, like in the present study, will further magnify this feature and also the easy handling of the final nanofabrics by the final users (*e.g.* farmers). Additionally, various combinations of valuable bacteria species and polymer fibers with different chemistries displaying distinct suitable BFR values could be selected to facilitate or limit the adhesion of specific microbial strains to surfaces. These results could also assist in the future development of biofilms and together with the employment of biodegradable and biocompatible materials could contribute to creating more efficient, eco-friendly and safe materials for target low-impact applications. Examples of such applications could include the creation of target-specific biostimulants

and biopesticides to be used in agriculture (replacing broad-spectrum synthetic chemical pesticides inducing resistance in target and non-target organisms), more efficient microbial fuel cells, selective materials for wastewater treatment and other environmental applications, bioreactors, specific biochemical catalysts, materials for biomedical applications (*e.g.* probiotics for restoration of gut microbiota), filtration systems, and so on. Oppositely, materials could be created aimed at reducing or preventing the adhesion of bacteria by tuning the size of fibers (in addition to materials) and then acting as antimicrobials for the biocontrol of pathogen-induced diseases in both agriculture and medicine. Moreover, the fiber size-based promotion or prevention of bacterial adhesion and surface colonization could be further combined with specific designs of the surface chemistry of fibers. The creation of specific OMVs loaded with compounds of interest could also be used in combination with the nanofibers of tailored size to create more effective fiber-based nanotopography materials aimed at inducing or hindering bacterial adhesion and biofilm formation on materials for applications of interest.

Further research studies might include analyses of interaction mechanisms based on the use of AFM and related modifications on single cell force spectroscopy (SCFM) as well as molecular analyses identifying the possible involvement of specific receptors on the bacterial cells, or the quorum sensing mechanisms of bacterial communication, and chemical analyses of the CF and EPS materials secreted on purpose by *B. terricola* in similar incubations. Other research studies could be focused on the mechanical properties of the nanofibers, for example, the flexural rigidity, and the charge density of the fibres and their effects on the interactions with the CF and the adhesion of *B. terricola* cells with PCL nanofibers. Macroscopic aspects such as the nanofibrous scaffold porosity and typical pore size could be further investigated to assess possible effects on such interactions. Microbial proliferation and microcolonies embedded in EPS with an

extended and diffused mature biofilm and the viability tests confirmed that PCL, depending on the ES parameters of deposition, can be considered a suitable framework housing alive and active microbial cells, capable of forming proper microbial communities like in proper soil ecosystems, where cells adhere to the surfaces of mineral particles and SOM (and roots), create colonies, communicate to organize their community (quorum sensing), form complex communities and develop mature biofilms for precision agriculture.

Acknowledgements

Acknowledgments to Dr. A. R. Taddei for sample preparations for Scanning Electron Microscopy (SEM) and Transmission Electron Microscopy (TEM), Prof. E. Di Mattia for bacteria strain selection and PCL incubation and Dr. F. De Cesare, for the experimental activity coordination and fruitful discussions.

Funding

ERA-NET COFUND - ERA-PLANET (H2020-SC5-15-2015): The European Network for Observing our Changing Planet – IGOSP Project: "Essential Variables workflows for resource efficiency and environmental management". Grant Agreement: 689443 (ITALY) (http://www.era-planet.eu/index.php/the-projects/igosp-integrated-global-observing-systems-for-persistent-pollutants), for financially supporting this research. COST Action MP1206 (AUSTRIA) "Electrospun nano-fibres for bio inspired composite materials and innovative industrial applications" (https://www.cost.eu/actions/MP1206/#tabs%7CName:overview) that promoted the present activity and the collaboration between scientists.

The results have been published in:

De Cesare F., Di Mattia E., Zussman E. and Macagnano A., A study on the dependence of bacteria adhesion on the polymer nanofibre diameter, Environ. Sci.: Nano, 2019,6, 778-797

Award: Back cover page of Environmental Science Nano Issue , 2019

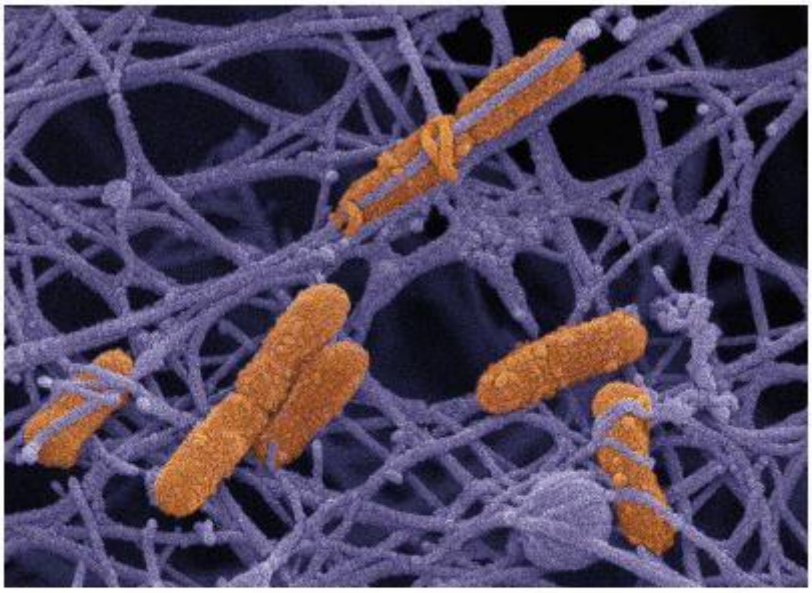

Featuring work from Dr. Fabrizio De Cesare at Department for Innovation in Biological, Agro-food and Forest Systems (DIBAF), University of Tuscia, Viterbo, Italy, and Antonella Macagnano at Institute of Atmospheric Pollution Research (IIA), National Research Council (CNR), Monterotondo, Italy.

A study on the dependence of bacteria adhesion on the polymer nanofibre diameter

Adhesion of bacteria to fibres is size-dependent with a preferential attachment to 100 nm wide nanofibres. The interaction mechanisms are investigated here. The presence of a conditioning film coating the nanofibres is found to be crucial for adhesion.

As featured in:

See Fabrizio De Cesare et al., *Environ. Sci.: Nano*, 2019, 6, 778.

Award: Runner up in the Materials Today cover competition 2016

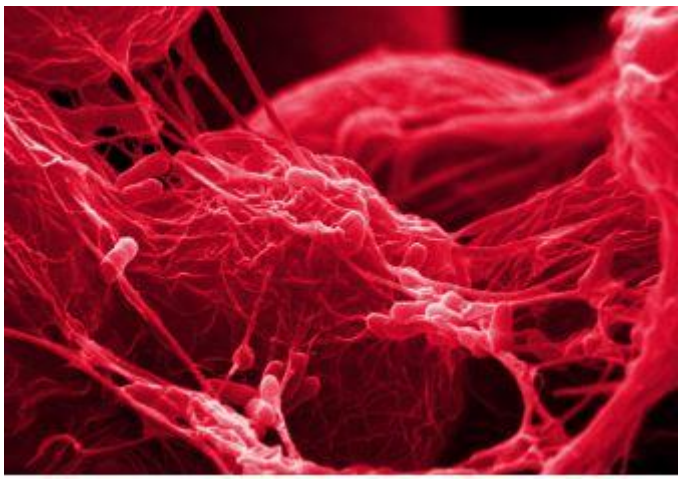

CHAPTER 5 - Strategies for novel eco-compatible nanofibrous sensors for gas and VOCs monitoring (APPROACH 3)

The final strategy concerned the chance to apply electrospinning technology to fabricate innovative sensors with potentials in precision agriculture applications.

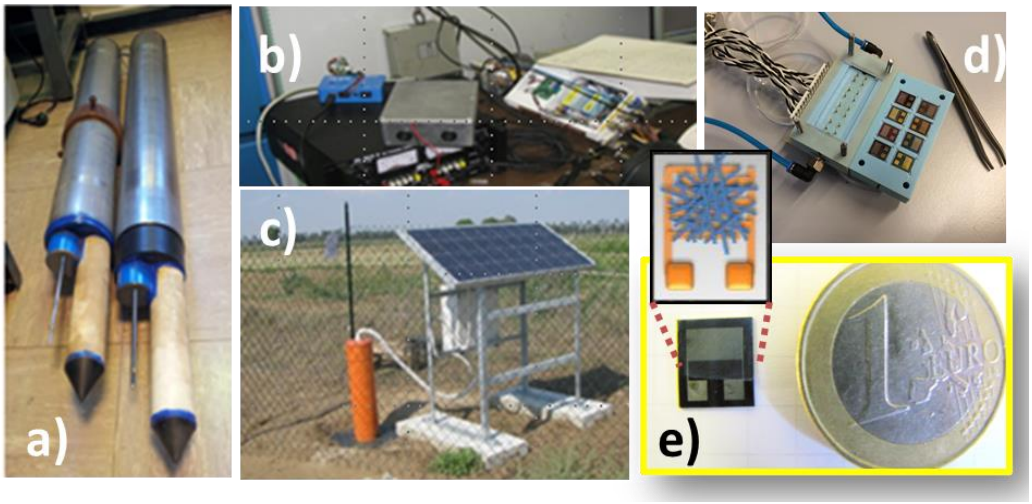

Figure 5.1. Some kind of devices developed for soil monitoring (CNR-UNITUS in SISA/POR-FESR Project): **a**) device housing VOCs commercial sensors, QCM sensors based on Me-porphyrins and IDEs based on conductive polymers to be buried in the soil; **b**) an home-made electronic nose to monitor the soil headspace; **c**) solar panel and monitoring device; **d**) sensor array chamber housing 8 IDEs (20 x 20 μm electrodes); **e**) an IDE electrode.

Indeed, soils may act as sources or sinks of volatile organic compounds (VOCs). Many of the formed VOCs are produced by microorganisms, and it would be a challenge to investigate soil microbial communities by studying their VOC profile. Such "volatilomics" would have the advantage of avoiding extraction steps that are often a limit in genomic or proteomic approaches (*Insam et al., 2010*). In soils, VOCs are mainly produced by plants and microorganisms. Volatile organic compounds emitted by plant roots (and associated mycorrhiza) or seedlings were also identified. Interactions between plants and microbes mediated by VOCs as well as plant VOC production, measurement, and the

influences of VOCs on plants have been matter of discussion in several reviews (*Cape, 2003; Tholl et al. 2006*). Investigation of soil VOC production is sophisticated as soil includes an enormous variability in parameters that influence VOCs production. Besides differences in soil-specific community composition, VOCs production in soils (e.g. limonene, cyclohexanone, aldehydes, branched chain alcohols, amines, esters, acids, alkyls) is strongly depending on nutrient and oxygen availability and on the physiological state of the microorganisms. The relationships between soil and VOCs and the chance to use VOCs as fingerprint of a soil, has opened novel perspectives in microbial ecology and agriculture (Figure 5.1).

Therefore, we designed two kinds of sensors to be differently and highly sensitive to several chemical classes of VOCS and gases. Initially we created and characterized a composite nanofibrous sensor and afterwards a similar sensor but loaded with a porphyrin in order to compare their sensing features and assess their potentials in an agricultural scenario.

A recent trend in planning sensors devices focuses on the attempt to develop portable and easy-to-use monitoring instruments for rapid and inexpensive analysis also of complex matrices, i.e., headspace containing various volatile and gaseous compounds, based on sensors arrays or matrices with broad and partially overlapping sensitivity to various chemicals (olfactory machines and electronic nose systems). Each sensor has to transduce chemical information concerning multi-component gaseous mixtures into a series of measurable signals (*Andrzej et al., 2012*). As a part of these systems, sensors are exploited independently and simultaneously, and then treated as independent sensing elements. Furthermore each sensor contributes to create a multivariate response, within a sensor array, of the analyzed matrix. In order to be effective and successful, all the sensors should be characterized by as much

chemical diversity as possible, on the assumption that they have not to be highly selective toward any given analyte, but highly and differently sensitive to every chemical class. On the other hand, the concept of an array of chemical sensors that can be used for any application is now outdated due to a series of difficulties, like the creation of universal databases from trained sensor arrays and the need to make the sensor array more selective to specific applications where gases or VOCs (Volatile Organic Compounds) to be revealed are present in trace amounts. For instance, in metal-oxide based sensors, that have been the most investigated and commercially used sensors, the working temperature is the main responsible of their sensitivity as well as their selectivity. Thus the same sensors, working at different working temperature values in order to detect various chemical classes with different sensitivity and selectivity, can be designed to create an array or a part of a suitable array for defined applications. For instance, SnO_2-based sensors can work between 25 and 500°C but their best sensing temperatures depend on the kind of gas to be detected (*Zakrzewski* et al., 2006): an optimal sensing temperature of a SnO_2 sensor to reveal CH_4 has been reported to be about 400°C while that for sensing CO has been 90°C, confirming that temperature could be an effective tuner of the sensing features. Obviously in the case of MeO_x semiconductors temperature is the main responsible parameter for the amount of O^- distribution on the sensors surface, which is necessary for them to work properly. Vice versa, sensors based on conductive polymers are designed to work at room temperature, in order to both avoid an eventual thermal degradation (*Zampetti et al., 2011*) of the chemical layer and to permit the adsorption and diffusion mechanisms of the analytes through the surface. Generally, the sensitivity and selectivity are commonly ruled by polymer chemical structure and arrangement within the sensing layer (*Sołoducho et al., 2016*). Conductive polymers were here preferred due to: i) rapid and

reversible adsorption and desorption kinetics at room temperature; ii) low energy consumption originated by the fundamental principles of conductive polymers and by the special low-power electronics required; iii) the interactions depending on the polarity and spatial structure characteristics of the odorous molecules; iv) the conductive organic sensors are sensitive only to the steric, ionic, hydrophilic and hydrophobic variations of the spectrum of molecules of the odorous substance; v)the volatile compounds existing in the environment, which can poison inorganic MOS sensors (for example sulfur compounds) can be detected without inactivating the polymers; vi) they are ease to be functionalized and modulated in sensitivity and selectivity.

Therefore, nanostructured and a nanocomposite polymer sensor has been designed, fabricated by electrospinning deposition, and then exposed to different chemical classes of VOCs and gas within a range of working temperatures, compatible with the thermal stability of the polymers, to ascertain that the temperature also could be a modulator of selectivity and sensitivity such as for metal-oxide based sensors. Obviously, in the case of polymer based sensors, the temperature changes are expected to affect different chemo-physical parameters of the sensing process. On the other hand, temperature can be a useful strategy for provisionally modifying the arrangement of both polymer chains and the hosted nanofillers, as well as the related electrical and sensing features.

Specifically, the attention has been focused on the challenging goal of obtaining conductive fibers electrospun by a mixture of two insulating polymers, polyhydroxibutyrate (PHB) (*Hankermeyer et al., 1999; Acevedo et al., 2018*) and polystyrene (PS), hosting a conductive nanopowder of mesoporous graphitized carbon (MGC). As described before, the polymers were mainly selected for several features like their versatility (generally used to make a wide variety of consumer products), but overall for their eco-compatibility due

to their biodegradability (PHB) and recyclability (PS) (*Wünsch, 2000; Uyaret al., 2008*) and good environmental resistance to thermal excursion. Indeed, both the polymers are classified as thermoplastics, i.e., they can be heated to their melting point (T_{PS}: 240°C, T_{PHB}: 175°C), cooled, and reheated again without significant degradation. Further, they were both soluble in $CHCl_3$, meaning that a unique and easily electrospun mixture could be provided, and insoluble in H_2O, meaning that the resulting fibers could be exposed to a wide range of relative humidity percentages without undergoing structural changes. Exploiting some of the properties of electrospinning technique, nanofibers have been designed in order to be rough and porous, in order to increase the exposed surface and facilitating gas and VOCs permeation. Thus, a mixing of two different organic solvents and a proper surfactant agent were used in the ES deposition mixture. Furthermore, a lot of polymer interfaces inside fibers were expected due to the incompatibility of the two polymers. About MGC, it was selected as the conductive nanofiller: its structure made of a single layer of sp^2 carbon atoms bonded in a hexagonal honeycomb crystalline structure displays outstanding physical properties as high carrier mobility [up to $350 \cdot 10^3$ $cm^2/(Vs)$], thermal stability (*Bolotin et al., 2008*), high mechanical strength (Young's module: 1 TPa and fracture strength: 130 GPa) and large availability of specific surface areas[2]. All these features were expected to provide both conductivity and a higher mechanical strength to the nanofibers. Graphitized carbon nanostructures have also been greatly investigated for their sensing features (*Wang et al., 2016*). The nanofillers, adopted for being included within the planned sensor, were provided also of a mesoporous membrane that conferred a larger available surface area (50–100 m^2/g) to the nanopowder as well as the potential to get high selectivity through effects of molecular size exclusion (137 Å average pore diameter). The resulting MGC arrangement within the electrospun polymer nanofibers was expected to depend both

on graphene/polymers mass ratio and its affinity to the hosting polymers, as well as on all the parameters of the electrospinning process. Electrical parameters are related to the quality of the MGC distribution within fibers, additionally to the MGC amount. Therefore, a rearrangement inside the polymer nanofibers due to temperature changes was expected to tune electrical parameters such as the sensing properties of the fibrous layer, thus suggesting an easy and novel strategy of tuning of selectivity and sensitivity of the polymer based sensors.

Afterwards, in the second research line, the same composite fibers were loaded with a further molecule as a sensing agent: a porphyrin free-base. Porphyrins have excellent sensing properties (their framework, peripheral substituents and the core that could be practically occupied by all metals of the periodic table) that make them an effective object of study and sensor applications of the last thirty years (*Paolesse et al, 2017*). In the literature, there are several cases of porphyrins subjected to electrospun deposition in combination with electrospinnable polymers, so that their dispersion (*Olkhov et al., 2018*) and arrangement inside fibers as well as their photocatalytic (*Shao et al., 2010*) and sensing features (*Hu et al., 2017*) have been investigated extensively (*Arai et al., 2012*). On the other hand, the best performances seem to be achieved when porphyrin occupies the outer part of the fiber (*Jang et al., 2011*) or when polymer fibers are very porous. Porphyrin was used also in a ternary combination with Nylon and graphene as sensor for acid vapours.

Porphyrin, due to its molecular structure, should be responsible of the planar coordination of graphene inside fibers, (changing their conductive properties) (*Avossa et al., 2018*), and the phenyl rings of PS (modifying fiber morphology and structure) and of the selective "capturing" of volatile organic compounds (VOCs) (tuning of sensor sensitivity and selectivity). Some steps of the procedure can be visualized in Figure 5.2.

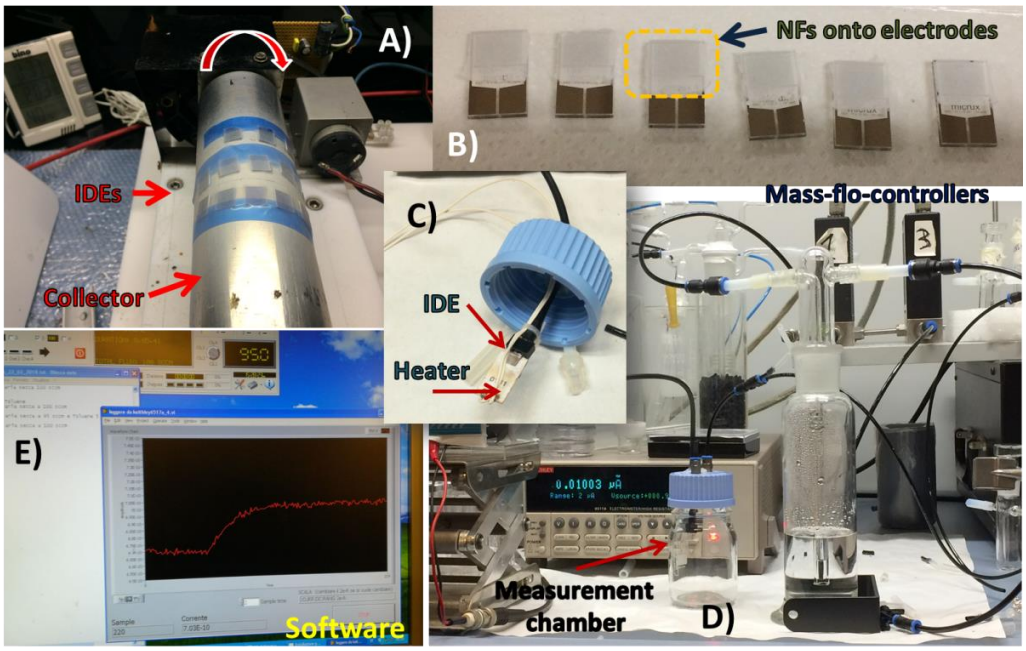

Figure 5.2. **A**) Grounded rotating collector housing a batch of IDEs coated with ESNFs; **B**) a set of IDEs showing microelectrodes coated with NF polymers; **C**) a commercial micro-heater nearby a sensor; **D**) a measurements chamber housing up two sensors; **E**) software.

5.1. Materials and Methods

Mesoporous Graphitized Carbon Nanopowder, MGC (<500 nm), Hexadecyltrimethylammonium Bromide, CTAB (~99%), Polystyrene, PS (Mw = 192,000 g/mol), Chloroform (≥99%), Acetone (≥99.5%), Toluene (≥99.8%), Polyvinylpyrrolidone, PVP (Mw = 1,300,000 g/mol), Acetic Acid, AcAc (≥99%), n-Butylamine (99.5%), Poly[(R)-3-hydroxybutyric acid, PHB (natural origin) were purchased from Sigma-Aldrich. Ethanol (≥99.8%) was obtained from Honeywell-Fluka. All chemical were used without further purification. A 5,10,15,20-tetraphenylporphyrin (H_2TPP) was prepared following literature protocol (*Fuhrop et al., 1975*). Standardized pure air (5.0) and NO_2 (5.00 ppm in N_2), were purchased from Praxair-RIVOIRA, Italy, and stored in cylinders. Interdigitated Electrodes (IDEs), provided by Micrux Technologies (Spain), were fabricated on glass substrate (IDE sizes: 10 x 6 x

0.75 mm, Pt/Ti electrodes, 120 pairs, 10 μm wide × 5 mm long × 150 nm thick, with 10 μm gap) and rinsed with soap and a "base piranha" mixture at 60°C for ~15 min, (3:1, v:v, ammonia water and hydrogen peroxide water solution) and finally with Milli-Q water (~18 MΩ cm) before any use.

First research line deposition. The electrospun dispersion for fibers no-porphyrin loaded (PS/PHB/MGC) was prepared by mixing two different solutions: one containing the matrix of the fibers (PS and PHB) called Sol1 and the other one, called Sol2, containing the carbon nanopowder dispersion stabilized by a small amount of PVP. Sol1 solution (1:0.1:0.3 = PS:PHB:CTAB, mass ratio) was prepared, first, solubilizing 450 mg of PS pellets into 9 mL of chloroform under magnetic stirring. After completely dissolution, 60 mg of PHB were added into the solution and mixed at 45°C for 2 *h*. Then CTAB 150 mg and 1 mL of ethanol were poured into the system and mixed overnight at 45°C under magnetic stirring. Sol2 dispersion (1:0.4 = MGC:PVP, mass ratio) containing 50 mg of MGC, 20 mg of PVP, 1.8 mL of chloroform and 0.2 mL of ethanol were mixed and then sonicated for ~2 *h*. Sol1 and Sol2 (1.2 mL and 36 μL, respectively) were mixed under magnetic stirring for 1 h (1:0.1:0.3:0.003:0.001 = PS:PHB:CTAB: MGC:PVP, mass ratio). The resulting dispersion was loaded into a glass syringe (1 cm long stainless steel tip) and connected to a syringe pump. The fibers deposition was carried out in a home-made ventilated clean box equipped at ambient condition. The electrospinning apparatus consisted of a high power AC-DC converter, a high voltage oscillator (100 V) driving a high voltage (ranging from 1 to 50 kV), a syringe pump (Model KDS 200, KD Scientific) and a rotating conductive pipe with a 45 mm diameter grounded collector. The fibrous layers were fabricated by applying 2.9 kV of electrostatic DC voltage between the syringe tip and the collector, at a pump feeding rate of 900 μl/h. Once the potential was applied, the

polymeric dispersion jet coated the IDEs placed on the grounded rotating collector (800 rpm), opposite to the syringe pump, at the distance of 8 cm. Deposition time was fixed at 2 min in order to obtain a thin coverage of the electrodes and water contact angle measurement.

Chemoresistors were housed in a measurement glass chamber (~100 mL volume) and connected to an electrometer (Keithley 6517) capable of measuring their electrical parameters and sending data to a PC (LabVIEW Software). The current was recorded by applying potential values from −7.0 to 7.0 V in ten steps of 0.7 V at different temperatures (20, 40, 60, 80, 100°C) generated by a micro-heater placed below each sensing area of the IDE. Currents values *vs*. applied voltage were used to calculate the resistance of the fibrous coated IDE and its correlation to the temperature.

Second research line deposition. The electrospinning procedure to get the fibers containing porphyrin were modified as follows: the dispersion for fibers containing g porphyrin was prepared by first solubilizing 450 mg of PS pellets into 9 mL of chloroform under magnetic stirring. After complete dissolution, 60 mg of PHB were added into the solution and mixed at 50 °C for 2 h. Then, 150 mg of CTAB and 1 mL of ethanol were poured into the system and mixed overnight at 50 °C under magnetic stirring. Suspensions composed of 1.3 mg of MGC with and without 15 mg of H_2TPP were poured into 2 mL of the PS/PHB/CTAB solution and sonicated for at least 1 h. The resulting polymer dispersions were loaded into glass syringes (1 cm long stainless steel and blunt tips) and connected to a syringe pump (Model KDS 200, KD Scientific). The fibers depositions were carried out in a home-made (IIA-CNR, Monterotondo, Rome, Italy) and ventilated clean box equipped at ambient condition. The electrospinning apparatus consisted of a high power AC-DC converter, a high voltage oscillator (100 V) driving a high voltage (ranging from 1 to 50 kV), a syringe pump

and a rotating conductive pipe with a 45 mm diameter grounded collector. The fibrous layers were fabricated by applying ~6 kV DC voltage between the syringe tip and the collector (8 cm of distance), at a pump feeding rate of 700 μL h^{-1}. Deposition time was fixed at 2 min to obtain a thin and adhering coverage of the surface (IDEs and SiO_2 wafers and High Precision Quartz slices). The porphyrin sensor working temperature ranged between 50 and 70 °C, such as the potential ranged between -4.0 and + 4V. For evaluating the effect of water and VOCs vapors (acetone, toluene, acetic acid, and n-butylamine) on the sensor conductivity, different compounds concentrations in air were generated by a bubbler filled with liquid water or VOCs and mixed with the gas carrier (air).

Porphyrin fibers STEM images were acquired in annular dark field mode (ADF) on a JEOL JEM-2200FS microscope operated at 200 kV and with a spot size of 2 nm (IMEM-CNR, Parma, Italy). The H_2TPP/PS-PHB-MGC fibers were deposited on a lacey carbon coated copper grid, to reduce electrostatic charging of the fibers under the electron beam. Chemical mapping of carbon and oxygen were obtained from energy dispersive X-ray spectroscopy (EDXS) using a Si-Li detector (JEOL JED-2400, Akishima, Tokyo, Japan).

The whole instrumentation used for optical and morphological characterization has been previously described.

All the batches of the chemoresistors fabricated in different dates but keeping the identical deposition parameters reported the same electrical features confirming the reproducibility of the deposition technique.

A total gas flow of 300 sccm passed through the measurement chamber, housing the IDEs. Each measurement was carried out after the complete recovery of the starting current (the baseline) under dry and clean air flow. IDE responses were calculated as $\Delta I/I_0$, where ΔI is the current variation and I_0 is the current when the air flowed.

5.2. Results and Discussion

The nanocomposite fibrous layers were grown up by electrospinning deposition using a single-needle. A diagram depicting the sensor development and its working is shown in Figure 5.2.

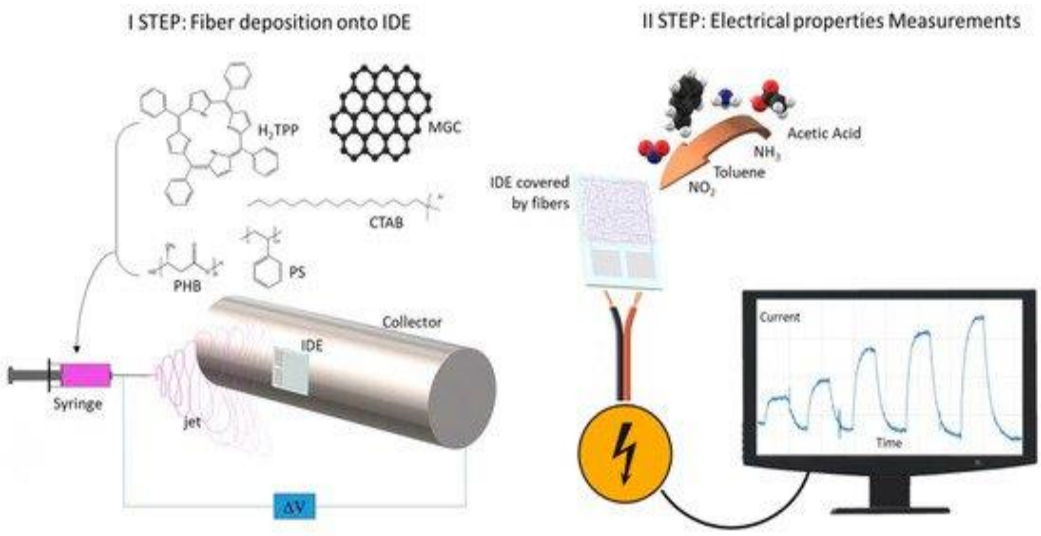

Figure 5.3. Sensor developing and usage scheme. The polymer mixture loaded in the syringe **(Left)** was electrospun by applying a voltage between the tip and the cylindrical collector where an interdigitated electrode is fixed and coated with the fibers. The coated IDE was used as transducer **(Right)** and connected to a PC for sensing current changes upon interaction with gases molecules.

The polymer drop on the needle tip, comprising PHB, PS, and MGC was subjected to an electrical field generating electric charges on the liquid surface, then repulsive electrical forces, elongation between the needle tip and collector up to the solvent evaporation and fibers formation. The transducers were fixed onto the grounded rotating cylinder in order to collect the ejected fibers on their electrodes and then be able to measure their electric and sensing features when exposed to the selected analytes. Despite the multiplicity of the components in the mixture, the electrospun traveling liquid jet stream proceeded without interruptions, micro-drops or nozzle fillings. All the substrates, i.e., IDEs, SiO_2 wafers, and Al-foils, were fixed on the cylindrical collector and aligned

within the deposition cone. After deposition IDEs and SiO_2 wafers appeared coated with a thin fibrous fabric. The heterogeneous system was collected for a few minutes on the interdigitated electrodes in order to link the metal fingers with a thin and highly porous film. Such fabrics resulted white/light grey, soft, and easy to peel off. Instead, a free-standing mat was got after at least 20 min of deposition onto the Al foil. After thermal incubation at 60°C for 12 h, the samples were investigated to outline their morphological, electrical, and sensing properties. UV-Vis spectra (data not shown) of MGC (Sol2) and MGC in PHB-PS have the typical shape of graphene dispersion in chloroform except for the main peaks due to polystyrene absorbance (260 nm). The absorption band centered at 232 nm is ascribed to π-π* transitions of aromatic C–C bonds (signals in saturation). Instead the absorbance band at 269 nm is presumed to be due to the redshift of the graphene band due to the flakes dispersion and orientation within the polystyrene suspension (*Khan et al., 2002*; *Çiplak et al., 2015*; *Uran et al., 2017*).

The morphology of the electrospun fibers is summarized in Figure 5.3. The three-component nanofibers, obtained from the mixture of PS/PHB, that are immiscible polymers, and MGC, all diluted in a $CHCl_3$ and EtOH, appeared extremely rough on the surface and decorated with jagged islands, which may indicate phase separation, but homogeneous in shape and diameter (d: 550 ± 170 nm). The long and continuous fibers as the beads absence suggested that an appropriated combination of electrospinning set of parameters was achieved (e.g., potential applied, nozzle-ground distance, the feed rate, chemical combination of solvents, viscosity, molecular weight, and structure of the carrier polymers, etc.).

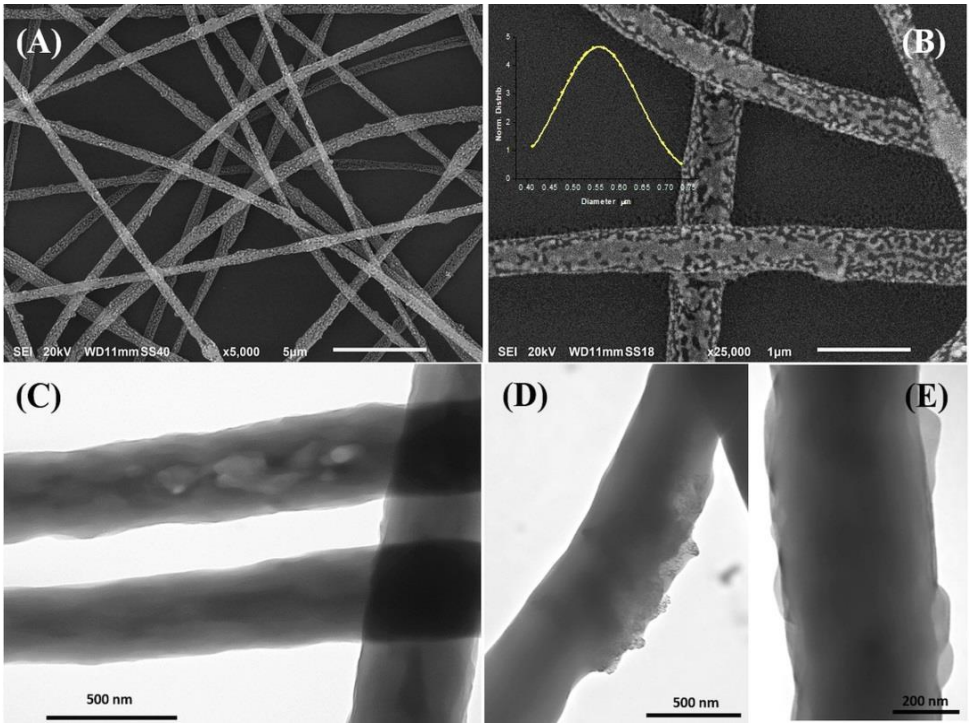

Figure 5.4. SEM (A,B) and TEM (C–E) micrographs of electrospun fibers at different magnifications. The inset in Figure B represents the diameter distribution of the fibers collected from the SEM micrographs. SEM micrographs showed cavities and roughness on the surface while TEM highlighted protrusions (E), zones with different density (C), and the MGC particles finely dispersed within the matrix (D).

Therefore the resulting IDE coating was a highly porous network of nanofibers with interconnected void volumes (high porosity) and high surface-to-volume ratios (specific surface area). Several parameters are expected to be the main responsible of the resulting fibers structure:

a) The use of an organic solvent combination ($CHCl_3$: EtOH) whereas each component has a different rate of evaporation (T_b: 61 < 78°C, respectively), viscosity (η: 0.57 < 1.20 cP, respectively) and relative polarity (0.259 < 0.654, respectively).

b) The use of a mixture of chloroform and ethanol (9:1 v/v) that are solvent and non-solvent for the polymers respectively may induce a phase separation during the electrospun fibers formation. Qi *et al*. produced highly porous Poly(L-lactic acid) (PLLA) fibers by a solvent (dichloromethane) and nonsolvent mixture (Butanol), suggesting that the higher amount of nonsolvent and volatility

difference between the nonsolvent and solvent the higher the porosity (*Qi et al., 2009*). In other works, the porosity was regulated by the humidity percentage: water (acted as a non-solvent for the polymer) diffused into the polymer jet solution causing phase separation and formation of porous fibers (*Megelski et al., 2002; Pai et al., 2009*).

c) The use of two polymers soluble in the same solvent ($CHCl_3$) but incompatible with each other, hence separating in different domains. Zhong *et al.* formed a blend of polymers by electrospinning a solution of poly(ethylene oxide) (PEO) and PS, where PEO separated in smaller domains within the PS fibers (*Zhong et al., 2011*). Bognitzki *et al.* produced fibers possessing co-continuous phase morphologies resulted from phase separation processes occurring during fiber formation of Poly(L-lactic acid) and PVP (*Bognitzki et al., 2001*).

d) The introduction of a quaternary ammonium surfactant capable of increasing polymer surface roughness. In fact, CTAB salt, increasing the charge density of the polymeric solution, can affect the average fiber diameter such as the presence of crystalline particles, can increase the surface roughness (*Sarac, 2016*).

Figure 5.3.C-E is a composition of TEM micrographs of fibers details, confirming an irregular edge of the fibers, with plicas and globosity. Since the mass ratio between PHB and PS is 0.13 and due to their immiscibility, the resulting fibers might be composed with a matrix of PS hosting a randomly dispersion of PHB in the form of small aggregates (Figure 5.3.C), that may be enhanced by the clearest areas along the fibers (lighter grey). Due to the rapid stretching of the electrified jet and the fast solvent evaporation, polymer macromolecules are forced to be oriented in the direction of elongation. This rapid event is able to inhibit the polymer chains from going back to their equilibrium conformations. As a result, electrospun nanofibers are featured by a high degree of molecular

orientation. Thus PHB and PS chains were subjected simultaneously to the same electric field strengths, but since they are basically incompatible, the stretching of the PHB chains is probably limited by the incompatibility with the PS ones, as reflected by their phase. Indeed, the phase separation was distinctly apparent with small aggregates of a polymer confined in the immiscible matrix. About the distribution of MGC along fibers, due to the low contrast between MGC sheets and the polymer matrix, it is difficult to observe the MGC networks. At higher TEM magnification darker areas appear to be finely distributed within the fiber (darker areas, Figure 5.3.D) without assembling into beads, but aggregated into clusters more or less densely packed through the fibers, where some of them protruded from the fibers. According to the MGC description provided by the supplier, they had a sheet configuration with an approximate diameter of 35 nm, forming aggregates in the 175 nm size range and then agglomerates in the 400 nm range. Further, MGC had a 137 Å average pore diameter. The resulting fibrous layer, comprising a lot of interfaces as well as the rough fibers and pores, was expected to be an intriguing system for the development of chemical sensors, due to both the wide adsorption surface and the surface energy potentials involved. The microtransducers coated with the 2 min-deposited fibers and placed on a customized micro-heater of alumina (Figure 5.2) were able to measure the electrical parameters of the resulting chemoresistor at increasing temperature values up to 100°C. However fibers coating the electrodes appeared encapsulating black MGC aggregates (optical micrograph picture of Figure 5.4 inset) suggesting that the graphene distribution was not completely homogeneous. Current-Voltage curves displayed a quasilinear relationship between the current changes and the increasing imposed voltage values. Such a chemoresistor reported a resistance value (R) of about $3.33 \cdot 10^6$ MΩ when it worked at 20°C.

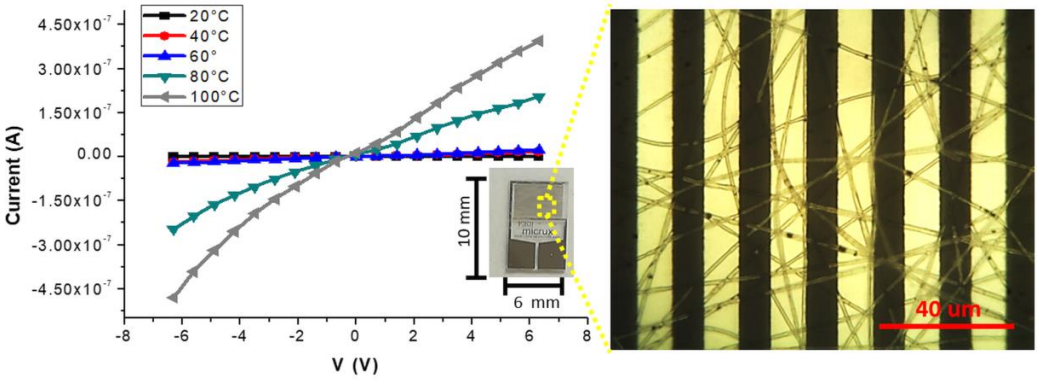

Figure 5.5. Current-Voltage curves at different temperatures (20, 40, 60, 80, 100°C) for the fibers coated IDE (inset) are plotted. On the right, an optical micrograph shows a homogeneous coverage of the transparent fibers onto the interdigitated platinum bars. The optical image highlighted the presence of sub-micrometric MGC clusters.

Obviously, electrical conductivity was strictly related to the MGC content. Changing the amount of MGC the resistance value dramatically changed (data not shown). The MGC concentration here described (0.93% mass percentage) is related to the fibrous layer containing the minimum concentration that allowed the generation of stable and reproducible electrical signals at room temperature (close to the percolation threshold). At room temperature, whereas the carbon nanopowder is dispersed inside fibers forming a non-contact mode networks, the tunneling of electrons should dominate the conduction of the composite system according to the percolation theory. Such a theory (*Mutlay et al., 2014*) proposes that below a critical concentration, conducting fillers are individually isolated in an insulating polymer. As the concentration of the nanofillers increases, an inter-connected network of particles distributed inside the matrix is formed. This arrangement makes the material to sharply change from insulator to semi-metal conductor. Beyond the critical concentration (percolation threshold) all the particles appear divided only by a thin polymer layer that allows the quantum mechanical tunneling. Further concentrating the particle network will generate saturation

and conductivity achieves an upper limit which is quite below the conductivity of pure nanofillers (metal-like). Alekseev *et al.* reported that, when conductive fillers are incorporated into polymer matrices, both their state of dispersion and their orientation are also significant for determining electrical conduction of composites (*Alekseev et al., 2012*). The relative high resistance value of MGC in PS-PHB nanofibers suggest that the graphitic powder was organized into a network allowing the fibrous layer being conductive. Further, I-V curve shape seems to be affected by the metal-like conductivity occurring within the "darker dots" where MGC were more densely packed. However, when the transducer was microheated up to 100°C, the chemoresistor reported a nonlinear increase in the current values (resistance decrease). Specifically, R abruptly decreased $9 \cdot 10^3$ times, i.e., from $3.33 \cdot 10^6$ to $3.61 \cdot 10^2$ MΩ, when temperature was increased from 20 to 40°C. The chemoresistor reached 14 MΩ resistance when the working temperature was set at 100°C. The temperature dependence of conductivity was non-linear but showed always a positive behavior upon heating. This result suggests the domination of the tunneling resistance in comparison with the contact one (*Gao et al., 2018*). The latter usually dominates in highly filled composites when physical contact between particles occurs, while the former is depending on the small dielectric barriers (insulating polymer) between the particles (*Sheng, 1980*). Polymer heating effects can be found in the chain reorientation due to a group rotation on the polymer backbone (*Alexander, 1999*), including phenyl group rotation in polystyrene. Such reorganization presumably affects the temperature dependence of conductivity due to strong π-π interaction existing between aromatic organic molecules and the basal plane of the graphene. According to Cao *et al.*, graphene sheets inside polystyrene films are able to build thermodynamically unstable networks at higher temperatures,

(*Cao et al., 2009*), thus improving the connectivity of the conductive networks and then enhance the electrical conductivity.

Measurements were carried out between 40° and 80° C since noisy at room temperature and potentially stressed at higher temperature. First of all sensors were exposed to different percentages of humidity. Thus, standard pure air with increasing percentages of water vapors was flowed throughout the measuring chamber and the changes of the sensor current were reported in Figure 5.5.A. The humidity is everywhere in the environment, thus it is crucial to control this parameter as well as to know its effects on the designed sensor (*Macagnano et al., 2016*). Indeed, water molecules in the air are commonly known as potential interfering agents in the interactions between the chemical sensors and the VOCs/gases. Measurements were ranging between dry and 50% humid air. The plot depicts a linear relationship between humidity and current changes (Figure 5.5.B), with current linearly increasing when humidity percentage increased. When the T_w (the working temperature) was set at 40°C and relative humidity was 50%, the normalized current increased by $7.46 \cdot 10^{-1}$ times. Similarly, the same measurements were carried out with the sensor set at increased temperature values. As previously reported, the current increased linearly with the humidity, but the sensor sensitivity to water vapor decreased at higher temperature. Therefore the normalized response to 50% of relative humidity, calculated as $(I-I_0)/I_0$, where I is the current value due to the reaction with the analyte and I_0 is the current value when sensor is under clean air, decreased to $3.58 \cdot 10^{-1}$ from $7.46 \cdot 10^{-1}$ when the T_w was set at 80°C. Measuring the sensitivity values at 60 and 80°C, they diminished of about 44 and 55%, respectively. Sensitivity, defined as the ratio of the incremental change in the sensor's output (Δy) to the incremental change of the measured in input (Δx), was calculated as the slope of the response curves (i.e., calibration curves) (*Kalantar-zadeh, 2013*). As a matter of fact, the fibers

were designed to get a poor interaction with water molecules. Both the polymers were hydrophobic and planar structure of MGC should prefer π-π interactions, despite H-bonds due to structural defects and terminal carboxyl groups. Instead, the experimental results reported unexpected findings. As confirmation, contact angle measurement (Figure 5.5.C-D) showed that once a droplet of water (5 µL) touched the surface of the ES mat (20 min deposition) a low water contact angle (~15°) was formed, demonstrating that fibers possessed an hydrophilic behavior, hence high affinity with water. More parameters were supposed to contribute to the unexpected sensor responses to the water, as the porosity and the interfaces among each component. Furthermore, since MGC has been designed with a mesoporous structure, it should easily entrap water molecules and interact by the oxygen atoms making part of the framework of each MGC sheet. Finally, the salt used to allow the mixing of such a heterogeneous ES suspension, being a water soluble cationic surfactant, should facilitate the adsorption of H_2O molecules on to the fiber surface. The general decreasing in sensitivity to water molecules when temperature increased is presumably related to the lowering the molecules diffusion due to the backbone motion of the polymer chains (*Ramesh and Duda, 2000*). The current variations of the sensor when exposed to a carboxylic acid (weak acid) and an amine (weak base) are reported in Figure 5.6. The shape of the transient responses indicated that the sensor responded quickly to both the analytes and it was regenerated in a few minutes by pure air. Further, the transient response shapes suggested two different VOC-surface rate of adsorption: very fast and with the reaching of a plateau in a few minutes for the amine (Langmuir-like kinetics) and linear without reaching an equilibrium phase for the acid.

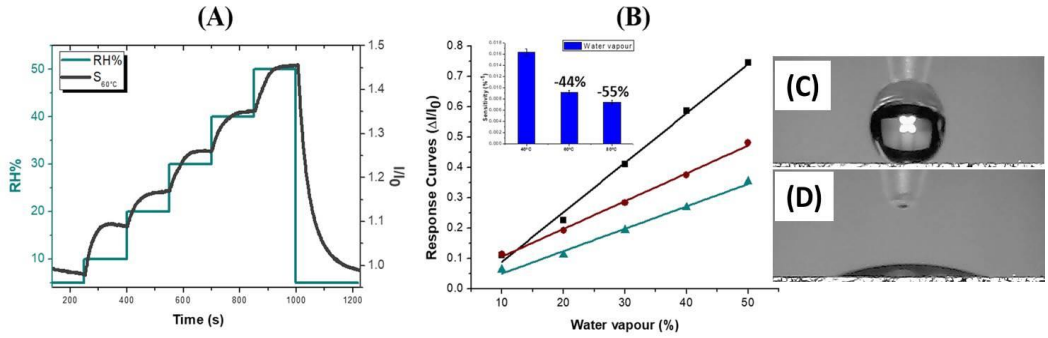

Figure 5.6. Sensor electrical features at 60°C (S60°C) in dependence on %RH: the Normalized current curves (I/I0, black) and Relative Humidity percentage (green) VS time are depicted **(A)**. Sensor Response Curves *vs.* Relative Humidity percentage at 40, 60, 80°C (green, brown and black, respectively) with an inset showing the Sensitivity values at 40, 60 and 80°C are reported **(B)**. Pictures of a water droplet of 5 µL before **(C)** and after **(D)** touching the electrospun mat.

The kinetics of AcAc (Figure 5.6, *right*) seems related to participation of multiple sites of interactions, possible lateral interactions between adsorbed molecules and a multilayer formation. The response curves depicted also different shapes within the measured ranges, meaning different affinity between the adsorbent fibers and the two VOCs. Specifically, they were linear for the amine and exponential for AcAc, but at higher concentrations.

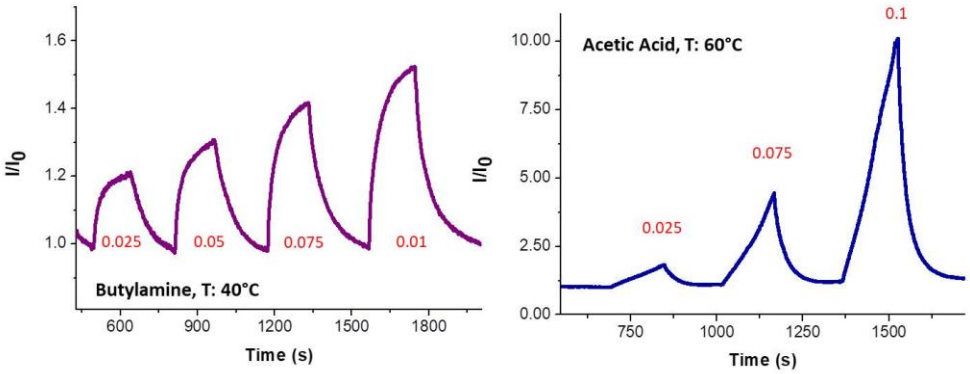

Figure 5.7. Transient response curves (Normalized current *vs* time) for Acetic Acid (*right*) and n-Butylamine (*left*).

The response curves to the increasing vapors of further tested VOCs, i.e. toluene (aromatic hydrocarbon) and acetone (ketone),

respectively, have been plotted in Figures 5.8.A,B showing curves with linear shapes, but different slopes (sensitivities). Transient response curves as the calibration curves are related to the ad/absorbing mechanisms that result in the chemical affinity of the VOCs to the material. The fibers are a heterogeneous system where MGC are the responsible of the electrical parameter: the adsorption of both polar and apolar VOCs onto mesopores (or structural defects) and planar surfaces of graphene, respectively, determine the changes in the charges density. The mesoporous structure could work as nucleation centre for entrapping and growing molecules, like AcAc, with multiple functional groups. On the other hands, these organic compounds can provide conformational changes of the hosting polymer chains, thus contributing to the redistribution of the graphene network, which is responsible for the charge flow. Since all the VOCs induced a rise in current, the effect on network distribution inside fibers could be the dominant one. A comparison of the sensitivities to several VOCs and at different T_w is reported in Figure 5.9.

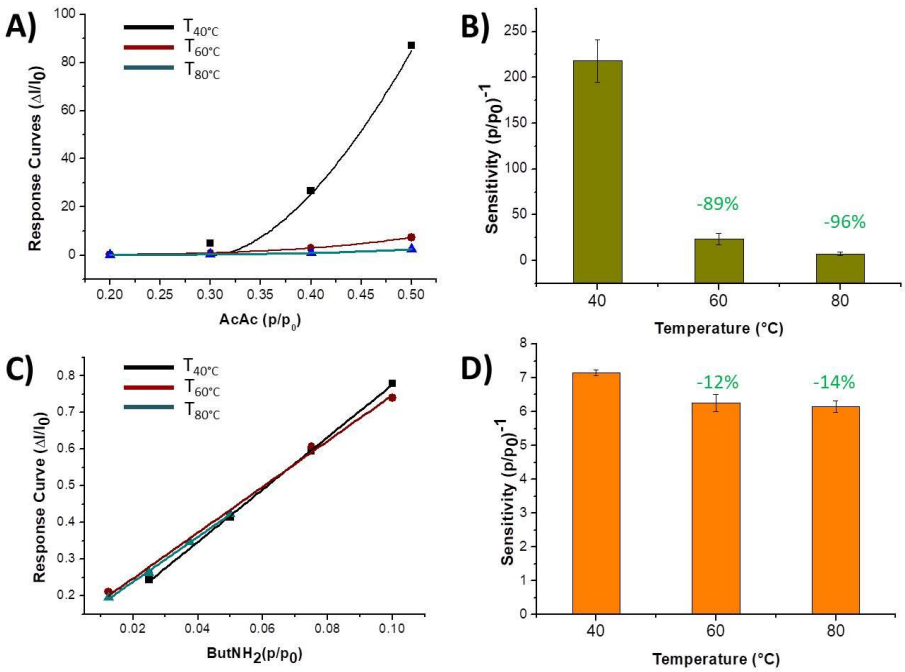

Figure 5.8. Response curves *vs* relative partial pressure at 40, 60, 80°C for Acetic Acid (A) and n-Butylamine (C) are depicted. Sensitivity of Acetic Acid (B) and n-Butylamine (D) were estimated.

When T_w increased to 60°C and then 80°C, the sensitivity to the amine (Figure 5.7.D) decreased slightly (−12 and −14%, respectively), but enormously to the acid (Figure 5.7.B) (−89 and −96%), acetone (−62 and −81%), and toluene (−50 and −78%) (Figure 5.8.C).

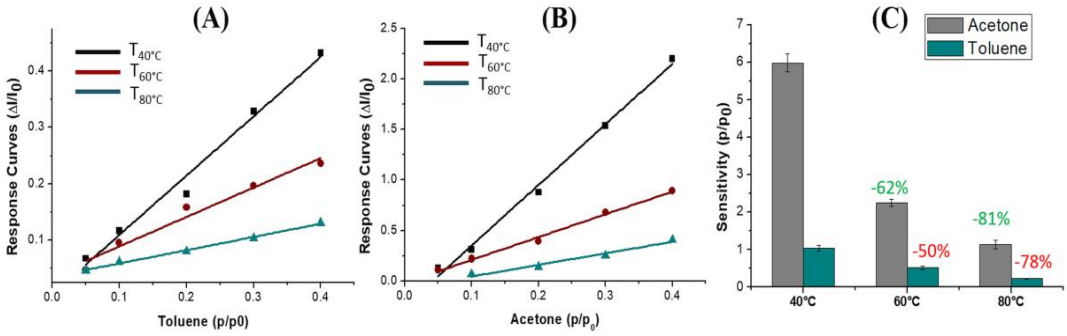

Figure 5.9. Response curves *vs* relative partial pressure at 40, 60, 80°C for Toluene **(A)** and Acetone **(B)** and corresponding sensitivity values **(C)**.

When compared to the other ones, the sensitivity to AcAc remained the highest at all temperature values, although the VOCs sensitivities ratios radically changed, reducing the global sensor selectivity (Figures 5.9).

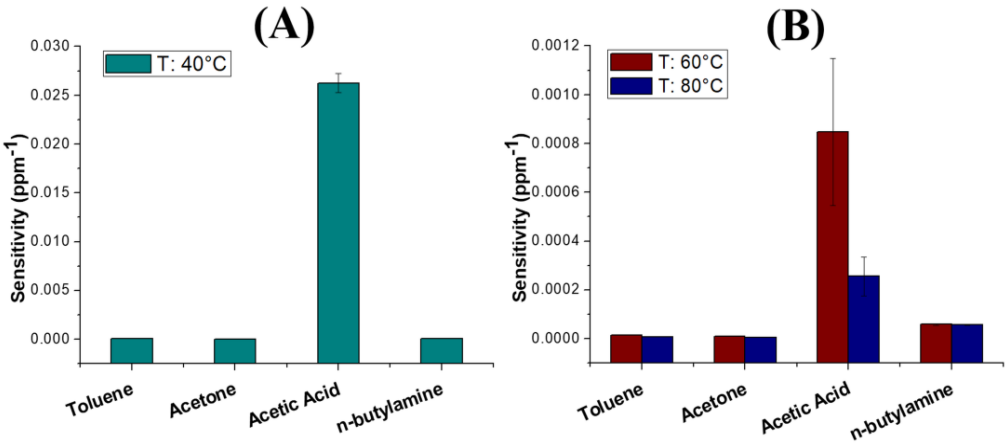

Figure 5.10. Diagram plotting sensitivity values (ppm^{-1}) of Toluene, Acetone, Acetic Acid, n-Butylamine at 40°C **(A)** and 60, 80°C **(B)**.

Higher temperature seemed to increase the permeation of amines despite the other VOCs, indeed the selectivity to n-butylamine

lightly augmented with the increase in the temperature, enhancing poor efficacy of a thermal role in the permeation and binding of the aliphatic amine with the fibers.

Since graphene and overall graphene-oxide, has been investigated as highly sensitive materials to the nitrogen oxides compounds (NOx) (*Novikov et al., 2016*), the sensor was exposed to increasing concentrations of NO_2 and the electrical signals in real time were reported in Figure 5.10.A showing an abrupt increase in current as the gas entered the measuring chamber and a likewise decrease until the baseline when pure air was flowed. More specifically, response and recovery time (t^{90}) values were measured to be <40 and <100 s, respectively. Despite to the VOCs results, when T_w increased, the sensitivity to NO_2 increased too, going from $3.91 \cdot 10^{-5}$ to $5.7 \cdot 10^{-5}$ and then to $1.16 \cdot 10^{-4}$ ppb^{-1} at 40, 60, and 80°C, respectively (Figure 5.10.B). Here the sensitivity was calculated as the slope of the curves in the linear range (i.e., at lower concentrations). The affinity of the chemosensor to NO_2 is depicted by the Langmuir-like calibration curves, as well as the significant effect of the temperature to the gas detection. Since NO_2, that is an electron withdrawing, causes an increase in current, the MGC inside fibers is supposed to perform as a p-type semiconductor, delivering electrons to the gas molecules, leading an increase of hole concentration and leading so to an increase of graphene's conductivity. The high polymer porosity seems to allow the gas diffusion. Further the sensitivity at 80°C was valued to be 4 times higher than at 40°C. The increase in sensitivity could be due to the redistribution and orientation of graphene within polymer fibers due to the heating, allowing the gas adsorption onto a larger number of exposed binding sites, despite of the unfavorable energies involved in the phenomena of ad-adsorption. The $LOD_{80°C}$ (defined as 3 * standard deviation of the blank) has been calculated to be ~2 ppb. In literature, chemoresistors based on

graphene hybrids, reported limits of detections ranging between 10 ppm and 64 ppb at room temperature (*Latif and Dickert, 2015*).

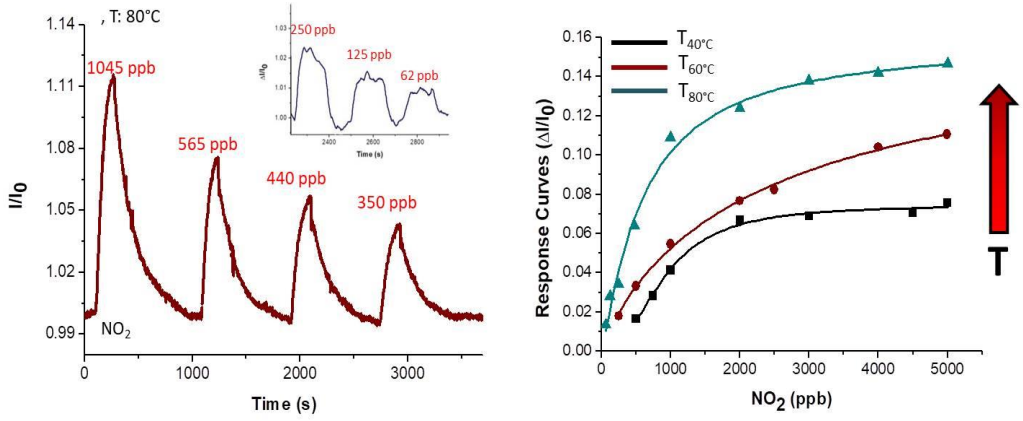

Figure 5.11. Transient response curve (normalized current *vs* time) at 80°C **(A)** and Response curves *vs* concentration at 40, 60, 80°C for NO_2 are depicted **(B)**. The inset in A showed an increase in current at lower concentration of NO_2 (150, 125, 62 ppb)

Let's move the following research line. When porphyrin was loaded, the nanocomposite fabrics appeared pink coloured (Figure 5.11.c) and porous, turning to orange when the thickness increased but white/light gray (Figure 5.11.d) if porphyrin-free. The fibers combined with H_2TPP (H_2TPP-PsB-MGC) kept the same circular cross-sectional shape but appeared much smaller in size (d: 174 ± 50 nm) (Figure 5.11.a) probably due to the decreasing of the polymer percentage in the solution. Furthermore, a higher voltage applied to the porphyrin mixture necessary to engage the electrospun process ($V_{H2TPP\text{-}PsB\text{-}MGC}$ =≈ 6 kV; $V_{PsB\text{-}MGC}$ = 2.9 kV) could also be responsible for the fiber diameter reduction when combined to a lower feed rate (i.e., 700 μL h^{-1} and 900 μL h^{-1} used for H_2TPP- PsB-MGC and PsB-MGC suspensions, respectively) (Wang et al., 2006). Porphyrin fibers looked smoother and had small spherical/elliptical bumps protruding from the whole the surface of the fibers. Therefore, the addition of the porphyrin to the composite system seemed to substantially change the morphology of the resulting fibers: in addition to dispersion forces, H_2TPP could interact with PS and graphene by π−π interactions and with PHB by

hydrogen bond. However, long, continuous and unbeaded fibers proved an appropriate combination of electrospinning set of parameters.

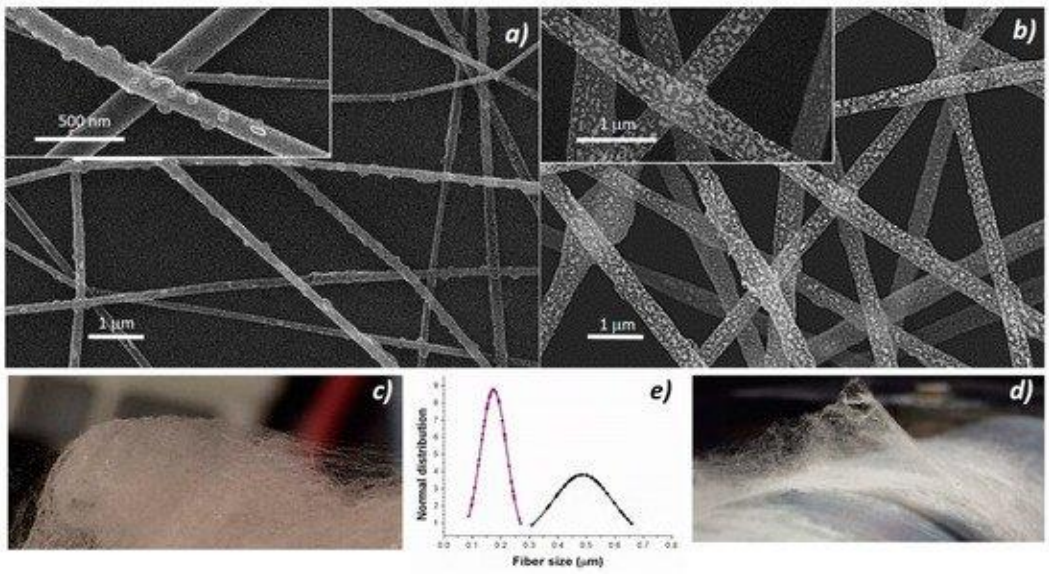

Figure 5.12. SEM micrographs of H_2TPP-PsB-MGC (**a**) and PsB-MGC (**b**) [**23**] and their respective pictures placed under (**c**,**d**). Diameter distribution graph (**e**) of H_2TPP-PsB-MGC (purple) (**a**) and PsB-MGC fibers (black) (**b**).

Figure 5.12. shows a magnified TEM micrograph focusing on a single H_2TPP-PsB-MGC fiber. The shape is regular but the heterogeneity of the fiber seems to be confirmed by areas with different contrast among the diverse nanoaggregates. For ADF-STEM imaging, the contrast (brightness/darkness) is approximately proportional to the square of the averaged atomic number projected in beam direction *z* and it depends linearly on the thickness (in particular, the bigger is the atomic number, the brighter is the image). The bright regions inside the polymer/porphyrin fiber could be due to Br^-, counterion to CTA^+ (Cetyltrimethylammonium) in the surfactant. The cationic surfactant was used to decrease the aggregation of MGC particles and improve their solubility/stability in the polymer matrix. Thus, the brightest area (a higher scattering, i.e., higher intensity in the image) distributed along the inner part of the fiber is supposed to be consequently and indirectly related also to graphene dispersion. As concerns the distribution of both polymers (PS and PHB) in the

electrospun nanofibers, we hypothesize a bulk matrix mainly composed of one of the two polymers hosting an approximately inhomogeneous dispersion of the second polymer, as a consequence of the poor polymer–polymer miscibility. According to the literature, when two polymers are soluble in the same solvent but incompatible with each other, they solidify in different domains during fiber formation. In the inset of Figure 5.12.A, the EDXS chemical map is shown, as obtained from C-K (blue) and O-K peaks (green). Oxygen looks to be more concentrated at the surface of the fiber, leading us to suppose a higher presence of PHB at the surface (carbonyl, hydroxyl and ether groups). On the other hand, the distribution of the porphyrin can hardly be highlighted by this technique since H_2TPP is also substantially constituted by C atoms with the exception of the four N atoms in the core of the macrocycle (but having close atomic number); thus, the contrast is too low to recognize the porphyrin. A high affinity between PS and H_2TPP (π−π stacking of the aromatic rings) is reported in literature where the homogeneous dispersion of the porphyrin in the surface and inside PS electrospun fibers is described using fluorescence microscopy (homogeneously red colored fibers). A weak π–π stacking could also occurs between graphene flakes surface and porphyrin molecules. Therefore, we hypothesize that porphyrin could be fairly dispersed among PS chains and MGC nanofillers in fiber inner part, and PHB arranged to the outermost part.

The UV-Vis diffuse reflectance (R%) spectrum of a H_2TPP-PsB-MGC fibrous layer (Figure 5.12.B) showed the characteristic features of the H_2TPP chromophore, with the Soret (reflectance minimum about 2.5% at 415 nm) and Q bands well defined (VI: 516 nm, R: 13%; III: 550 nm, R: 19%; II: 591 nm, R: 23%; I: 648, R: 22%). Although the Soret band showed the expected broadening in the solid state, the absence of wavelength shifts seemed to indicate that the porphyrin could be well dispersed in

the polymeric matrix. This hypothesis is also supported by the narrow Q bands.

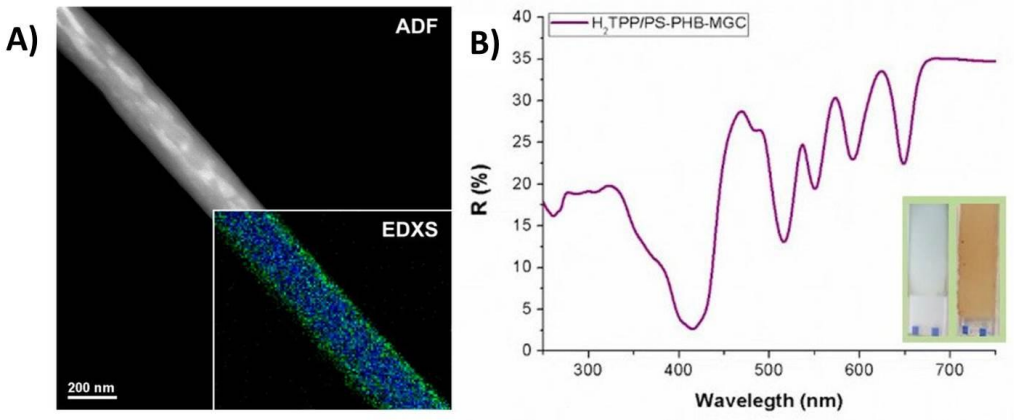

Figure 5.13. **A**) Annular dark field mode-scanning - transmission electron microscopy (ADFM-STEM) image of a porphyrin doped fiber. The inset shows the corresponding energy dispersive X-ray spectroscopy (EDXR) chemical map from carbon (blue) and oxygen (green); **B**) Diffuse reflectance ultraviolet-visible (DR-UV-Vis) spectrum of a H_2TPP PsB-MGC thick fibrous layer (the orange one in inset). Inset shows also the porhyrin-free fibrous coating (the white-grey one)

Optical microscope pictures (Figure 5.13.b) depicted a Pt-Ti microtransducer coated with 2 min-deposited fibers, which appeared optically transparent and with some small black MGC aggregates spread inside fibers (as in the fibers without porphyrin), suggesting that the graphene distribution was not completely homogeneous but enclosed within the polymer wires. Increasing the deposition time, a thicker layer was obtained, but the adhesion resulted inhomogeneous and it was more easily peelable from the transducer. To measure the electrical parameters of the resulting chemiresistor, both at room and increasing temperatures up to 70 °C, each IDE, during the current *vs*. voltage measurements, was positioned onto a customized micro-heater fabricated on alumina substrate. The supplied voltage ranged between −4 V and +4 V. Current–voltage curves displayed a quasilinear relationship between the current changes and the voltage values. Indeed, both PS and PHB, being thermoplastics, can be heated to their melting

point (T_{M_PS}: 240 °C; T_{M_PHB}: 175 °C), cooled, and reheated again without substantial degradation. The experimental melting point of porphyrin is also high enough (T_{M_H2TPP}: ≥300 °C) to allow the sensor to work properly in the established range. However, further heating involved an initial increase in current followed by a slow and irreversible increase in resistance, probably due to an irreversible arrangement of MGC inside fibers. For this reason, all experiments were carried out up to 70 °C. To compare fibers and to understand the contribution of the porphyrin to the chemiresistor electrical features, we used the same amount of graphene (≈1% mass). At room temperature (25 °C), porphyrin chemiresistor was more resistive (about 1.2×10^8 MΩ) than the porphyrin-free one (about 3.4×10^6 MΩ). The current inside fibers is supposed to occur by tunneling of electrons among MGC particles through a small insulating barrier (percolation theory). The electrical properties of such fibrous layers depend on both the quantity and the quality of the "texture" covering the electrodes. Therefore, the resulting measured electrical resistance is related to the individual fiber resistance (due to its dimension and shape), the fiber density (number of fibers per unit of surface area) and the electrode coverage. In porphyrin-fibers, nanofillers appeared distributed within the inner part of fibers, whereas the MGC aggregation inside PsB-MGC was supposed outer, then closer to the IDE metal-electrodes and with a smaller polymer barrier. A reason of this effect could be due to the arrangement of MGC inside fibers due to the porphyrin addition. Furthermore, it is known that conductivity can increase more than one order of magnitude when fiber diameter increases (*Mac Diarmid et al., 2001*). Porphyrin fibers were estimated to be much thinner than PsB-MGC one. On the other hand, thinner fibers are commonly preferred for sensor applications, since smaller-diameter wires are expected to have a faster response associated with a quicker diffusion of gas molecules through the fiber. Additionally, the collected porphyrin fibrous

coatings showed a lower density of the PsB-MGC nanofibers over the electrodes (i.e., layer more porous, Figure 5.13.b), although it increased with the same deposition time. This result could be a further reason to explain a lower conductivity of H_2TPP fibrous chemiresistor. The electrical signals at 25 and 40 °C were noisy, thus the porphyrin chemiresistor did not seem to work properly. Conversely, increasing the electrode working temperature, current increased considerably, especially when temperature value was set at 70 °C. Consequently, the signal to noise ratio increased too, and the baseline looked more stable.

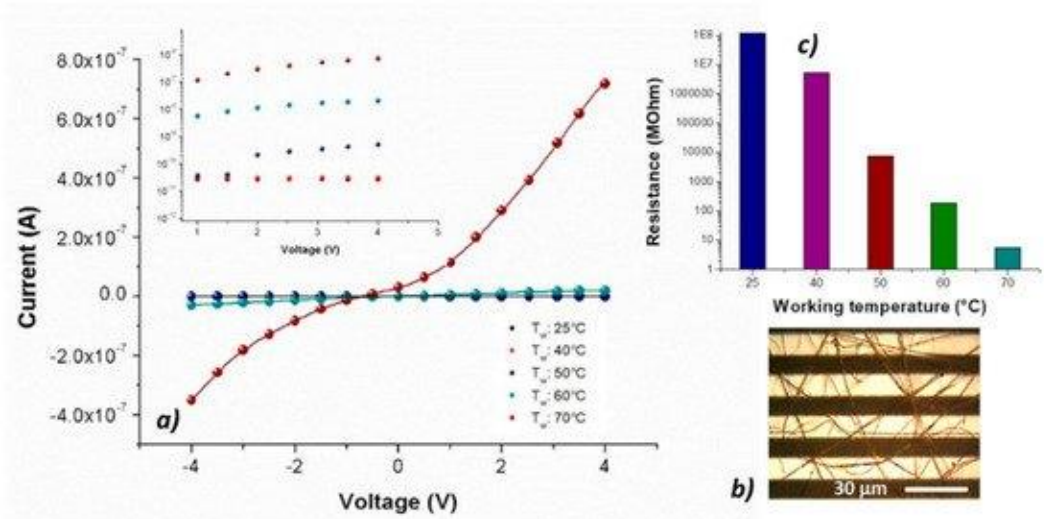

Figure 5.14. Current *vs*. voltage diagram at 25, 40, 50, 60 and 70 °C and 25, 40, 50 and 60 °C in the inset (**a**); optical image of the IDE covered by H_2TPP-PsB-MGC fiber (**b**); and resistance values diagram at 25, 40, 50, 60 and 70 °C (**c**).

When the sensor was heated from 25 to 40 °C, the electrical resistance changed by two orders of magnitude (from 10^8 to 10^6 MΩ) (Figure 5.13.c and inset). The exponential decreasing of the resistance values to the increasing 10 °C steps has been reported in the semi-logarithm bar-plot of Figure 5.13.c, where resistance changed from ≈7 × 10^3 to ≈5 MΩ, going from 50 to 70 °C. Such a non-linear dependence of conductivity on the heating apparently confirms the prevalence of the tunneling current (depending on the small dielectric barriers (insulating polymer) between the particles (*Sheng, 1980*) in comparison with the

contact one (*Syurik et al., 2013; Gao et al., 2018*), which usually should dominate in highly filled composites in contact with each other. The tunnel contribution is described by Equation (1):

$$\rho_T = e^{\left(\frac{\pi w}{2}\sqrt{\frac{2mV_0}{\left(\frac{h}{2\pi}\right)}}\right)}$$

where *ρT* is the tunnel resistivity, m is the electron rest mass, h is Planck's constant, V_0 is the height of the barrier, and w is its width (*Celzard et al., 1998*). Commonly, in a polymer nanocomposite matrix, the gap among nanofillers tends to increase with temperature due to the polymer phase volume expansion (i.e., polymer crystalline phase melting (*Feller et al., 2002*) or the amorphous phase softening (*Pillin et al., 2002*) during melting, resulting in a resistivity rise of several decades. In the fibrous chemiresistors here described, with and without porphyrin, the different results could be explained by the phenyl group rotation in polystyrene (polymer backbone chain reorientation, which allow strong π–π interactions existing between aromatic organic molecules and the basal plane of MGC. Such a rearrangement could be responsible for the connectivity improvement of the conductive network of the nanofillers, inducing the enhancement of the electrical conductivity. The interfacial force between graphene and PS could be enhanced by surface modification, which reduced the interfacial thermal resistance and dispersed graphene more uniformly. A significant contribution to the MGC rearrangement inside fibers could also be generated by the aromatic planes of H_2TPP facing graphene surfaces. Indeed, comparing both the fibrous layers resistance values, H_2TPP-PsB-MGC became less resistive than PsB-MGC, when the working temperature reached and went over 60 °C (Figure 5.14) notwithstanding the disadvantaged parameters listed above of the porphyrin layers to be conductive. More specifically, its resistance value reached ≈5.7 MΩ versus ≈81.6 MΩ of PsB-MGC measured at the same temperature (T_w: 70 °C) in dry and clean air. It means that at

lower temperature H_2TPP-PsB-MGC could work as barrier while at higher temperature it should promote conduction. By comparing both the data linear fitting, H_2TPP showed a greater sensitivity to working temperature changes (R/T=-0.172±0.016 MOhm/°C; R^2:0.97) than PsB-MGC (R/T=-0.0764±0.0288 MOhm/°C; R^2:0.78). Vapor measurements were carried out according to a dynamic mode: the sensor was exposed to a gaseous stream of molecules, the content of which was ruled by blending a stream of pure air with a second stream saturated with the vapor to be analyzed. Thus, the fibrous chemosensor was firstly deployed to increasing percentages of water vapors, ranging 0–50% with increments of 10%, and with working temperature values set at 40, 50 and 60 °C.

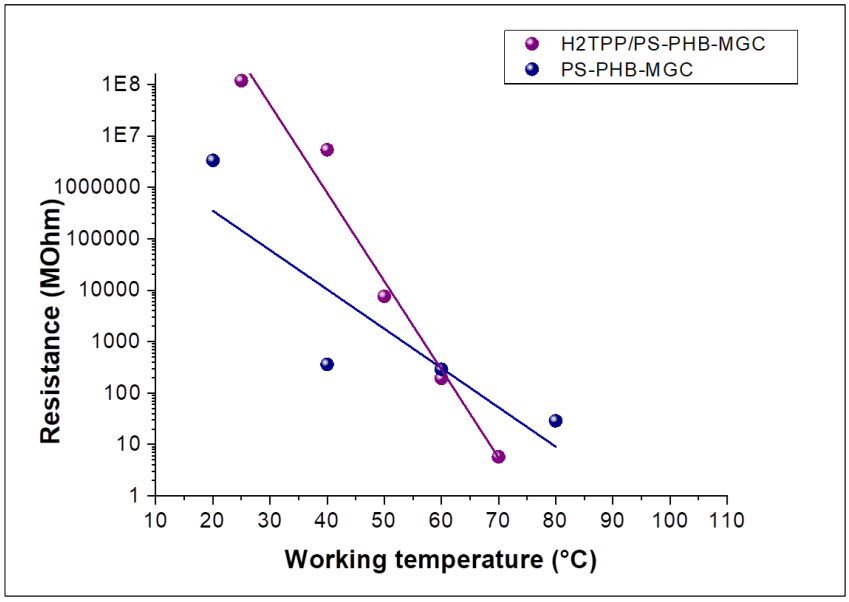

Figure 5.15. Linear fitting of resistance *vs*. working temperature for H_2TPP-PsB-MGC (purple) and PsB-MGC (blue) fibers.

Response curves are depicted in Figure 5.15.a. The current linearly increased when humidity percentage increased, too. A reason for this positive trend was the presence of the cationic surfactant inside the fibers that facilitated the dispersion of the carbon nanostructures. Another reason could be related to the porous structure of the nanofillers. When the chemosensor (T_w: 50

°C) was exposed to 50% relative humidity, it became seven times more conductive than the dried one. As expected, an inverse relationship occurred when working temperature increased: under 50% RH (relative humidity), the sensor became six (60 °C) and three times (70 °C) more conductive than under dry air, therefore generally the sensor responses to water vapors decreased with temperature. The related sensitivity values, defined as the change of measured signal per analyte concentration unit, i.e., the slope of the sensor responses graph (Figure 5.15.b), showed a decrease of 64% and 78% when the sensor worked, respectively, at 60 and 70 °C. The lowering of the affinity index to vapor due to the heating should be presumably caused by the decrease of the vapor molecules diffusion mainly due to the backbone polymer chains motion. In addition, in agreement with the kinetic theory of matter, the sorbed molecules (H-bonds and Van der Waals forces), gaining kinetic energy when heated, were able to "fly" out of the binding site. Indeed, furnishing the sufficient kinetic energy to desorb the "captured" material is the usual strategy to restore/regenerate an adsorbent. A very similar behavior is reported for PsB-MGC nanosensors.

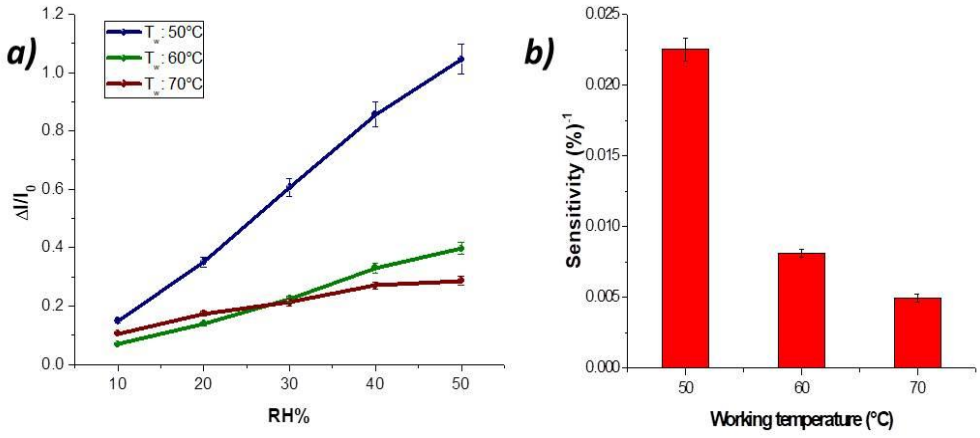

Figure 5.16. $\Delta I/I_0$–RH percentage diagram (response curves) (**a**); and sensitivity of the H_2TPP-PsB-MGC electrode at the different working temperatures (**b**).

To investigate a potential role of the porphyrin as a selective sensing agent, the fibrous chemosensor was deployed to toluene

and acetic acid vapors, the two chemicals that, among the VOC chemical classes previously tested, reported the lowest and the highest, respectively, affinity to PsB-MGC fibers. Additionally, when working temperature increased, the PsB-MGC sensitivity values decreased greatly, making that sensor suitable to work at room (or close to room) temperature for VOC detection. Finally, both acetic acid and toluene, being solvents of PHB and PS, respectively, were expected to be able to easily penetrate inside fibers. However, the analyzed vapors flowed in low concentrations (acetic acid and toluene up to 1000 and 1200 ppm, respectively) to avoid the poisoning of the sensing layers. Such a missing effect (i.e., the poisoning) was supported by no change in the baseline of the transient sensor responses, confirming that no chemical interaction had resulted in a permanent variation of the polymer structure. Thus, known concentrations of toluene vapors were generated and flowed throughout the sensor measuring chamber, and the related electrical changes are depicted in Figure 5.16. The shape of the transient responses (Figure 5.16.a) pointed out quick responses to toluene at each temperature, ranging between 50 and 70 °C, suggesting a Langmuir-like kinetics and reaching the plateau in a few minutes. However, unexpectedly, the sensor response (current values) increased by heating, reporting the highest sensitivity at 70 °C (S_{Tol70}: 1.76×10^{-3} ppm^{-1}; S_{Tol50}: 9.63×10^{-5} ppm^{-1}). The exposure to acetic acid vapors also induced fast responses, linearly related to increasing concentrations of the sample (Figure 5.17). At higher temperature, sensitivity to acetic acid increased too (S_{AcAc70}: 14×10^{-3} ppm^{-1}; S_{AcAc50}: 4.4×10^{-4} ppm^{-1}) according to an exponential rate (Figure 5.17.d,e). Further, a better signal/noise ratio was gathered as the temperature increased.

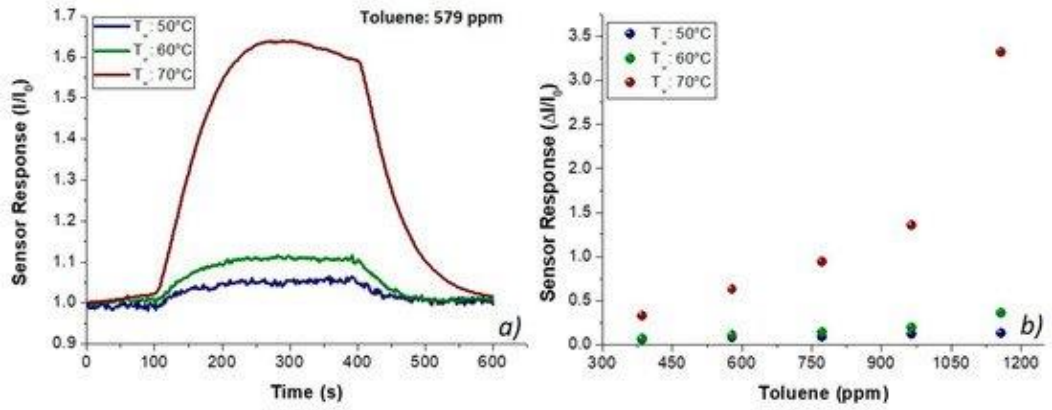

Figure 5.17. Transient responses (I/I_0 versus time) upon injection of 579 ppm of toluene in dry air (**a**); and response curves ($\Delta I/I_0$) to different toluene concentrations at increasing temperature values (50, 60 and 70 °C) (**b**).

Figure 5.18 depicts, in semi-logarithm scale, a comparison among the sensitivities to the selected chemicals, enhancing the different affinity of the material to each analyte, the same positive trend for the VOCs and the divergent trend (i.e., sensitivity decreasing) for water vapors. Therefore, going from 50 to 70 °C, the sensitivity to water vapors became five times lower; conversely, to acetic acid and toluene, it was about 32 and 18 times greater, respectively. Another significant sensor feature is the limit of detection (LOD) defined as the lowest concentration of the analyte that can be detected by the sensor under given conditions, particularly at a given temperature. Thus, LOD_{AcAc70} and LOD_{Tol70} (three standard deviations of the blank) were lowered up to ~1 and ~3 ppm, respectively.

Porphyrin contribution to the sensor features was highlighted by the shape of the normalized response rate, which described the current variation per ppm in time during the exposure to the VOCs flow (Figure 5.19).

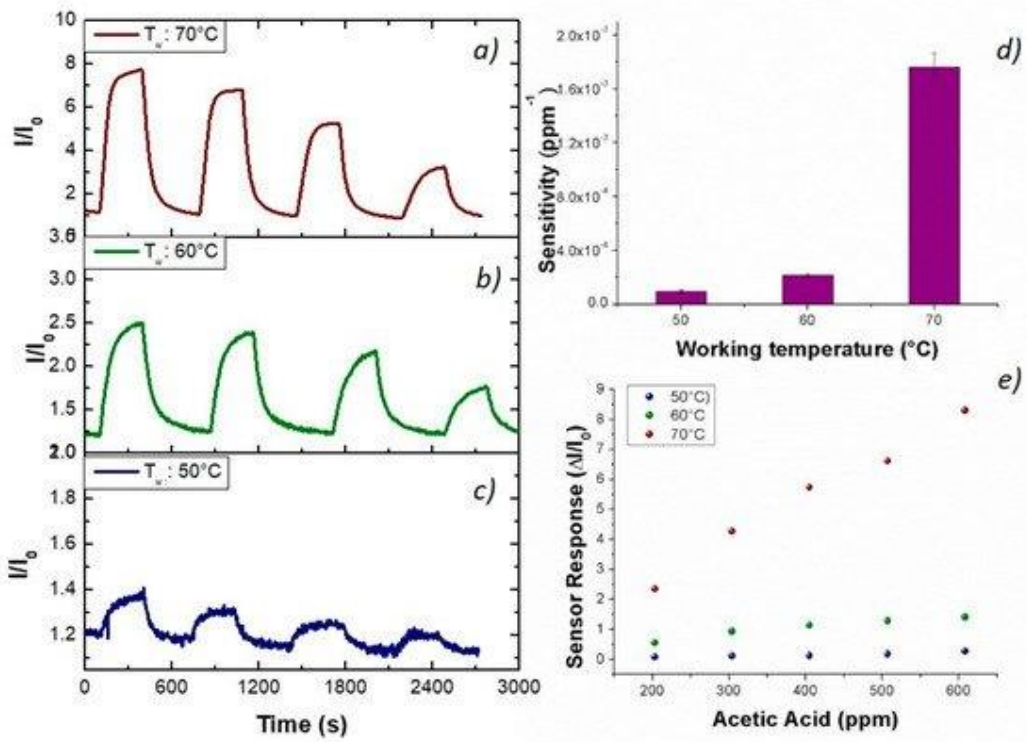

Figure 5.17. Transient responses (I/I_0 versus time) upon injection of different concentration of acetic acid in dry air at: 70 °C (**a**); 60 °C (**b**); and 50 °C (**c**); sensitivity dependence on the working temperature (**d**); and response curves ($\Delta I/I_0$) to increasing acetic acid concentrations and increasing temperature (**e**).

When toluene molecules kept in touch with the fibrous surface within the first 60 s (60 °C), a seven times higher response rate to toluene was measured for H_2TPP-PsB-MGC sensor than PsB-MGC (specifically from $6.75 \times 10^{-4} \pm 1.95018 \times 10^{-5}$ ppm^{-1} s^{-1} to $4.90 \times 10^{-3} \pm 6.27 \times 10^{-5}$ ppm^{-1} s^{-1}).

This temperature value was chosen because the current values of both sensors were comparable. The kinetic adsorption profile followed a classical Langmuir profile in both sensors but with different magnitude and adsorption rate. Since both sensors were operating at the same temperature and same toluene concentration, the main parameters involved in the sensor response were expected to be related to the number of the available binding sites and the adsorption energy (features defining the affinity between analyte and surface). Additionally, toluene could efficiently mediate the electron transfer between porphyrin and MGC.

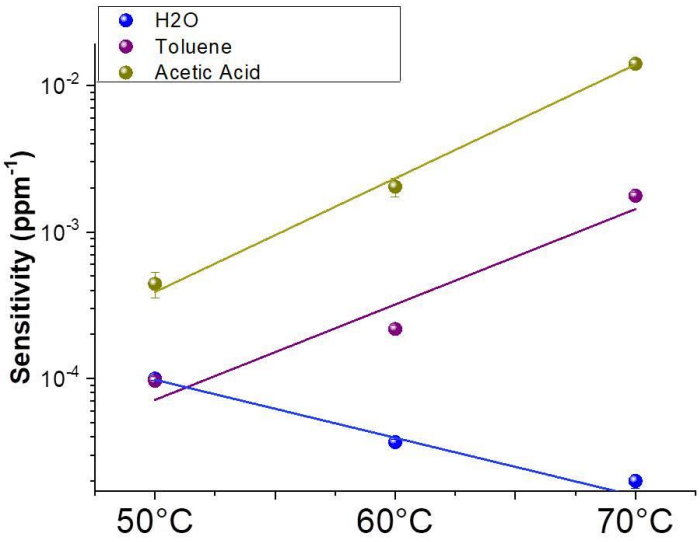

Figure 5.19. Linear fitting of the sensor sensitivity to water vapors, toluene and acid acetic, respectively, depending on the working temperature (Acetic Acid: $S/T_W=0.77\pm0.05 ppm^{-1}/°C$; Toluene: $S/T_W=0.65\pm0.17 ppm^{-1}/°C$; Water vapor: $S/T_W=-0.39\pm0.04 ppm^{-1}/°C$)

On the other hands, this organic compound could provide conformational changes of both macromolecules and hosting polymer chains (PS), thus contributing to the redistribution of the graphene network, which is responsible for the charge flow. When the sensors were exposed to acetic acid, the H_2TPP inside fibers apparently was responsible for the changes in both response magnitude and adsorption curve shape, Langmuir-like and Henry-like to with and without porphyrin sensor, respectively, indicating a higher affinity of porphyrin fibers to the analyte (Figure 5.19.a,c). Both transient response and calibration curves are the results of the ad/absorbing processes that depend on the chemical affinity of the VOCs to the material. The nanofibrous thin film can be considered as a complex and heterogeneous system where MGCs, and their arrangement through the fibers, are responsible for the resulting electrical features. Thus, the analytes have to be able to diffuse through the polymer–porphyrin matrix to be adsorbed onto the mesopores (or structural defects) and/or the planar surfaces of graphene, determining the changes in the charge density. The mesoporous structure could work as nucleation center for

entrapping and growing molecules, such as AcAc, with multiple functional groups. Simultaneously, specific hydrogen bond interaction with the four nitrogen atoms, arranged in the core of the macrocycle structure, could occur (*Nardis et al., 2011*).

Since all VOCs induced a rise in current, the effect on network distribution inside fibers could be considered the dominant one. The active contribution of porphyrin to the VOCs adsorption and to the electrical mechanisms is visualized in Figure 5.19.b,d, whereas the changes of sensitivities in temperature for both sensors enhanced the opposite curve trend: sensitivity decreasing by heating in PsB-MGC sensor and conversely increasing in H_2TPP-PsB-MGC.

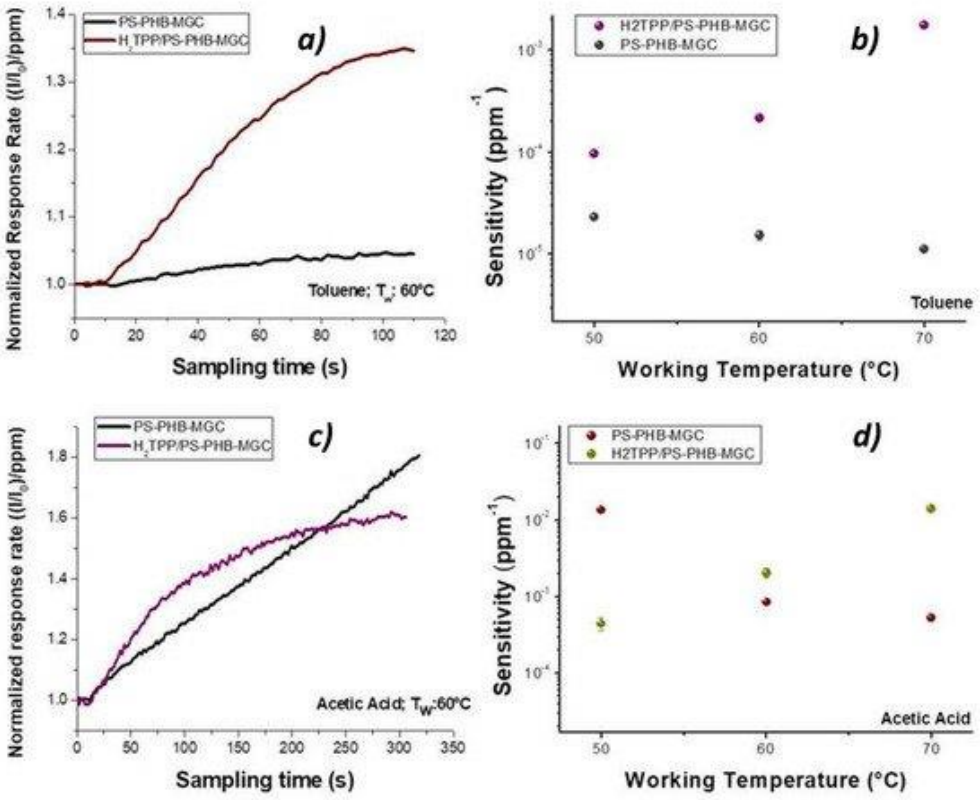

Figure 5.20. Comparison of the normalized response rate (**a**,**c**) and sensitivities (**b**,**d**) of H_2TPP-PsB-MGC and PsB-MGC to toluene (**a**,**b**) and acetic acid (**c**,**d**), respectively.

5.4. Preliminary conclusions

In my PhD thesis, conductive materials based on eco-compatible polymers were designed, created and tested in laboratory as sensors for gaseous compounds and VOCs. Electrospinning technology was exploited to get nanofibers of both a ternary and quaternary combinations of materials. Thus, nanocomposite fibers, resulting by a combination of PS, PHB and mesoporous MGC, were easily generated. The sensing surface resulted extremely porous, improving the diffusion process. Sensor could be tuned in order to be more selective to a gas (NO_2, 80°C) or a VOC (carboxylic acid, at room temperature). At this working temperature the role of the potential interferents in complex environments (as VOCs, and RH) could be significantly lowered. It is worth of nothing that the sensitivity to NO_2 is comparable to the commercial devices one. The introduction of a fourth component (H_2TPP), which is a well-known sensing agent, modified dramatically the sensing properties of the nanofibers (in addition to the morphological ones). Here, fibers were more conductive at higher temperature (60-70°C) and more sensitive to VOCs, especially to aromatic hydrocarbon (toluene, LOD: 3 ppm) and more selective, too, since these fibers seem less sensitive to NO_2 and other gas.

5.5. Outlooks

Nanofibrous sensors driven by temperature and a plethora of differently functionalized porphyrins can be designed in a series of new combinations and they should be: i) able to work alone or in array; ii) promising smart sensing textiles; iii) no-expensive; iv) low power; v) fast responses; vi) easy to be produced in large-scale and vi) to be applied for multifaceted environments; vii) first step towards eco-sensing-devices.

The results here reported were deeply described in the following scientific papers:

Avossa J., Zampetti E., De Cesare F., Bearzotti A., Scarascia-Mugnozza G., Vitiello G., Zussman E. and **Macagnano A**. Thermally Driven Selective Nanocomposite PS-PHB/MGC Nanofibrous Conductive Sensor for Air Pollutant Detection. *Frontiers in Chemistry* **2018**. doi: 10.3389/fchem.2018.00432

Avossa J., Paolesse R., Di Natale C., Zampetti E., Bertoni G., De Cesare F., Scarascia Mugnozza G. and **Macagnano A.** Electrospinning of Polystyrene/Polyhydroxybutyrate Nanofibers Doped with Porphyrin and Graphene for Chemiresistor Gas Sensors. *Nanomaterials* **2019**, 9(2), 280; https://doi.org/10.3390/nano9020280

Funding

This research was funded by a 2-Year National Project, BRIC ID.12 2016—National Institute for Insurance against Accidents at Work (INAIL), titled: "Design and development of a sensory system for the measurement of volatile compounds and the identification of job-related microorganisms".

Acknowledgments

The authors gratefully thank G. Tranfo of National Institute for Insurance against Accidents at Work for her crucial support in the BRIC ID.12 2016 Project and A.R. Taddei of High Equipment Centre, Electron Microscopy Section, University of Tuscia (VT), Italy, for providing SEM micrographs; Dr. Avossa (CNR) for his cooperation in fabricating electrospun fibers; Prof. Zussman (Technion) for fruitful discussion about the structure of fibers; Prof. Paolesse (University of Tor Vergata) for synthesizing porphyrin; Prof. Di Natale for his suggestions in sensing strategy; Prof. De Cesare (University of Tuscia) for productive discussions about the sensing application in agriculture.

6. GENERAL CONCLUSIONS

The exceptional specific surface area of the nanofibrous scaffolds created on purpose via electrospinning, together with the employment of biodegradable and biocompatible materials, resulted in efficient, eco-friendly and safe products for agriculture.

Through the exploitation of this versatile, easy to use, cost-effective and scalable technology, some nanofibrous fabrics were designed, developed and investigated as potential innovative tools within a sustainable and innovative triple approach aimed at supporting and improving agriculture productivity.

By a proper tuning of the deposition process parameters, it was possible to obtain nanofibers with desired morphology and diameter.

Furthermore, different structures of nanofibers, such as, blends or composite, hollow and porous, could be achieved by using special spinnerets or by playing with solution types and ambient conditions.

The resulting nanostructured materials were featured by high porosity, stability, permeability, and a large surface-to-volume ratio.

They were here designed and tested trying to mimic natural strategies according to specific approaches: i) providing nutrients to plants, specifically iron, by loading Fe chelating agents like phytosiderophores (mugineic acid) and phenolic compounds (catechol) on suitable biodegradable scaffoldings, then releasing them in the surroundings, in order to mobilize insoluble iron and make it absorbable by plants; ii) delivering nutrients to plants by supporting the successful colonization of soil (rhizosphere) by the adhesion and growth of beneficial microorganisms (plant growth promoting rhizobacteria, PGPR) on suitable nanofibrous supports; iii) designing and testing selective nano-composite conductive

sensors based on biodegradable and recyclable polymers, capable of detecting some biogenic gases and volatile compounds in traces (like amines, carboxylic acids, ketones, aromatic hydrocarbons, and nitrogen oxides) released in the soil upon treatments and metabolic activities.

Therefore nanostructured fabrics based on different combinations of PHB and PCL polymers were loaded with natural molecules selected on purpose, able to both mobilize insoluble iron from the environment (making it available to plant nutrition) and promote the colonization of bacteria beneficial to plants in croplands.

Thus, electrospinning procedure preserved the effectiveness of the loaded compounds as well as the modulation of the 3D-arrangement seemed a promising strategy to control their delivery rate into the surroundings.

Nanosized fibrous scaffold facilitated the adhesion of bacteria, up to biofilm formation, and keeping active the fabric for months. Similarly, nanofibrous composite polymer based sensors were set up exploiting the specific features of metalloporphyrins and graphene to create sensitive and selective sensors. They were easily generated to be used within precision agriculture systems for monitoring crop health status, with the aim of optimizing crop yield, and supporting more sustainable agro-system practices and management.

In sensor design, the employment of eco-friendly thermoplastic polymers allowed to use defined temperature values for enhancing and modulating gas-VOCs selectivity. The use of the selected thermoplastics for designing sensors allowed the temperature to be a useful parameter for modulating their selectivity, similarly to what happens for the metal oxide sensors, so that a sensor array might be created based on the same sensor working at different temperatures. The introduction of a free-base porphyrin made

fibers more sensitive to VOCs, especially to aromatic hydrocarbon and less sensitive to gas and other interferents (humidity).

We are aware that further and deeper studies are necessary to confirm the effectiveness of the proposed tools, here tested in model systems, in real and more complex ecosystems. Similarly, the efficacy of the products here proposed might be assessed also employing different molecules and polymers.

7. PERSPECTIVES

Electrospinning has been confirmed to be an attractive and suitable technology able to fit circular economy strategies, where natural derivatives can be easily redesigned, modulated and properly functionalized in order to be converted in a plethora of more sustainable outfits, like sensors, bio-scaffoldings and smart tools for agriculture.

Furthermore, economic and environmental impacts are expected by applying the developed tools in agriculture, as more efficient practices, agrochemicals and products based on natural agents able to reduce the environmental impacts of agricultural systems, but preserve their competitiveness in crop productivity.

The nanofibrous structures are expected:

i) to preserve the soil ecosystem, considered as global natural capital;
ii) to develop resource-efficient, green and competitive approaches for agricultural systems based on the use of eco-sustainable materials (biological, biodegradable and recycled materials) to create nanofibrous matrices acting as both nano(bio)fertilizers (i.e. nanostructured fertilizers loading chemical fertilizers or nutrient releasing systems composed of molecules, macromolecules or microorganisms) and nanosensors capable of monitoring the ecosystem health, quality and safety;
iii) to protect the environment from eutrophication and contamination (e.g. through the slow release of nutrients, the use of eco-friendly compounds, the employment of natural strategies);
iv) to monitor ecosystems with novel sensors based on electrospun technology;

v) to couple the nano(bio)fertilizers and the nanosensors products, created on purpose to provide nutrients and monitor environments, in an integrated system capable of releasing nutrients (controlled release) in soil and detecting and monitoring, directly or indirectly, the presence of excessive nutrients in soil ecosystems, to reduce further fertilizations and prevent the possible contamination of natural resources.

As concerns the creation of delivering nanostructures to be used as nano(bio)fertilizers, biomaterials as polyhydroxibutyrate (PHB), biodegradable polymers like polycaprolactone (PCL), and waste polymeric materials as recycled polystyrene (circular economy) have been properly processed and used to design ES nanofibrous smart fabrics with potential in providing nutrients, "nutrient-mobilising" molecules and microorganisms to soil in various combinations in order to:

i) provide nutrients mostly in a single and easy operation, to reduce the application rate and frequency;
ii) release nutrients directly into the root zone (for higher efficacy and fast absorption);
iii) minimize leaching and runoff losses (lower contamination of groundwater and surface water);
iv) combine macro- and micronutrients

Further advantages will be also related to the independence from irrigation plan, no excess of fertilisers (= no saline stress) and no fixation of nutrients onto soil particles (better efficiency).

Finally, same polymer materials (biodegradable and recycled) have been used to create sensors (low cost, low environmental impact) able to monitor gas and VOCs that could be of potential interest in precision agriculture.

In conclusion, electrospinning technology can be thought as a significant promoter of a new green revolution with reduced

farming risks, low costs and smart managing. In fact, electrospinning can work in agreement with the worldwide demand of producing renewable bio-based raw materials to replace the petroleum-based raw materials and polymers. Thus, the use of ES bio-derived polymer fabrics will be able to easily replace a number of plastic outfits also commonly used in the commercial slow-release fertilizers. Additionally, the use of natural strategies to improve crops productivity will also be able to reduce the global impact on the environment and health. The application of such bioactive products in agriculture (but also in nurseries and gardening) could become a powerful tool to improve crop production and consequently contribute in fulfilling the demand by human populations for healthy and safe foods and environment preservation. Taking into account further applications, the described polymer scaffolds could be promising candidates for more efficient microbial fuel cells, selective materials for wastewater treatment and other environmental applications, bioreactors, specific biochemical catalysts, materials for biomedical applications (*e.g.* probiotics for restoration), filtration systems, and so on. Similarly, ES represent a powerful tool to create more sustainable nanofibrous sensors, designed and developed in a series of new combinations and configurations, to detect selectively defined chemicals in different compartments (air, water and soil), according to desired arrangements towards eco-sensing-devices for precision agriculture.

8. FULL LIST OF REFERENCES

Beech I. B. , R. Gubner , V. Zinkevich , L. Hanjangsit and R. Avci, Characterisation of conditioning layers formed by exopolymeric substances of Pseudomonas NCIMB 2021 on surfaces of AISI 316 stainless steel, Biofouling, 2000, 16 , 93 —104

Flemming H. C. and J. Wingender , The biofilm matrix, Nat. Rev. Microbiol., 2010, 8 , 623 —633

Garrett T. R. , M. Bhakoo and Z. Zhang , Bacterial adhesion and biofilms on surfaces, Prog. Nat. Sci., 2008, 18 , 1049 —1056

Grossen P. , D. Witzigmann , S. Sieber and J. Huwyler , PEG-PCL-based nanomedicines: A biodegradable drug delivery system and its application, J. Controlled Release, 2017, 260 , 46 —60 .

Peters R, Brandhoff P, Weigel S, Marvin H, Bouwmeester H., Inventory of nanotechnology applications in the agricultural, feed and food sector, EFSA 2014. http://www.efsa.europa.eu/it/supporting/pub/621e/.

Abideen Z.U., Katoch A., Kim J.H., Kwon Y.J., Kim H.W., Kim S.S., Excellent gas detection of ZnO nanofibers by loading with reduced graphene oxide nanosheets, Sens. Actuators B Chem. 221 (2015) 1499e1507, http:// dx.doi.org/10.1016/j.snb.2015.07.120.

Acevedo, F., Villegas, P., Urtuvia, V., Hermosilla, J., Navia, R., and Seeger, M. (2018). Bacterial polyhydroxybutyrate for electrospun fiber production. Int. J. Biol. Macromol. 106, 692–697. doi: 10.1016/j.ijbiomac.2017.08.066

Adewopo J.B.; Van Zomeren, C.; Bhomia, RK.; et al. Top-Ranked Priority Research Questions for Soil Science in the 21st Century, *Soil Science Society of America Journal* 78 (2), 2014, 337-347. DOI: 10.2136/sssaj2013.07.0291

Albertsson, P.-A.; Andreasson, E. The constant proportion of grana and stroma lamellae in plant chloroplasts. *Physiol. Plant.* **2004**, *121*, 334–342.

Alekseev, A., Chen, D., Tkalya, E. E., Ghislandi, M. G., Syurik, Y., Ageev, O., et al. (2012). Local organization of graphene network inside graphene/polymer composites. Adv. Funct. Mater. 22, 1311–1318. doi: 10.1002/adfm.201101796

Alexander, G. M. (1999). Anomalous temperature dependence of the electrical conductivity of carbon–poly (methyl methacrylate) composites. Mater. Res. Bull. 34, 603–611.

Ali M.A., Jiang H. Mahal N.K., Weber R.J., Kumar R., et al., Microfluidic impedimetric sensor for soil nitrate detection using graphene oxide and conductive nanofibers enabled sensing interface, *Sens. Actuators B Chem.* 239 (2017) 1289e1299, http://dx.doi.org/10.1016/j.snb.2016.09.101.

Amenta V., Aschberger K., Arena M., et al., Regulatory aspects of nanotechnology in the agri/feed/food sector in EU and non-EU countries, Regulatory Toxicology and Pharmacology 73 (2015) 463e476. https://doi.org/10.1016/j.yrtph.2015.06.016

Andrzej, S., and Maciejewsk, M. (2012). "Gas sensor array with broad applicability,"in *Sensor Array*, ed Wuqiang Yang InTech. Available online at: http://www.intechopen.com/books/sensor-array/gas-sensor-array-with-broad-applicability.

Antisari, L.V.; Carbone, S.; Gatti, A.; Vianello, G.; Nannipieri, P. Uptake and translocation of metals and nutrients in tomato grown in soil polluted with metal oxide (CeO_2, Fe_3O_4, SnO_2, TiO_2) or metallic (Ag, Co, Ni) engineered nanoparticles. *Environ. Sci. Pollut. Res.* **2015**, *22*, 1841–1853

Arai, T.; Tanaka, M.; Kawakami, H. Porphyrin-Containing Electrospun Nano fi bers: Positional Control of Porphyrin Molecules in Nano fibers and Their Catalytic Application. *Appl. Mater. Interfaces* **2012**.

Avossa, J.; Zampetti, E.; De Cesare, F.; Bearzotti, A.; Scarascia-Mugnozza, G.; Vitiello, G.; Zussman, E. Thermally Driven Selective Nanocomposite PS-PHB/MGC Nanofibrous Conductive Sensor for Air Pollutant Detection. *Front. Chem.* **2018**, *6*, 1–14

Baker, N.R. Chlorophyll Fluorescence: A Probe of Photosynthesis In Vivo. Annu. Rev. Plant Biol. **2008**, 59, 89–113

Bansal P. *Water-Based Polymeric Nanostructures for Agricultural Applications.* PhD Thesis 2010 Philipps-Universitat Marburg. http://archiv.ub.uni-marburg.de/diss/z2010/0643/pdf/dpb.pdf

Bisotto-de-Oliveira R, De Jorge B C, Roggia I, Sant'Ana J, Pereira C N. Nanofibers as a Vehicle for the Synthetic Attactant TRIMEDLURE to be Used for Ceratitis capitata Wied: (Diptera, Tethritidae) Capture. *Journal of Research Updates in Polymer Science* 2014; 3: 40.

Bisotto-de-Oliveira R, Morais R M, Roggia I, Silva S J N, Ana J S, Pereira C N. Polymers nanofibers as vehicles for the release of the synthetic sex pheromone of Grapholita molesta (Lepidoptera, Tortricidae). *Revista Colombiana de Entomologia* 2015; 41: 262.

Bognitzki, M., Czado, W., Frese, T., Schaper, A., Hellwig, M., Steinhart, M., et al. (2001). Nanostructured fibers via electrospinning. Adv. Mater. 13, 70–72. doi: 10.1002/1521-4095(200101)13:1<70::AID-ADMA70>3.0.CO;2-H

Bolhar-Nordenkampf, H.R.; Long, S.P.; Baker, N.R.; Oquist, G.; Schreiber, U.; Lechner, E.G. Chlorophyll fluorescence as a probe of the photosynthetic competence of leaves in the field: A review of current instrumentation. *Funct. Ecol.* **1989**, *3*, 497–514.

Bolotin, K. I., Sikes, K. J., Jiang, Z., Klima, M., Fudenberg, G., Hone, J., et al. (2008). Ultrahigh electron mobility in suspended graphene. Solid State Commun. 146, 351–355. doi: 10.1016/j.ssc.2008.02.024

Briat, J.F.; Dubos, C.; Gaymard, F. Iron nutrition, biomass production, and plant product quality. *Trends Plant Sci.* **2015**, *20*, 33–40

Bugnicourt, E.; Cinelli, P.; Lazzeri, A.; Alvarez, V. Polyhydroxyalkanoate (PHA): Review of synthesis, characteristics, processing and potential applications in packaging. *Express Polym. Lett.* **2014**, *8*, 791–808

Canarini, A.; Kaiser, C.; Merchant, A.; Richter, A.; Wanek, W. Root exudation of primary metabolites: Mechanisms and their roles in plant responses to environmental stimuli. *Front. Plant Sci.* **2019**, *10*, 157.

Cao, Q., Song, Y., Tan, Y., and Zheng, Q. (2009). Thermal-induced percolation in high-density polyethylene/carbon black composites. Polymer 50, 6350–6356. doi: 10.1016/j.polymer.2009.10.059

Cape JN (2003) Effects of airborne volatile organic compounds on plants. Environ Pollut 122:145–157

Castro-Enriquez D D, Rodriguez-Felix F, Ramirez-Wong B, Torres-Chavez P I, Castillo-Ortega M M, Rodriguez-Felix D E, Armenta-Villegas L, Ledesma-Oasuna A I. Preparation, Characterization and Release of Urea from Wheat Gluten Electrospun Membranes. *Materials* 2012; 5: 2903.

Celzard, A.; McRae, E.; Marêché, J.F.; Furdin, G.; Sundqvist, B. Conduction mechanisms in some graphite– polymer composites: Effects of temperature and hydrostatic pressure. *J. Appl. Phys.* 1998, *83*, 1410–1419.

Chakraborty S. , S. Mukherji and S. Mukherji , Surface hydrophobicity of petroleum hydrocarbon degrading Burkholderia strains and their interactions with NAPLs and surfaces, Colloids Surf., B, 2010, 78 , 101 —108

Choi S.-W., Zhang J., Akash K., Kim S.S., H2S sensing performance of electrospun CuO-loaded SnO2 nanofibers, Sens. Actuators B Chem. 169 (2012) 54e60, http://dx.doi.org/10.1016/j.snb.2012.02.054

Çiplak, Z., Yildiz, N., and Çalimli, A. (2015). Investigation of Graphene/Ag nanocomposites synthesis parameters for two different synthesis methods. Fullerenes Nanotub. Carbon Nanostruct. 23, 361–370. doi: 10.1080/1536383X.2014.894025

Costerton J. W. Introduction to biofilm, Int. J. Antimicrob. Agents, 1999, 11 , 217 —221

Dalla Torre, G.; Mujika, J.I.; Formoso, E.; Matito, E.; Ramos, M.J.; Lopez, X. Tuning the affinity of catechols and salicylic acids towards Al(III): Characterization of Al-chelator interactions. *Dalton Trans.* **2018**, *47*, 9592

Damasceno R, Roggia I, Pereira C, Sa E. Rhizobia survival in seeds coated with polyvinyl alcohol (PVA) electrospun nanofibres. *Can. J. Microbiol.* 2013; 716.

Darbani, B.; Briat, J.F.; Holm, P.B.; Husted, S.; Noeparvar, S.; Borg, S. Dissecting plant iron homeostasis under short and long-term iron fluctuations. *Biotechnol. Adv.* **2013**, *31*, 1292–1307

De Cesare F., Di Mattia E., Pantalei S., Zampetti E., Vinciguerra V., Canganella F., Macagnano A., Use of electronic nose technology to measure soil microbial activity through biogenic volatile organic compounds and gases release, *Soil Biology and Biochemistry* (2011) 43: 2094-2107

De Cesare F., Di Mattia E., Zussman, Macagnano A., A study on the dependence of bacteria adhesion on the polymer nanofibre diameter Env Sci Nano 6 **2019** 778-797 (a)

De Cesare F., E. Di Mattia and A. Macagnano , Fishing bacteria with a nanonet, Mater. Today, 2017, 20 , 284 —285 .

De Cesare F., Pietrini F., Zacchini M., Scarascia Mugnozza G. and Macagnano A., Catechol-Loading Nanofibrous Membranes for Eco-Friendly Iron Nutrition of Plants, Nanomaterials 2019, 9(9), 1315; https://doi.org/10.3390/nano9091315 (b)

De Cesare F., Pantalei S., Zampetti E., Macagnano A., Electronic nose and SPME techniques to monitor phenanthrene biodegradation in soil, *Sensors and Actuators B* 131 (2008) 63–70

De Gregorio PR, Michavila G, Ricciardi Muller L, de Souza Borges C, Pomares MF, Saccol de Sá EL, Pereira C, Vincent PA. Beneficial rhizobacteria immobilized in nanofibers for potential application as soybean seed bioinoculants. *PLoS ONE* 2017; 12(5): e0176930.

Du Jardin, P. Plant biostimulants: Definition, concept, main categories and regulation. *Sci. Hortic.* **2015**, *196*, 3–14.

Dunne, W. M. Bacterial adhesion: Seen any good biofilms lately?, Clin. Microbiol. Rev., 2002, 15 , 155 —166 .

Fares S., Scarascia Mugnozza G., Corona P, Palahí M., Five steps for managing Europe's forests. *Nature* 519, 2015 407–409

Feller, J.F.; Linossier, I.; Grohens, Y. Conductive polymer composites: comparative study of poly(ester)—Short carbon fibres and poly(epoxy)—Short carbon fibres mechanical and electrical properties. *Polym. Adv. Technol.* **2002**, *57*, 64–71.

Figueiredo MV, Seldin L., et al., Plant growth promoting Rhizobacteria: fundamentals and applications in Plant Growth and Health Promoting Bacteria, 2010. DOI: 10.1007/978-3-642-13612-2_2

Flemming H. C. Ecological Biochemistry: Environmental and Interspecies Interactions , G.-J. Krauss and D. H. Nies, Wiley-VCH Verlag GmbH & Co. KGaA, 2015, pp. 277–291

Fraceto L.F., Grillo R., de Medeiros G.A., Scognamiglio V., Rea G., Bartolucci C., Nanotechnology in Agriculture: Which Innovation Potential Does It Have?, *Front. Environ. Sci*., 22 March 2016 | https://doi.org/10.3389/fenvs.2016.00020

Fuhrhop, J.H.; Smith, K.M. Laboratory methods. In *Porphyrins and Metalloporphyrins*; Smith, K.M., Ed.; Elsevier Science: Amsterdam, The Netherlands, 1975; pp. 757–869.

Gao, C., Liu, P., Ding, Y., Li, T., Wang, F., Chen, J., et al. (2018). Non-contact percolation of unstable graphene networks in poly(styrene-co-acrylonitrile) nanocomposites: electrical and rheological properties. Compos. Sci. Technol. 155, 41–49. doi: 10.1016/j.compscitech.2017.11.023

Gao, C.; Liu, P.; Ding, Y.; Li, T.; Wang, F.; Chen, J.; Zhang, S.; Li, Z.; Yang, M. Non-contact percolation of unstable graphene networks in poly(styrene-co-acrylonitrile) nanocomposites: Electrical and rheological properties. *Compos. Sci. Technol.* **2018**, *155*, 41–49.

Garcia-Rodríguez, A.; Matamoros, V.; Fontàs, C.; Salvadó, V. The ability of biologically based wastewater treatment systems to remove emerging organic contaminants—A review. *Environ. Sci. Pollut. Res.* **2014**, *21*, 11708–11728

Gouda S, Kerry RG, Das G, Paramithiotis S, Shin HS, Patra JK. Revitalization of plant growth promoting rhizobacteria for sustainable development in agriculture. Microbiol Res. 2018 Jan;206:131-140. doi: 10.1016/j.micres.2017.08.016.

Han, J.; Liang C.; Cui, Y.; Xiong, L.; Guo, X.; Yuan, X.; Yang, D.; Encapsulating Microorganisms inside Electrospun Microfibers as a Living Material Enables Room-Temperature Storage of Microorganisms, ACS Appl. Mater. Interfaces 10 (45) **2018** 38799-38806

Hankermeyer, C. R., and Tjeerdema, R. S. (1999). Polyhydroxybutyrate: plastic made and degraded by microorganisms, in Rev Env Contam Toxicol, ed G. W. Ware (New York, NY: Springer), 1–24.

He C., Nie W., Feng W., Engineering of biomimetic nanofibrous matrices for drug delivery and tissue engineering, *Journal of Materials Chemistry B* 45 2014 7828-7848

Heege H.J., *Precision in Crop Farming*, 2013, 1-349. Springer Science+Business Media Dordrecht 2013. DOI: 10.1007/978-94-007-6760-7.ISBN 978-94-007-6760-7

Hider, R.C.; Kong, X. Chemistry and biology of siderophores. *Nat. Prod. Rep.* **2010**, *27*, 637–657

Hu, M.; Kang, W.; Zhao, Y.; Shi, J.; Cheng, B. A fluorescent and colorimetric sensor based on a porphyrin doped polystyrene nanoporous fiber membrane for HCl gas detection. *RSC Adv.* **2017**.

Ingale A.G. and Chaudhari A.N., Biogenic Synthesis of Nanoparticles and Potential Applications: An EcoFriendly Approach. *Journal of Nanomedicine & Nanotechnology*, 2013, 4:165. doi:10.4172/2157-7439.1000165

Insam H., Seewald Martin S.A., Volatile organic compounds (VOCs) in soils Biology and Fertility of Soils 46 2010 199-213

Jang, K.; Baek, I.W.; Back, S.Y.; Ahn, H. Electrospinning of porphyrin/polyvinyl alcohol (PVA) nanofibers and their acid vapor sensing capability. *J. Nanosci. Nanotechnol.* **2011**, *11*, 6102–6108.

Kalantar-zadeh, K. (2013). Sensors. New York, NY: Springer Science+Business Media. doi: 10.1007/978-1-4614-5052-8_2

Kampeerapappun P, Phanomkate N. Slow Release Fertilizer from Core-Shell Electrospun Fibers. *Chiang Mai J Sci* 2013: 40: 775

Khalil A., Kim J.J., Tuller H.L., Rutledge G.C., Hashaikeh R., Gas sensing behavior of electrospun nickel oxide nanofibers: effect of morphology and microstructure, Sens. Actuators B Chem. 227 (2016) 54e64, http:// dx.doi.org/10.1016/j.snb.2015.12.012

Khan, M. S., Khan, W., Khan, S. A., and Iqbal, Y. (2002). UV absorbance studies of dilute polystyrene solutions in different solvents. J. Chem. Soc. Pak. 24, 237–240

Krishnamoorthy V, Rajiv S., An eco-friendly top-down approach to nutrient incorporated electrospun seed coating for superior germination potential, *Journal of Advanced Applied Scientific Research* 2017, 1:1

Ladd T. I. and J. W. Costerton , 9 Methods for Studying Biofilm Bacteria, Methods Microbiol., 1990, 22 , 285 —307

Latif, U., and Dickert, F. L. (2015). Graphene hybrid materials in gas sensing applications. Sensors15, 30504–30524. doi: 10.3390/s151229814

Lee J.H., Katoch A., Choi S.W., Kim J.H., Kim H.W., Kim S.S., Extraordinary improvement of gas-sensing performances in SnO2 nanofibers due to creation of local p-n heterojunctions by loading reduced graphene oxide nanosheets, ACS Appl. Mater. Interfaces 7 (2015) 3101e3109, http://dx.doi.org/ 10.1021/am5071656.

Lemanceau, P.; Bauer, P.; Kraemer, S.; Briat, J.F. Iron dynamics in the rhizosphere as a case study for analyzing interactions between soils, plants and microbes. *Plant Soil* **2009**, *321*, 513–535.

Leng, R.A. *Duckweed: A Tiny Aquatic Plant with Enormous Potential for Agriculture and Environment*; FAO: Rome, Italy, 1999

Levi, S.; Rovida, E. The role of iron in mitochondrial function. *Biochim. Biophys. Acta Gen. Subj.* **2009**, *1790*, 629–636.

Li, J.; Hu, J.; Ma, C.; Wang, Y.; Wu, C.; Huang, J.; Xing, B. Uptake, translocation and physiological effects of magnetic iron oxide (γ-Fe_2O_3) nanoparticles in corn (*Zea mays* L.). *Chemosphere* **2016**, *159*, 326–334

Lichtenthaler, H.K. Plastoglobuli, Thylakoids, chloroplast structure and development of plastids. In *Plastid Development in Leaves during Growth and Senescence*; Biswal, B., Krupinska, K., Biswal, U.C., Eds.; Springer Netherlands: Dordrecht, The Netherlands, **2013**; Volume 36, pp. 337–361. ISBN 978-94-007-5723-3.

Macagnano A., Zampetti E., Kny, E., *Electrospinning for high performance Sensor*, 2015, Springer International Publishing, ISBN: 978-3-319-14405-4

Macagnano, A.; Perri, V.; Zampetti, E.; Bearzotti, A.; De Cesare, F. Humidity effects on a novel eco-friendly chemosensor based on electrospun PANi/PHB nanofibres. *Sens. Actuators B Chem.* **2016**, *232*, 16–27.

MacDiarmid, A.G.; Jones, W.E., Jr.; Norris, I.D.; Gao, J.; Johnson, A.T., Jr.; Pinto, N.J.; Hone, J.; Han, B.; Ko, F.K.; Okuzaki, H.; et al. Electrostatically-generated nanofibers of electronic polymers. *Synth. Met.* **2001**, 27–30.

Megelski, S., Stephens, J. S., Bruce Chase, D., and Rabolt, J. F. (2002). Micro- and nanostructured surface morphology on electrospun polymer fibers. Macromolecules 35, 8456–8466. doi: 10.1021/ma020444a

Mercante L.A., Scagion V.P., Migliorini F.L., Mattoso L.H.C, Correa D.S., Electrospinning-based (bio)sensors for food and agricultural applications: A review, Trends in Analytical Chemistry 91 (2017) 91e103

Mikandawire, M.; Teixeira Da Silva, J.A.; Dudel, E.G. The *Lemna* bioassay: Contemporary issues as the most standardized plant bioassay for aquatic ecotoxicology. *Crit. Rev. Environ. Sci. Technol.* **2014**, *44*, 154–197

Mondal, D.; Griffith, M.; Venkatraman, S.S. Polycaprolactone-based biomaterials for tissue engineering and drug delivery: Current scenario and challenges. *Int. J. Polym. Mater. Polym. Biomater.* **2016**, *65*, 255–265

Morales, F.; Belkhodja, R.; Abadía, A.; Abadía, J. Photosystem II efficiency and mechanisms of energy dissipation in iron-deficient, field-grown pear trees (*Pyrus communis* L.). *Photosynth. Res.* **2000**, *63*, 9–21.

Mutlay, I., and Tudoran, L. B. (2014). Percolation behavior of electrically conductive graphene nanoplatelets/polymer nanocomposites: theory and experiment. Fullerenes Nanotub. Carbon Nanostruct. 22, 413–433. doi: 10.1080/1536383X.2012.684186

Nardis, S.; Pomarico, G.; Tortora, L.; Capuano, R.; D'Amico, A.; Di Natale, C.; Paolesse, R. Sensing mechanisms of supramolecular porphyrin aggregates: a teamwork task for the detection of gaseous analytes. *J. Mater. Chem.* **2011**, *21*, 18638.

Novikov, S., Lebedeva, N., Satrapinski, A., Walden, J., Davydov, V., and Lebedev, A. (2016). Graphene based sensor for environmental monitoring of NO2. Sensors Actuators B Chem. 236, 1054–1060. doi: 10.1016/j.snb.2016.05.114

OECD Guideline 221: Lemna sp. Growth Inhibition Test. In Guidelines for the Testing of Chemicals; OECD Publishing: Paris, 2006 ISBN 9789264016194

Olkhov, A.A.; Karpova, S.G.; Tubayeva, P.M.; Lobanov, A.V.; Kurnosov, A.S.; Mastalygina, E.E.; Iordanskii, A.L. Supramolecular structure of electrospun ultrathin fibers based on poly-(3-hydroxibutirate) with zinc-tetraphenylporphyrin complex. *AIP Conf. Proc.* **2018**, *2051*.

Osório, J.; Osório, M.L.; Correia, P.J.; de Varennes, A.; Pestana, M. Chlorophyll fluorescence imaging as a tool to understand the impact of iron deficiency and resupply on photosynthetic performance of strawberry plants. Sci. Hortic. (Amsterdam). 2014, 165, 148–155

Pai, C. L., Boyce, M. C., and Rutledge, G. C. (2009). Morphology of porous and wrinkled fibers of polystyrene electrospun from dimethylformamide. Macromolecules 42, 2102–2114. doi: 10.1021/ma802529h

Palvannan T, Saravanakumar T, Unnithan A R, Chung N J, Kim D H, Park S M. Efficient transformation of phenyl urea herbicide chloroxuron by laccase immobilized on zein polyurethane nanofiber. Journal of Molecular Catalysis B: Enzymatic 2014; 99: 156

Pang Z., Fu J., Luo L., Huang F., Wei Q., Fabrication of PA6/TiO2/PANI composite nanofibers by electrospinning-electrospraying for ammonia sensor, Coll. Surf. A Physicochem. Eng. Asp. 461 (2014) 113e118, http://dx.doi.org/ 10.1016/j.colsurfa.2014.07.038

Paolesse, R.; Nardis, S.; Monti, D.; Stefanelli, M.; Di Natale, C. Porphyrinoids for Chemical Sensor Applications. *Chem. Rev.* **2017**, 2517–2583.

Paramonova, N.V.; Shevyakova, N.I.; Kuznetsov, V.V. ultrastructure of chloroplasts and their storage inclusions in the primary leaves of *Mesembryanthemum crystallinum* affected by putrescine and NaCl. *Russ. J. Plant Physiol.* **2004**, *51*, 86–96.

Pietrini, F.; Bianconi, D.; Massacci, A.; Iannelli, M.A. Combined effects of elevated CO_2 and Cd-contaminated water on growth, photosynthetic response, Cd accumulation and thiolic components status in *Lemna minor* L. *J. Hazard. Mater.* **2016**, *309*, 77–86.

Pietrini, F.; Bianconi, D.; Massacci, A.; Iannelli, M.A. Combined effects of elevated CO2 and Cd-contaminated water on growth, photosynthetic response, Cd accumulation and thiolic components status in Lemna minor, J. Hazard. Mater. 2016, 309, 77–86

Prasad, P.V.V.; Djanaguiraman, M. Iron Chlorosis. In *Encyclopedia of Applied Plant Sciences*; Academic Press: Oxford, UK, 2016; Volume 1, pp. 246–255. ISBN 9780123948083

Qi, Z., Yu, H., Chen, Y., and Zhu, M. (2009). Highly porous fibers prepared by electrospinning a ternary system of nonsolvent/solvent/poly(l-lactic acid). Mater. Lett. 63, 415–418. doi: 10.1016/j.matlet.2008.10.059

Ramesh, N., and Duda, J. L. (2000). Diffusion in polymers below the glass transition temperature: comparison of two approaches based on free volume concepts. Korean J. Chem. Eng. 17, 310–317. doi: 10.1007/BF02699046

Ranjan S., Dasgupta N., Lichtfouse E., *Nanoscience in food and agriculture* 5, in Sustainable Agriculture Reviews, Springer International Publishing AG 2017, DOI: 10.1007/978-3-319-58496-6. ISBN 978-3-319-58495-9

Saito, A.; Shimizu, M.; Nakamura, H.; Maeno, S.; Katase, R.; Miwa, E.; Higuchi, K.; Sonoike, K. Fe deficiency induces phosphorylation and translocation of Lhcb1 in barley thylakoid membranes. *FEBS Lett.* **2014**, *588*, 2042–2048.

Sarac, A. (2016). Nanofibers of Conjugated Polymers. New York, NY: Pan Stanford.

Schmid, N.B.; Giehl, R.F.H.; Doll, S.; Mock, H.-P.; Strehmel, N.; Scheel, D.; Kong, X.; Hider, R.C.; von Wiren, N. Feruloyl-CoA 6′-Hydroxylase1-dependent coumarins mediate iron acquisition from alkaline substrates in *Arabidopsis*. *Plant Physiol.* **2014**, *164*, 160–172

Schoolaert E., Steyaert I., Vancoillie I., Geltmeyer J., Lava K., Hoogenboom R., De Clerck K., *Journal of Materials Chemistry* B 4(26) 2016 4507-4516

Schweigert, N.; Zehnder, A.J.B.; Eggen, R.I.L. Chemical properties of catechols and their molecular modes of toxic action in cells, from microorganisms to mammals. *Environ. Microbiol.* **2001**, *3*, 81–91

Shang Y., Hasan M.K., Ahammed G.J., Li M., Yin H., Zhou J., Applications of Nanotechnology in Plant Growth and Crop Protection: A Review. *Molecules* 2019, 24, 2558; doi:10.3390/molecules24142558

Shao, L.; Hu, B.; Dong, P.; Ji, W.; Qi, C. Electrospinning Fe(III)porphyrin/TiO2/poly(styrene) mixture: Formation of a novel nanofiber photocatalyst for the photodegradation of methyl orange. *J. Porphyr. Phthalocyanines* **2010**, *14*, 993–999.

Sheng, P. (1980). Fluctuation-induced tunneling conduction in disordered materials. Phys. Rev. B 21, 2180–2195. doi: 10.1103/PhysRevB.21.2180

Sheng, P. Fluctuation-induced tunneling conduction in disordered materials. *Phys. Rev. B* **1980**, *21*, 2180–2195

Singh, J.S; Pandey C.C.; Singh D.P. Efficient soil microorganisms: A new dimension for sustainable agriculture and environmental development. Agriculture, Ecosystems & Environment 140 (3-4) **2011** 339-353

Sołoducho, J., and Cabaj, J. (**2016**). "Conducting polymers in Sensor Design," in Conducting Polymers, ed F. Yilmaz (London: Intech), 27–48

Srilatha B., J. Nanotechnology in Agriculture, *Nanomedic Nanotechnol* **2011**, 2:7, http://dx.doi.org/10.4172/2157-7439.1000123

Syurik, J.; Ageev, O.A.; Cherednichenko, D.I.; Konoplev, B.G.; Alexeev, A. Non-linear conductivity dependence on temperature in graphene-based polymer, Carbon 63 **2013** 317-323

Tampau, A.; González-Martínez, C.; Chiralt, A. Release kinetics and antimicrobial properties of carvacrol encapsulated in electrospun poly-(ε-caprolactone) nanofibres. Application in starch multilayer films. *Food Hydrocoll.* **2018**, *79*, 158–169

Tholl D, Boland W, Hansel A, Loreto F, Röse USR, Schnitzler J-P (2006) Practical approaches to plant volatile analysis. Plant J 45:540–560

Timilsena, Y.P.; Adhikari, R.; Casey, P.; Muster, T.; Gill, H.; Adhikari, B. Enhanced efficiency fertilisers: A review of formulation and nutrient release patterns. *J. Sci. Food Agric.* **2015**, *95*, 1131–1142

Terra IAA, Mercante LA, Andre RS, Correa DS, Fluorescent and Colorimetric Electrospun Nanofibers for Heavy-Metal Sensing, Biosensors (Basel). 2017 Dec 15;7(4). pii: E61. doi: 10.3390/bios7040061.

Tuteja N., Gill S.S., *Crop Improvement Under Adverse Conditions*, 2013, Springer Science+Business Media New York 2013. DOI 10.1007/978-1-4614-4633-0 ISBN: 978-1-4614-4632-3

Uran, S., Alhani, A., and Silva, C. (2017). Study of ultraviolet-visible light absorbance of exfoliated graphite forms. AIP Adv. 7:4979607. doi: 10.1063/1.4979607

Uyar, T., and Besenbacher, F. (2008). Electrospinning of uniform polystyrene fibers: the effect of solvent conductivity. *Polymer* 49, 5336–5343. doi: 10.1016/j.polymer.2008.09.025

Varsano, T.; Kaftan, D.; Pick, U. Effects of iron deficiency on thylakoid membrane structure and composition in the alga *Dunaliella salina*. *J. Plant Nutr.* **2003**, *26*, 2197–2210.

Wang, T., Huang, D., Yang, Z., Xu, S., He, G., Li, X., et al. (2016). A review on graphene-based gas/vapor sensors with unique properties and potential applications. Nano-Micro Lett. 8, 95–119. doi: 10.1007/s40820-015-0073-1

Wang, X.; Cao, J.; Hu, Z.; Pan, W.; Liu, Z. Jet shaping nanofibers and the collection of nanofiber mats in electrospinning. *J. Mater. Sci. Technol.* **2006**, *22*, 536–540

Wendorff J.H., *Electrospinning: Materials, Processing and Applications*, 2012, Wiley, ISBN: 978-3-527-32080-6

Wünsch, J. R. (2000). Polystyrene: Synthesis, Production and Application. Shawbury, Shrewsbury: Rapra Technology Ltd

Yan, J. Yu, Y. Qiu, X. Yi, J. Lu, X. Zhou, X. Bai, Self-assembly of electrospun polymernanofibers: a general phenomenon generating honeycomb-patterned nanofibrousstructures, Langmuir 27 (8) (2011) 4285–4289

Yang G., Li X., He Y. et al., From nano to micro to macro: Electrospun hierarchically structured polymeric fibers for biomedical applications, Progress in Polymer Science 81 2018 80-113. DOI: 10.1016/j.progpolymsci.2017.12.003

Yang Y. , A. J. Wikieł , L. T. Dall'Agnol , P. Eloy , M. J. Genet , J. J. G. Moura , W. Sand , C. C. Dupont-Gillain and P. G. Rouxhet , Proteins dominate in the surface layers formed on materials exposed to extracellular polymeric substances from bacterial cultures, Biofouling, 2016, 32 , 95 —108

Yang, Y.; Wang, H.; Su, K.; Long, Y.; Peng, Z.; Li, N.; Liu, F. A facile and sensitive fluorescent sensor using electrospun nanofibrous film for nitroaromatic explosive detection. *J. Mater. Chem.* **2011**, 11895–11900.

Yao T., Chen H., Pinak S., et al., Self-assembly of electrospun nanofibers into gradienthoneycomb structures, Materials and Design 168 2019 107614

Yoon J., Chae S.K, Kim J-M., *J. Am. Chem. Soc*., 2007, 129 (11), 3038–3039

Zakrzewski, J., Domanski, W., Chaitas, P., and Laopoulos, T. (2006). Improving sensitivity and selectivity of SnO2 gas sensors by temperature variation. IEEE Trans. Instrum. Meas. 55, 14–20. doi: 10.1109/TIM.2005.862039

Zampetti E., Pantalei S., Muzyczuc A., Bearzotti A., De Cesare F., Spinella C., Macagnano A., *Sensors and Actuators B* 176 2013 390-398

Zampetti E., Pantalei S., Scalese S., Bearzotti A., De Cesare F., Spinella C, Macagnano A., *Biosensors and Biolectronics* 26 (5) 2011 2460–2465

Zampetti, E., Muzyczuk, A., Macagnano, A., Pantalei, S., Scalese, S., Spinella, C., et al. (2011). Effects of temperature and humidity on electrospun conductive nanofibers based on polyaniline blends. J. Nanoparticle Res. 13, 6193–6200. doi: 10.1007/s11051-011-0310-6

Zhong, G., Wang, K., Zhang, L., Li, Z. M., Fong, H., and Zhu, L. (2011). Nanodroplet formation and exclusive homogenously nucleated crystallization in confined electrospun immiscible polymer blend fibers of polystyrene and poly(ethylene oxide). Polymer 52, 5397–5402. doi: 10.1016/j.polymer.2011.09.045

9. Student's Scientific Publications pertinent to the PhD Thesis

F De Cesare, E Di Mattia, **A Macagnano**

Fishing bacteria with a nanonet. Materials Today 20 (5) 2017 284-285. DOI: https://doi.org/10.1016/j.mattod.2017.05.005

A. Macagnano, V. Perri, E. Zampetti, AM. Ferretti, F. Sprovieri, N. Pirrone, A. Bearzotti, F. De Cesare

A smart nanofibrous material for adsorbing and detecting elemental mercury in air. Atmospheric Chemistry and Physics 17 (11) 2017, 6883-6893

A. Macagnano, V. Perri, E. Zampetti, F. Sprovieri, N. Pirrone, G. Esposito, A. Bearzotti, F. De Cesare.

Elemental mercury vapor chemoresistors employing TiO_2 nanofibers photocatalytically decorated with Au-nanoparticles, Sensors and Actuators B: Chemical 247 2017, 957-967

A. Macagnano, F. De Cesare.

Electrospinning: A versatile technology to design biosensors and sensors for diagnostics. In: Electrospun Materials for Tissue Engineering and Biomedical Applications (T. Uyar, E. Kny Eds) Woodhead Publishing Ltd., Cambridge (UK) 2017, pp. 385-418. ISBN. 978-0-08101022-8

Zampetti E.; Papa P.; Di Flaviano F.; Paciucci L.; Petracchini F.; Pirrone N.; Bearzotti A.; **Macagnano A**

Remotely controlled terrestrial vehicle integrated sensory system for environmental monitoring. *Lecture notes in electrical engineering* 431 2018 338-343**,** Springer**,** ISSN: 1876-1100

Avossa, J.; Zampetti, E.; De Cesare,F.; Bearzotti, A.; Scarascia-Mugnozza, G.; Vitiello, G.; Zussman, E.; **Macagnano, A**.

Thermally driven selective nanocomposite PS-PHB/MGC nanofibrous conductive sensor for air pollutant detection, *Frontiers in Chemistry* 6, 2018, 432; DOI: 10.3389/fchem.2018.00432

De Cesare F., Pietrini F., Zacchini M., Scarascia-Mugnozza and **Macagnano A**.

Catechol-Loading Nanofibrous Membranes for Eco-Friendly Iron Nutrition of Plants., Nanomaterials 2019, 9(9), 1315; https://doi.org/10.3390/nano9091315

F De Cesare, E Di Mattia, E Zussman, **A Macagnano**

A study on the dependence of bacteria adhesion on the polymer nanofibre diameter, Environmental Science: Nano 6 (3) 2019, 778-797. **HOT ARTICLE**

J. Avossa, R. Paolesse, C. Di Natale, E. Zampetti, G. Bertoni, F. De Cesare, G. Scarascia-Mugnozza, **A. Macagnano**

Electrospinning of Polystyrene/Polyhydroxybutyrate Nanofibers Doped with Porphyrin and Graphene for Chemiresistor Gas Sensors, Nanomaterials 9 (2), 2019, 280

Awards

2019. F. De Cesare, E. Di Mattia, E. Zussman, **A. Macagnano** (2019).

Back cover, Environmental Science: Nano, vol. 6 (3), pp. 993-994, DOI: 10.1039/C9EN90016K (http://dx.doi.org/10.1039/C9EN90016K).

2017. COVER PAGE WINNER in Materials Today, F. De Cesare, E. Di Mattia, **A. Macagnano**

Materials Today Cover Competition 2016: Fishing bacteria with a nanonet.
http://www.materialstoday.com/amorphous/comment/fishing-bacteria-with-a-nanonet/

Conferences

F. De Cesare, **A. Macagnano**,
Novel approaches and tools to reduce environmental impacts in agrosystems - 19th EGU General Assembly, EGU2017, Proceedings 19 2017, 17704 (23-28 April, 2017 Vienna, Austria)

F. De Cesare, E Di Mattia, **A Macagnano**,
Nanorhizosphere: a new approach to study the interactions between plant and soil microorganisms – The effect of pollutants. 19th EGU General Assembly, EGU2017, Proceedings 19 2017, 17765 (23-28 April, 2017 Vienna, Austria)

V. Perri, E. Zampetti, B. Richichi, N. Pirrone, F. De Cesare, **A. Macagnano**
CdSe/ZnS-TiO_2 nanofibers: a suitable combination for a low cost and effective sensor device. ElectrospinCY2017, International Conference on Electrospinning: from design and processing to advanced nanomaterials and application, New Campus of the University of Cyprus, Nicosia – Cyprus 19-21 Aprile 2017 (INV.2, p.18)

F. De Cesare, E. Di Mattia and **A. Macagnano**
Development of Smart Nanofibrous Plant Growth Promoting Rhizobacteria (PGPR) Biofilms for Agricultural Applications**.** ElectrospinCY2017, International Conference on Electrospinning: from design and processing to advanced nanomaterials and application, New Campus of the University of Cyprus, Nicosia – Cyprus 19-21 Aprile 2017 (INV.23, p.41)

De Cesare, F.; Pietrini, P.; Patti, V; Zacchini, M.; Scarascia Mugnozza, G.; A. **Macagnano, A.**

Nanostrategies in iron supply to plants, ELECTROSPIN2018" - 5th International Conference on Electrospinning, Stellenbosch (South Africa) 16-18/01/2018 (poster presentation)

Macagnano, A.; De Cesare, F.; Zampetti, E.; Bearzotti, A.; Scarascia-Mugnozza, G.; Pirrone, N.

Design of eco-friendly and sustainable nanofibrous sensors for detecting environmental pollutants. ELECTROSPIN2018" - 5th International Conference on Electrospinning, Stellenbosch (South Africa) 16-18/01/2018 (oral presentation)

Macagnano, A.; Avossa, J.; Zampetti, E.; Pirrone, N.; Scarascia Mugnozza, G.; Di Natale, C.; R. Paolesse, R.; De Cesare F.

Composite Electrospun Fibers Based on Sustainable and Biodegradable Polymers for Monitoring Air Pollution, SETAC Europe 28th 13-17/05/2018, Rome (Italy), (poster presentation)

Macagnano, A.; Avossa, J.; Zampetti, E.; Papa, P., Bearzotti, A.; De Cesare F.

Sviluppo di sensori low-cost ed eco-sostenibili per il monitoraggio della qualità dell'aria Conferenza d'Istituto IIA-CNR, 9-10/05/2018 (http://www.iia.cnr.it/conferenza-distituto-2018/) (oral presentation)

Macagnano, A.; Avossa J.; Zampetti E.; De Cesare F.; Paolesse R.; Di Natale C.

Tetraphenylporphyrin in a Heterogeneous Nanofbrous Polymer Layer to get Ultra-Sensitive Conductive Sensors, International Conference on Porphyrins & Phtalocyanines, ICPP-10, Munich, July 1-6, 2018 (oral presentation)

Avossa, J.; Zampetti, E.; Scarascia Mugnozza, G.; De Cesare, F.; Paolesse, R.; Di Natale, C.; **Macagnano, A.**

Gas sensing properties of Porphyrins-Graphene composite electrospun fibers, 17th International Meeting on Chemical Sensors, July 15-19, 2018, University of Vienna, Austria (*Proceedings Book: DOI 10.5162/IMCS2018/GS4.3*) (oral presentation)

Avossa, J.; Zampetti, E.; Paolesse, R.; Di Natale, C.; Scarascia-Mugnozza, G.; De Cesare (3), F.; **Macagnano, A.**

Porphyrin and Graphene as smart nanofillers for eco-friendly, sustainable and selective polymer nanofibrous sensors for IAQ monitoring, Nanoinnovation2018-Conference and Exhibition, Rome (Italy) September, 11-142018 (poster presentation)

Macagnano A.

Nanocomposite nanofibers in chemical sensors for air pollution, POLYMAR 2018 (2nd Conference for Early Stage Researchers in Polymer Science through the Aegean), October 8-12, 2018 (oral presentation)

J. Avossa, E. Zampetti, G. Scarascia Mugnozza, F. De Cesare, C. Di Natale, R. Paolesse, **A. Macagnano**

Composite electrospun fibers based on PS-PHB blend and graphene-porphyrine for conductive gas-sensors, POLYMAR 2018 (2nd Conference for Early Stage Researchers in Polymer Science through the Aegean), October 8-12, 2018 (oral presentation)

A. Macagnano, J. Avossa, E. Zampetti, R. Paolesse, G. Scarascia Mugnozza, C.Di Natale, F. De Cesare

Porphyrin, graphene and polymers: smart combinations for selective nanofibrous chemosensors for gas and VOCs, European Polymer Conference 2019 EUPOC2019, Como, 12-16 May 2019 (oral presentation)

A. Macagnano, E. Zampetti, J. Avossa, G. Scarascia-Mugnozza, F. De Cesare Fabrizio

Electrospun nanocomposite nanofibers in chemical sensors for gaseous compounds, Nano-M&D 2019, "Fabrication, Properties, and Applications of Nano-Materials and Nano-Devices" International Conference, Savoy Beach Hotel, Paestum, Salerno (Italy), June 04-08, 2019 (invited talk).